

VILNIUS GEDIMINAS TECHNICAL UNIVERSITY

Athanasios IOANNIDIS

ELECTRODYNAMICAL INVESTIGATION OF THE PHOTONIC METAMATERIALS

DOCTORAL DISSERTATION

TECHNOLOGICAL SCIENCES
ELECTRICAL AND ELECTRONIC ENGINEERING (T 001)

Vilnius, 2023

The doctoral dissertation was prepared at Vilnius Gediminas Technical University in 2019–2023.

Scientific Supervisor

Assoc. Prof. Dr Tatjana GRIC (Vilnius Gediminas Technical University, Electrical and Electronic Engineering – T 001).

The Dissertation Defence Council of Scientific Field of Electrical and Electronic Engineering of Vilnius Gediminas Technical University:

Chairman

Assoc. Prof. Dr Andrius KATKEVIČIUS (Vilnius Gediminas Technical University, Electrical and Electronic Engineering – T 001).

Members:

Dr Igor MEGLINSKI (Aston University, United Kingdom, Electrical and Electronic Engineering – T 001),

Assoc. Prof. Dr Dalius SELIUTA (Vilnius Gediminas Technical University, Electrical and Electronic Engineering – T 001),

Dr Habil. Kęstutis STALIŪNAS (Vilnius University, Physics – N 002),

Prof. Dr Nerija ŽURAUSKIENĖ (Vilnius Gediminas Technical University, Electrical and Electronic Engineering – T 001).

The dissertation will be defended at the public meeting of the Dissertation Defence Council of Electrical and Electronic Engineering in the SRA-I Meeting Hall of Vilnius Gediminas Technical University at **10 a.m. on 18 December 2023**.

Address: Saulėtekio al. 11, LT-10223 Vilnius, Lithuania.

Tel.: +370 5 274 4956; fax +370 5 270 0112; e-mail: doktor@vilniustech.lt

A notification on the intended defence of the dissertation was sent on 17 November 2023.

A notification on the intended defence of the dissertation was sent on 9 January 2023. A copy of the doctoral dissertation is available for review at Vilnius Gediminas Technical University repository <https://etalpykla.vilniustech.lt> and the Library of Vilnius Gediminas Technical University (Saulėtekio al. 14, LT-10223 Vilnius, Lithuania) and at the Library of State Research Institute Center for Physical Sciences and Technology (Saulėtekio al. 3, LT-10257 Vilnius, Lithuania).

Vilnius Gediminas Technical University book No 2023-049-M

doi:10.20334/2023-049-M

© Vilnius Gediminas Technical University, 2023

© Athanasios Ioannidis, 2023

athanasios.ioannidis@vilniustech.lt

VILNIAUS GEDIMINO TECHNIKOS UNIVERSITETAS

Athanasios IOANNIDIS

FOTONINIŲ METAMEDŽIAGŲ ELEKTRODINAMINIS TYRIMAS

DAKTARO DISERTACIJA

TECHNOLOGIJOS MOKSLAI,
ELEKTROS IR ELEKTRONIKOS INŽINERIJA (T 001)

Vilnius, 2023

Disertacija rengta 2019–2023 metais Vilniaus Gedimino technikos universitete.

Mokslinis vadovas

doc. dr. Tatjana GRIC (Vilniaus Gedimino technikos universitetas, elektros ir elektronikos inžinerija – T 001).

Vilniaus Gedimino technikos universiteto Elektros ir elektronikos inžinerijos mokslo krypties disertacijos gynimo taryba:

Pirmininkas

doc. dr. Andrius KATKEVIČIUS (Vilniaus Gedimino technikos universitetas, elektros ir elektronikos inžinerija – T 001).

Nariai:

dr. Igor MEGLINSKI (Astono universitetas, Jungtinė Karalystė, elektros ir elektronikos inžinerija – T 001),

doc. dr. Dalius SELIUTA (Vilniaus Gedimino technikos universitetas, elektros ir elektronikos inžinerija – T 001),

habil. dr. Kęstutis STALIŪNAS (Vilniaus universitetas, fizika – N 002),

prof. dr. Nerija ŽURAUSKIENĖ (Vilniaus Gedimino technikos universitetas, elektros ir elektronikos inžinerija – T 001).

Disertacija bus ginama viešame Elektros ir elektronikos inžinerijos mokslo krypties disertacijos gynimo tarybos posėdyje **2023 m. gruodžio m. 18 d. 10 val.** Vilniaus Gedimino technikos universiteto SRA-I Posėdžių salėje.

Adresas: Saulėtekio al. 11, LT-10223 Vilnius, Lietuva.

Tel. (8 5) 274 4956; faksas (8 5) 270 0112; el. paštas doktor@vilniustech.lt

Pranešimai apie numatomą ginti disertaciją išsiųsti 2023 m. lapkričio 17 d.

Disertaciją galima peržiūrėti Vilniaus Gedimino technikos universiteto talpykloje <https://etalpykla.vilniustech.lt> ir Vilniaus Gedimino technikos universiteto bibliotekoje (Saulėtekio al. 14, LT-10223 Vilnius, Lietuva) ir Valstybinio mokslinių tyrimų instituto Fizinių ir technologijos mokslų centro bibliotekoje (Saulėtekio al. 3, LT-10257 Vilnius, Lietuva).

Abstract

The dissertation investigates the possibilities of applying the Maxwell–Garnett approach for homogenising different types of metamaterial structures, such as conventional nanowires, spiral nanowires, and nanostructured composite cases. The research aims to study the dispersion maps of the surface plasmon polaritons (SPPs) propagating at different interfaces, such as metallic nanowire metamaterial interface and the hollow-core metamaterial interface, nanostructured metamaterial and corrugated metal interface, spiral nanowire metamaterial and air interface, nanocomposite and hypercrystal interface.

This dissertation aims to analyse the properties of the dispersion and loss of SPPs at the investigated interfaces, aiming to achieve absorption enhancement, enabling the possible creation of the aircraft coating model, and allowing for the cancellation along with the antenna systems. The dissertation enables to analyse system engineering tools, such as the angle of the spiral, the number of grooves, etc., aiming to conclude the tunability possibilities of the structure's properties.

Relevant dispersion relations are derived by matching the tangential components of the electrical and magnetic fields. It is demonstrated that tuning can be achieved by modifying the parameters of the metamaterial building blocks. Moreover, the tunability of the nanowire metamaterials can be enhanced further by changing either the metamaterial filling ratio or metamaterial cell geometry. Calculated dispersion relations and propagation lengths of plasmon modes in the system are presented. It has been concluded that the frequency range of the surface waves' existence can be significantly increased by dealing with the nanowire metamaterial interface. The possible application of the proposed tunable structures is in antenna and aircraft noise reduction system design.

Reziumė

Disertacijoje nagrinėjamos Maxwell–Garnett metodo taikymo galimybės skirtingų tipų metamedžiagų struktūroms, tokioms kaip įprastinė nanovielinė metamedžiaga, spiralinė nanovielinė metamedžiaga, nanostruktūrinė metamedžiaga, homogenizuoti. Siekiama ištirti paviršinių plazmonų poliaritonų (SPP), sklindančių įvairiose sandūrose, tokiose kaip metalinės nanovielinės metamedžiagos ir tuščiaavidurės šerdies metamedžiagos sandūra, nanostruktūrinės metamedžiagos ir gofruoto metalo sandūra, spiralinė nanovielinė metamedžiaga ir oro sandūra, nanokompozito ir hiperkristalo sandūra, dispersines diagramas.

Disertacinio darbo tikslas – išanalizuoti PPP sklaidos ir nuostolių ypatybes tiriamose sandūrose, siekiant pagerinti absorbciją, leidžiančią sukurti orlaivio dangos modelį, taip pat ir antenų sistemas, su tikslu slopinti triukšmą. Disertacija taip pat leidžia išanalizuoti sistemos derinamumo priemones, tokias kaip spiralės kampas ir griovelių skaičius, siekiant padaryti išvadą apie konstrukcijų savybių derinimo galimybes.

Taikant elektrinių ir magnetinių laukų tangentinių komponentų suderinimo metodą gaunami atitinkami dispersijos ryšiai ir parodoma, kad derinimą galima pasiekti modifikuojant metamedžiagų dalelių parametrus. Be to, nanovielinių metamedžiagų derinamumą galima dar labiau pagerinti keičiant metamedžiagos užpildymo koeficientą arba metamedžiagų ląstelių geometriją. Pateikiami apskaičiuoti dispersijos santykiai, taip pat SPP sklidimo ilgiai sistemoje. Padaryta išvada, kad naudojant nanovielinių metamedžiagų sandūrą galima žymiai padidinti paviršinių bangų egzistavimo dažnių diapazoną. Galimas siūlomų derinamų konstrukcijų pritaikymas mažinant antenų ir orlaivių triukšmą.

Notations

Symbols

β – propagation constant (liet. *sklidimo pastovioji*);
 ε_m – permittivity of metal (liet. *metalo santykinė dielektrinė skvarba*);
 ε_d – permittivity of dielectric (liet. *dielektriko santykinė dielektrinė skvarba*);
 ω – cyclic frequency (liet. *ciklinis dažnis*);
 c – speed of light (liet. *šviesos greitis*);
 ρ – filling fraction (liet. *užpildos koeficientas*);
 k – wave number (liet. *bangos skaičius*);
 λ – wavelength (liet. *bangos ilgis*);
 σ – conductivity (liet. *laidumas*);
 L_p – propagation length (liet. *sklidimo ilgis*).

Abbreviations

ENP – epsilon near pole (liet. *epsilon arti ašigalio*);
ENZ – epsilon near zero (liet. *epsilon arti nulio*);
FB – Ferrell Berreman (liet. *Ferrell Berreman*);
ITO – indium tin oxide (liet. *indžio alavo oksidas*);
MM – metamaterial (liet. *metamedžiaga*);
PbS – lead sulfide (liet. *švino sulfidas*);
PEC – perfect electric conductor (liet. *tobulas elektros laidininkas*);

SP – surface plasmon (liet. *paviršiniai plazmonai*);

SPP – surface plasmon polariton (liet. *paviršiniai plazmoniniai polaritonai*);

TCO – transparent conducting oxide (liet. *skaidrus laidus oksidas*).

Contents

AUTHOR’S CONTRIBUTION TO THE PUBLICATIONS.....	XIII
INTRODUCTION	1
Problem formulation	1
Relevance of the dissertation.....	2
The object of the research	2
The aim of the dissertation	2
The objectives of the dissertation	2
Research methodology	3
Scientific novelty of the dissertation	3
Practical value of the research findings.....	4
The defended statements	4
Approval of the research findings	5
Structure of the dissertation.....	5
1. PHOTONIC METAMATERIALS MODELLING TECHNIQUES	7
1.1. Anisotropic medium homogenisation techniques.....	7
1.2. Propagation of surface plasmons and surface plasmon polaritons	8
1.3. Attempts to design models for aeroacoustics and electronics	10
1.4. Homogenisation method.....	11
1.4.1. Mixing rules to homogenise metamaterials	11
1.4.2. Maxwell Garnett formula to homogenise layered nanostructured metamaterial	12

1.5. Transfer matrix method to obtain the dispersion relation of surface plasmon polaritons	13
1.6. Conclusions of the First Chapter and formulation of the dissertation tasks	16
2. SURFACE PLASMON POLARITONS: INVESTIGATION METHODOLOGY	19
2.1 Analytical models of the investigated systems.....	19
2.1.1. Surface plasmon polaritons at the interface separating nanocomposite and hypercrystal	20
2.1.2. Surface plasmon polaritons propagating at the boundary of spiral wire metamaterial	22
2.2. Conclusions of the Second Chapter.....	25
3. SURFACE PLASMON POLARITONS: INVESTIGATION RESULTS AND CONCLUSIONS.....	27
3.1. Theoretical studies of the tunable surface plasmon polaritons	27
3.1.1. Propagation of surface plasmon polariton at the interface of nanowire metamaterial	28
3.1.2. Propagation of surface plasmon polaritons at the interface of the corrugated metamaterial	32
3.1.3. Propagation of surface plasmon polaritons at the interface of spiral wire metamaterial	35
3.1.4. Propagation of surface plasmon polaritons at the interface of the acoustic metamaterial	38
3.1.5. Propagation of surface plasmon polaritons at the interface of nanocomposite and hypercrystal	41
3.1.6. Conductivity-dependent surface plasmon polaritons propagating at the boundary of nanocomposite and hypercrystal	45
3.2. Conclusions of the Third Chapter.....	47
GENERAL CONCLUSIONS	49
REFERENCES	51
AUTHOR'S PUBLICATIONS COLLECTION.....	57
Article 1. Ioannidis et al. (2022). Tunable polaritons of spiral nanowire metamaterials (https://doi.org/10.1080/17455030.2020.1774095).....	59
Article 2. Ioannidis et al. (2021). Controlling surface plasmon polaritons propagating at the boundary of low-dimensional acoustic metamaterials (https://doi.org/10.3390/app11146302)	68
Article 3. Ioannidis et al. (2021). Looking into surface plasmon polaritons guided by the acoustic metamaterials (https://doi.org/10.1007/s11468-021-01377-x).....	76
Article 4. Ioannidis et al. (2021). The study of the surface plasmon polaritons at the interface separating nanocomposite and hypercrystal (https://doi.org/10.3390/app11115255)	81

Article 5. Ioannidis et al. (2020). Surface plasmon polariton waves propagation at the boundary of graphene based metamaterial and corrugated metal in THz range (https://doi.org/10.1007/s11082-019-2128-x).....	96
Article 6. Ioannidis et al. (2019). Enhancing the properties of plasmonic nanowires (https://doi.org/10.1088/2053-1591/ab0a1b).....	108
SUMMARY IN LITHUANIAN.....	117

Author's contribution to the publications

Publication ¹	Formal contribution ²	Conceptualisation	Data curation	Formal analysis	Investigation	Methodology	Software	Validation	Visualisation	Writing – original draft	Writing – review & editing
Ioannidis et al. 2022	0.33	sole	joint	joint	main	sole	main	joint	main	joint	joint
Ioannidis et al. 2021	0.33	sole	joint	joint	main	sole	main	joint	main	joint	joint
Ioannidis et al. 2021	0.33	joint	joint	joint	main	main	main	sole	main	joint	joint
Ioannidis et al. 2021	0.33	sole	joint	main	main	main	main	joint	main	joint	joint
Ioannidis et al. 2020	0.33	sole	joint	joint	main	main	main	sole	main	joint	joint
Ioannidis et al. 2019	0.2	joint	joint	joint	main	joint	main	joint	main	joint	joint
Total or max ³	1.85	sole	joint	main	main	main	main	sole	main	joint	joint

¹ – the published articles have been used here with the permission of relevant publishers.

² – the formal contribution is calculated as a fraction – $1/N_{\text{authors}}$.

³ – the total sum of the formal contribution values or the highest contribution achieved (in increasing order: none, joint, main, or sole) in the specified 10 of 14 roles (according to the CRediT taxonomy, <https://credit.niso.org/>).

All the above-mentioned articles' co-authors have no motive to use this published data to prepare other dissertations.

All the authors of the above-mentioned articles have agreed on the author's contribution statement.

Introduction

Problem formulation

For aerospace and antenna applications, traditional antenna materials – printed circuit boards, machined aluminium enclosures, and thermoset radomes – offer tried and true but costly approaches to building antennas. Another major disadvantage is the poor absorption properties, increasing noise levels. A key SPP-enabled property is the strong light confinement well beyond the diffraction limit in metallic nanostructures via the excitation of localised SPP resonances. This property can be used to build subwavelength-sized plasmonic nanoresonators extremely sensitive to tiny variations in their surroundings or plasmonic nanoantennas that efficiently convert confined into radiative fields and vice versa. A new approach is needed to meet next-generation antenna requirements. These types of problems can be solved by applying metamaterials (MMs). An MM is composed of nanostructures, which are called artificial atoms. These structures provide the metamaterial with unique properties that natural materials cannot have. These properties can be used to overcome optical limits caused by several effects, such as the diffraction limit, so using metamaterials can yield abnormal properties in the devices. The changeable properties of MMs have been achieved by introducing active materials, such as vanadium dioxide, indium tin oxide, polydime-

thylsiloxane, graphene, or liquid crystals. The former allows for achieving controllable characteristics. An active material provides a metamaterial with tunability, reversibility, repeatability and fast response to change. Incorporating responsive materials, such as semiconductors, liquid crystals, phase-change materials, or quantum materials (e.g., superconductors, 2D materials, etc.) imbue metamaterials with dynamic properties, facilitating the development of active and tunable devices harbouring enhanced or even entirely novel electromagnetic functionality.

Relevance of the dissertation

The importance of a doctoral dissertation lies in its ability to design, develop and disseminate novel tunable metamaterial models for possible applications in the aircraft industry and at high-frequency regions. The doctoral dissertation is a multidisciplinary project highly relevant to the aspects of the aircraft and electronic fields, including possible applications of the presented approaches in the antennas and aircraft industry fields. The work outcomes will not only result in completely new tunable metamaterial models, potentially applicable to perform noise cancellation functions, but also open a new route to novel platforms that could offer several practical implementations of novel antenna systems.

The object of the research

The research object is the design of various solutions for the propagation of surface plasmon polaritons (SPPs) based on the application of nanostructured and nanowire metamaterial models.

The aim of the dissertation

Creation of the theoretical novel models enabling investigation of the electrodynamic properties of SPPs propagating at the studied interfaces.

The objectives of the dissertation

The following objectives were formulated to solve the stated problem and reach the aim of the dissertation:

1. To investigate the possibilities of applying the Maxwell Garnett approach to homogenising different types of metamaterial structures, such as conventional nanowires, spiral wire, and nanostructured composite cases.
2. To study the dispersion maps of the SPPs propagating at different interfaces such as:
 - metallic nanowire metamaterial interface and the hollow-core metamaterial interface;
 - nanostructured metamaterial and corrugated metal interface;
 - spiral wire metamaterial and air interface;
 - nanocomposite and hypercrystal interface.
3. To analyse the properties of the dispersion and loss of SPPs at the investigated interfaces, aiming to achieve absorption enhancement, enabling possible creation of the aircraft coating model, allowing for noise cancellation along with the antenna systems.
4. To analyse system engineering tools, such as the angle of the spiral, number of grooves, etc., aiming to conclude the tunability possibilities of the structure properties.

Research methodology

Methods used in the dissertation:

- The effective medium approximation theory is based on the Maxwell Garnett approach and the transfer matrix approach, which was used to develop the novel SPP propagation models aiming to calculate electro-dynamical characteristics.
- SPP simulation methods were implemented to measure the absorption enhancement of the propagating mode, leading to possible applications in the antenna design.

Scientific novelty of the dissertation

- Novel computer models of SPP propagation at the novel metamaterial interfaces have been developed with *Matlab* to calculate the electro-dynamical parameters of the SPPs propagating at the interfaces under study.
- The influence of the metamaterial filling ratio on the transmission characteristics of SPPs has been determined, enabling the realisation of dimension-tunable SPPs.

- The tunability of the absorption enhancement (the imaginary part of the propagation constant) has been investigated by engineering metamaterial structural design.

Practical value of the research findings

New computer models based on novel metamaterials having a potential application in devices, such as antennae and noise cancellation films, were created, and existing models were improved. These models allow for analysing the propagation of SPPs at the boundary of novel interfaces. They also enable the calculation of their parameters and evaluation of electrodynamic characteristics. It investigates how the properties of the devices change by varying the metamaterial parameters. Algorithms and programs were created to predict electrodynamic characteristics of the SPPs propagating at the novel metamaterial interfaces.

The defended statements

1. A two times wider frequency range of surface waves existence, i.e. from 500 THz (600 nm) to approximately 1000 THz (300 nm), can be achieved if a nanowire metamaterial ($d = 10$ nm, $S = 60$ nm) interface is employed instead of a hollow-core metamaterial interface ($d = 10$ nm, $S = 60$ nm).
2. The absorption enhancement of nanowire metamaterial could be increased by ten times if transparent conducting oxides are employed in the nanowire metamaterial instead of the silver analogues.
3. The resonance frequency of the SPPs modes can be increased from 250 THz to 1000 THz by increasing the chemical potential from $\mu = 0.1$ eV till $\mu = 1.5$ eV.
4. The designed spiral wire metamaterial with a wire diameter d of 8 nm allowed to increase the highest operation frequency of the propagating modes regime to 500 THz compared to 300 THz, which is permitted by the smaller analogue ($d = 4$ nm).
5. The noise could be reduced by 1.1 factor (0.83 dB) if nanowire acoustic metamaterial ($d = 10$ nm, $S = 60$ nm) is applied and would reach its maximum efficiency if the metamaterial filling ratio equals $f = 0.7$.

Approval of the research findings

The main results of the dissertation were published in seven scientific publications: six in the *Clarivate Analytics Web of Science* database with an impact factor and one in other databases.

The research results on the dissertation's topic were presented at four scientific conferences:

- Metamaterials and Plasmonics Conference (META) 2022. Torremolinos, Spain.
- International Conference “Electrical, Electronic and Information Sciences“ (eStream) 2022. Vilnius, Lithuania.
- Metamaterials and Plasmonics Conference (META) 2021. Poland, Warsaw.
- Conference for Lithuania Junior Researchers “Science – Future of Lithuania” 2021. Vilnius, Lithuania.

Structure of the dissertation

The dissertation contains an introduction, analytical literature review, discussion of research methodology, summarized investigation results and conclusions, references, author's publications collection, and a summary in Lithuanian. The dissertation consists of 138 pages, 40 displayed equations, 23 figures, 1 table, and 69 references cited in the dissertation. The dissertation is structured around three main chapters.

The First Chapter reviews the concept of SPPs and their application in aviation. It concludes by formulating the main objective and tasks of the present investigation.

The Second Chapter explores numerical methods for investigating metamaterials. It presents homogenisation techniques for concluding the effective permittivity of considered metamaterial. Also, it considers *the novel* transfer matrix method used to derive the dispersion relation of SPPs propagating at the boundary of the novel metamaterials.

The Third Chapter presents numerical investigation results on analysing the propagation of SPPs at the boundaries of novel studied metamaterials. In this relation, the doctoral dissertation covers a wide range of investigations, starting from conventional nanowire cases and ending with exotic cases, such as spiral wire metamaterials.

Photonic metamaterials modelling techniques

This chapter reviews the concept of SPPs and their application in aviation, the main techniques for homogenising highly anisotropic media and dealing with the SPP propagation based on their dispersion relation. This chapter concludes by formulating the main objective and tasks of the investigation. The scientific publication was published on the topic of the first chapter (Ioannidis et al., 2021) and findings were presented at META 2021 and META 2022 conferences.

1.1. Anisotropic medium homogenisation techniques

In the last few decades, metamaterials have inspired scientists and engineers to think about waves beyond traditional constraints imposed by materials in which they propagate, conceiving new functionalities, such as subwavelength imaging, invisibility cloaking and broadband ultraslow light. Mainly for ease of fabrication, many of the metamaterial concepts have initially been demonstrated at longer wavelengths and for microwaves, and later, metamaterials have subsequently moved to photonic frequencies and the nanoscale. Recently, metamaterials have embedded new quantum materials, such as graphene, dielectric nanostructures and, as metasurfaces, surface geometries and surface waves while embracing new

functionalities such as nonlinearity, quantum gain and strong light-matter coupling. A significant number of attractive applications, e.g., ultra-compact wave plates (Min et al., 2015), broadband absorbers (Kong et al., 2017) and optical circuit boards (Min & Huang, 2015) have been enabled due to numerous unusual trends in anisotropic composites. These include an invisible cloak (Klotz et al., 2019), negative refraction (Kadic et al., 2019), and abnormal reflection (Ratni et al., 2018). It should be noted that electromagnetic features of composites can be engineered by lights (Dani et al., 2009), electrics (Anglin et al., 2011), magnetics (Han et al., 2008) and temperatures (Chen et al., 2010), engineering material structure or geometry of metamaterial unit cells.

Metamaterials can be engineered to obtain the desired unique properties depending on the application. Thus, the studied structures vary using different unit cell types, i.e., rectangular and hexagon. The presence of waves was originally demonstrated for dielectric materials placed over a metal surface or for the metallic surface with a periodic repetition of obstacles or holes in the direction of propagation (Pendry et al., 2004; Garcia-Vidal et al., 2005; Jiang et al., 2009). The mentioned structures have been homogenised by applying the Maxwell Garnett approach; however, no attempt was made to deal with the novel and more complicated metamaterial cases. Therefore, it is particularly interesting to examine the metamaterial structures with complicated geometry by applying the Maxwell Garnett approach.

It is particularly important to find a way to achieve tunability. It should be mentioned that metamaterials can be tuned to respond to different frequencies instead of only fixed ones. Therefore, in this great diverse environment of the design structures of metamaterials, depending on the case, they require low or high applied frequency ranges. Additionally, due to their dispersive abilities, the permittivity and permeability in the studied metamaterials depend on the incoming wave frequency.

1.2. Propagation of surface plasmons and surface plasmon polaritons

An important aspect of the present investigation is the propagation of SPPs at the boundary of geometrically different metamaterials. Surface plasmons (SPs) are introduced as collective oscillations of the delocalised electrons presenting at metal–dielectric interfaces in metamaterial structures. The resonant oscillations of free electrons at the interface of nanocomposite media due to optical radiations give rise to SPPs (Stiens et al., 1997). Another definition is that the strong level of interaction between light and free electrons in metals (Raether, 1988; Maier, 2007) causes quasiparticles called SPPs. The SPP propagation in nanocomposites

has been extensively studied (Singh et al., 2015; Singh et al., 2021; Singh, 2021). Composite media with metal nanoparticles are particularly essential, aiming to create nanostructured metal–insulator systems and novel approaches to manipulating light based on it. The calculations focus on dispersion properties and SPP propagation lengths at the boundary of nanostructured metamaterials, employing realistic material parameters. However, the mentioned studies report on investigating SPP propagation at conventional interfaces. Further steps are needed to enhance the interest-raising properties, such as absorption enhancement necessary for developing aircraft coverage films for noise cancellation and improved passenger comfort. Thus, it is particularly interesting to examine the SPP propagation in the enhanced system, i.e., at the interface separating metallic nanowire metamaterial and hollow-core metamaterial medium. The emergence of transparent conductive oxides (TCOs) has attracted tremendous interest within the scientific community. These are the alternative approach for plasmonics (Naik et al., 2016) in the near-infrared region. Contrary to noble metals, such TCOs as indium tin oxide (ITO) demonstrate a great tunability of their optical and electronic properties (Feigenbaum et al., 2010). Although TCOs have already been widely used as an advantageous metal alternative, studies are still lacking to allow for enhanced absorption and structure tunability. Doing so, the investigation of the nanocomposite and hypercrystal interface would provide fertile ground for the mentioned functionality due to the innovative TCO inclusions. Plasmonic behaviour in the visible to near-infrared light range is achievable due to the employment of metallic nanostructures. Absorption enhancement of silver and TCO nanowires with different diameters by effective medium approximation has already been investigated (Gric et al., 2018). The studies also report on the stronger enhancement of TCO nanowires. Surface-plasmon-based circuits are known to merge the fields of photonics and electronics at the nanoscale, thereby enabling it to overcome the existing difficulties related to the large size mismatch between the micrometre-scale bulky components of photonics and the nanometre-scale electronic chips. These applications, however, are generally limited to high electromagnetic (EM) frequencies (the UV, visible, and near-infrared ranges). This is because metals behave akin to perfect electric conductors (PECs) at lower frequency regimes and do not support SP modes. Early works showed that by corrugating metal surfaces, this limitation could be overcome, and they reported the excitation of highly confined SP-like EM modes at microwave frequencies (Gaubau et al., 1950; Harvey, 1960). In 2004, Pendry et al. introduced the concept of spoof SPs and demonstrated that plasmonic metamaterials constructed by patterning metal surfaces with subwavelength periodic features can mimic, at low frequencies (far IR, terahertz, or microwave regimes), the EM guiding characteristics of optical SPs (Pendry et al., 2004; Garcia-Vidal et al., 2005). It should be mentioned that ex-

ceptional SPP properties, such as subwavelength confinement and strong field enhancement, give rise to a wide range of innovative applications (Ioannidis et al., 2019; Gric et al., 2018; Lepeshov et al., 2018). However, studies are lacking on the absorption enhancement by corrugated systems. In the frame of the present dissertation, the investigation will focus on the spiral wire metamaterial and air interface, the nanostructured metamaterial and the corrugated metal interface. The former approach will bring absorption enhancement, which is highly desirable for aircraft coatings, with the system engineering tools, such as the angle of the spiral, the number of grooves, etc., to conclude the tunability of the structure properties.

1.3. Attempts to design models for aeroacoustics and electronics

Flexible electronics that break through the bottleneck and monopoly of traditional rigid electronics have aroused extensive interest in the research community and become one of the greatest cutting-edge interdisciplinary concerns. Broad innovative applications include wearable electronics (Shi et al., 2021; Hajiaghajani et al., 2021), epidermal electronics, implantable electronics (Song et al., 2019), soft robotics (Byun et al., 2018; Yang et al., 2018), etc. Over the last two decades, great progress has been achieved on advanced soft materials (Chen et al. 2019) and structural designs to enable flexible electronics. While the application of metamaterials for cloaking has been extensively covered, their use in THz and acoustic frequency ranges still requires scientists' attention. So, an intriguing application of metamaterials is in aeroacoustics, by mathematical analogy from electromagnetic waves. Maxwell electromagnetism, elasticity, and acoustics describe various classical waves via different equations. Analogies between these waves are very fruitful and repeatedly resulted in the mutual export of ideas between optics and acoustics. To name a few, acoustic crystals/metamaterials, vortex beams, and topological systems were developed in parallel with their optical counterparts and attracted great attention in the past decades. Surface waves at interfaces between continuous media, such as surface plasmon-polaritons, are highly important for modern optics. However, only some research efforts analyse acoustic analogues of such waves (Kiełczyński, 2022; Bliokh et al., 2019). The reason for this is that such waves (for linear longitudinal sound fields) appear only at interfaces with negative-density media, i.e., acoustic metamaterials. Surface electromagnetic waves also require media with negative parameters (permittivity or permeability), but there are natural media with such parameters, e.g., metals. Nonetheless, the dissertation aims to explore the fundamental origin of surface acoustic modes and show that this reveals nontrivial intrinsic properties of acoustic wave equations.

1.4. Homogenisation method

This section presents homogenisation techniques used to investigate novel types of metamaterials.

1.4.1. Mixing rules to homogenise metamaterials

Homogenisation theories are applied to assign effective material parameters (in metamaterials studies, especially effective permittivity and permeability) to materials of mixed and heterogeneous microstructure. The former approach establishes if the characteristic length of inhomogeneities in the mixture is sufficiently smaller than the wavelength of the operating electromagnetic field. This is at least the case for the non-resonant inclusions and positive-permittivity materials composing the whole mixture. However, it has been shown (Ferrari et al., 2015) that for negative-permittivity mixtures, basic mixing rules based on quasistatic principles give fairly accurate predictions when measured against full-wave simulations. This happens even surprisingly close to regions where plasmonic resonances appear, although, of course, the failure in accounting for all the detailed resonance structures cannot be avoided. Below, the simplest classical mixing rules are described. Isotropic phases (background medium and inclusions) form the considered mixtures, and the inclusions are assumed to be spheres. The presented rule is applied to homogenise novel metamaterials presented in the doctoral dissertation.

The polarisability α describes the first-order response of an isotropic dielectric sphere that is small compared to the wavelength. It is the ratio between the induced dipole moment and the amplitude of the external electric field (Poddubny et al., 2013):

$$\alpha = V (\varepsilon_i - \varepsilon_e) \frac{3\varepsilon_e}{\varepsilon_i + 2\varepsilon_e}, \quad (1.1)$$

where the permittivities of the inclusion and its environment are denoted by ε_i and ε_e , respectively. The volume of the sphere is V . Note that the polarisability is a scalar. This is because the inclusion material is isotropic, and its shape is spherically symmetric. The presented mixing rule (1.1) will serve as a basis to derive analytical homogenisation formulas for the novel metamaterials.

1.4.2. Maxwell Garnett formula to homogenise layered nanostructured metamaterial

Consider a mixture where small (in comparison with the wavelength) spherical dielectric inclusions (with permittivity ε_i) are embedded in a host material of permittivity ε_e . The number density of the inclusions is n . Then, the effective permittivity of the mixture, according to the so-called Clausius–Mossotti formula (Pod-dubny et al., 2013), is as follows:

$$\frac{\varepsilon_{eff} - \varepsilon_e}{\varepsilon_{eff} + 2\varepsilon_e} = \frac{n\alpha}{3\varepsilon_e}. \quad (1.2)$$

The dilute-mixture approximation can be written by taking the limit of small n :

$$\varepsilon_{eff} \approx \varepsilon_e + n\alpha. \quad (1.3)$$

In practical applications, it is not always convenient to use quantities like polarisabilities and scatterer densities. Rather, it is preferred to deal with the permittivities of the components of the mixture. When this is the case, it is advantageous to combine the Clausius–Mossotti formula with the polarisability expression (Eq. 1.1). Then, the equation can be written as follows:

$$\frac{\varepsilon_{eff} - \varepsilon_e}{\varepsilon_{eff} + 2\varepsilon_e} = f \frac{\varepsilon_i - \varepsilon_e}{\varepsilon_i + 2\varepsilon_e}, \quad (1.4)$$

where $f = nV$ is a dimensionless quantity signifying the volume fraction of the inclusions in the mixture. It is worthwhile noting that because only the volume fraction and the permittivities appear in the mixing rule, the spheres are not required to have the same size if only all of the objects are small compared to the wavelength.

The Maxwell Garnett formula stands for the most common mixing rule (Eq. 1.4) written explicitly for the effective permittivity:

$$\varepsilon_{eff} = \varepsilon_e + 3f\varepsilon_e \frac{\varepsilon_i - \varepsilon_e}{\varepsilon_i + 2\varepsilon_e - f(\varepsilon_i - \varepsilon_e)}. \quad (1.5)$$

This formula opens wide avenues for researchers. The beauty of the Maxwell Garnett formula is in its simplicity combined with its wide applicability. It satisfies the limiting processes for vanishing inclusion phase $f \rightarrow 0$, giving $\varepsilon_{eff} \rightarrow \varepsilon_e$, and for vanishing background $f \rightarrow 1$, it can be concluded that $\varepsilon_{eff} \rightarrow \varepsilon_i$.

The mixing equation for dilute mixtures ($f \ll 1$) is given by the perturbation expansion of the Maxwell Garnett rule:

$$\varepsilon_{eff} \approx \varepsilon_e + 3f\varepsilon_e \frac{\varepsilon_i - \varepsilon_e}{\varepsilon_i + 2\varepsilon_e} + 3f^2\varepsilon_e \left(\frac{\varepsilon_i - \varepsilon_e}{\varepsilon_i + 2\varepsilon_e} \right)^2. \quad (1.6)$$

An improved version of the Maxwell Garnett formula has been given by Lord Rayleigh (Hoffman et al., 2007):

$$\varepsilon_{eff} = \varepsilon_e + \frac{3f\varepsilon_e}{\frac{\varepsilon_i + 2\varepsilon_e}{\varepsilon_i - \varepsilon_e} - f - 1.305 \frac{\varepsilon_i - \varepsilon_e}{\varepsilon_i + 4\varepsilon_e / 3} f^{10/3}}. \quad (1.7)$$

The difference between the predictions by the Maxwell Garnett and Rayleigh mixing rules lies in the similarity of the coefficients up to the fourth power of f in the case of the series expansions in terms of the volume fraction around $f = 0$. However, the deviation becomes large for higher volume fractions of the inclusion phase. If the permittivity contrast is large enough ($\varepsilon_i/\varepsilon_e > 4.735$), the Rayleigh mixing rule predicts a value for ε_{eff} approaching infinity for increasing f .

The effective permittivities of the layered nanostructured metamaterial composed of alternating graphene and dielectric layers are as follows (Khromova et al., 2014):

$$\varepsilon_{\parallel} = \frac{\varepsilon_g d_g + \varepsilon_d d_d}{d_g + d_d}; \quad (1.8)$$

$$\varepsilon_{\perp} = \frac{\varepsilon_g \varepsilon_d (d_g + d_d)}{\varepsilon_g d_d + \varepsilon_d d_g}, \quad (1.9)$$

where ε_g , ε_d are the permittivities of the graphene and dielectric layers, correspondingly; d_g , d_d are the thicknesses of the graphene and dielectric layers, correspondingly.

1.5. Transfer matrix method to obtain the dispersion relation of surface plasmon polaritons

The transfer matrix approach is also applied to derive the dispersion relationship for SPP waves. It is worthwhile noting that the former is unique for every system presented in the doctoral dissertation. The transfer matrix method is a chosen technique used to derive the parameters related to the architecture of the metamaterial

designed and investigated. It relates the incoming waves to the outgoing (scattered) waves to understand the properties of the metamaterial. Especially for an arbitrary number of material layers, the transfer matrix technique becomes indispensable in simulating the reflection, absorption, and transmission.

As an example, a plane wave of wavelength λ incident normally on a stack of dielectric materials of various thicknesses t_j and indices of refraction n_j is considered. Naturally, the impinging light will have reflected and transmitted components, which is illustrated in Fig. 1.1 (Balili, 2012).

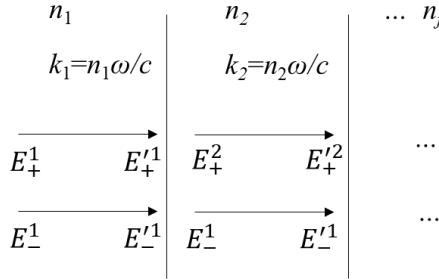


Fig. 1.1. Transmission and reflection on stacks of dielectric

The field components, after propagating through the system, can be solved by a transfer matrix equation $E' = T_M E$, where T_M is the effective matrix contribution of all the layers and interfaces. To solve for the effective matrix, the electric field is written as a sum of forward and backwards-moving waves. The fields across an interface are then given in a matrix form by

$$\begin{pmatrix} E'_+ \\ E'_- \end{pmatrix} = \begin{pmatrix} e^{ik_j t_j} & 0 \\ 0 & e^{-ik_j t_j} \end{pmatrix} \begin{pmatrix} E_+ \\ E_- \end{pmatrix}. \quad (1.10)$$

Hence, the transfer matrix across a layer is

$$T_{layer} = \begin{pmatrix} e^{ik_j t_j} & 0 \\ 0 & e^{-ik_j t_j} \end{pmatrix}. \quad (1.11)$$

Across an interface, the contributions to the electric field are observed due to the transmission from the left, reflection from the right and vice versa.

$$E_+^2 = \frac{2n_1}{n_2 + n_1} E_+^1 + \frac{n_2 - n_1}{n_1 + n_2} E_-^2; \quad (1.12)$$

$$E_-'^2 = \frac{n_1 - n_2}{n_2 + n_1} E_+'^1 + \frac{2n_2}{n_1 + n_2} E_-^2. \quad (1.13)$$

Eq. (1.12), (1.13) can be then simplified in matrix form

$$\begin{pmatrix} E_+^2 \\ E_-^2 \end{pmatrix} = \frac{1}{2} \begin{pmatrix} n+1 & -(n-1) \\ -(n-1) & n+1 \end{pmatrix} \begin{pmatrix} E_+^1 \\ E_-^1 \end{pmatrix}, \quad (1.14)$$

where $n = n_1/n_2$. Therefore, the transfer matrix across an interface can be written as follows:

$$T \frac{1}{2} \begin{pmatrix} n+1 & -(n-1) \\ -(n-1) & n+1 \end{pmatrix}_{int}. \quad (1.15)$$

The same procedure is followed for the transfer matrix across an interface for oblique incidence. The transfer matrix across the interface for arbitrary incident angle θ is

$$T \frac{1}{2} \begin{pmatrix} 1 & r \\ r & 1 \end{pmatrix}_{int}, \quad (1.16)$$

where t and r are the regular Fresnel transmission and reflection coefficients derived by Balili (2012). Finally, the effective matrix T_M is obtained as a resultant product of all the different matrices across the layers and interfaces.

$$T_M = \begin{pmatrix} t_{11} & t_{12} \\ t_{21} & t_{22} \end{pmatrix} = T_N \dots T_3 T_2 T_1. \quad (1.17)$$

For light incident on a complete stack of materials, incident and reflected light on one side and just transmitted light on the other can be considered. This is described by the following matrix equation:

$$\begin{pmatrix} E_{trans} \\ 0 \end{pmatrix} = \begin{pmatrix} t_{11} & t_{12} \\ t_{21} & t_{22} \end{pmatrix} \begin{pmatrix} E_{inc} \\ E_{ref} \end{pmatrix}. \quad (1.18)$$

Then, the transmitted and reflected electric fields are given by

$$E_{trans} = \frac{\det(T_M)}{t_{22}} E_{inc}, \quad E_{ref} = -\frac{t_{21}}{t_{22}} E_{inc}. \quad (1.19)$$

In general, chosen methods for designing metamaterials can drastically reduce the expenses of product development and prototyping by replacing costly

experimental trial-and-error with computational experiments. There is, however, always a level of discrepancy between the experimentally measured and the numerically calculated response. Improving the accuracy and performance of the numerical models to overcome such discrepancies is vital and, therefore, remains an area of extremely active research.

1.6. Conclusions of the First Chapter and formulation of the dissertation tasks

Although concepts of metamaterials and SPPs and their physical properties and various applications have already been extensively covered, the possible application of the physical essence of surface waves in aeroacoustics remains an unsolved problem. Thus, the present dissertation bridges this gap by classical electrodynamics and acoustics. So, this study is a multidisciplinary approach discussing the possibilities of combining both disciplines.

Based on the literature survey, the following objectives should be formulated:

- Investigate the possibilities of applying the Maxwell Garnett approach for homogenising different metamaterial structures, such as conventional nanowires, spiral wire, and nanostructured composite cases.
- To study the dispersion maps of the SPPs propagating at different interfaces such as:
 - metallic nanowire metamaterial interface and the hollow-core metamaterial interface,
 - nanostructured metamaterial and corrugated metal interface,
 - spiral wire metamaterial and air interface,
 - nanocomposite and hypercrystal interface.
- To analyse the dispersion properties and SPP loss at the investigated interfaces to achieve absorption enhancement, enabling the possible creation of the aircraft coating model for noise cancellation and antenna systems.
- To analyse system engineering tools, such as the angle of the spiral, number of grooves, etc., to conclude the tunability possibilities of structure properties.

Based on the literature survey, the following hypothesis could be provided:

- Graphene-based nanostructured and nanowire metamaterial structures with the hexagonal unit cell can help to achieve tunable SPP features.

- Absorption enhancement could be controlled by changing the filling ratio of the nanowire metamaterial.
- The use of nanowire metamaterial ($d = 10$ nm, $S = 60$ nm) interface allows for a significant increase of the frequency range of surface waves existence.

Surface plasmon polaritons: investigation methodology

This chapter presents the methodology for investigating the system tunability. It presents numerical methods used to investigate metamaterials and homogenisation techniques for concluding the effective permittivity of the considered metamaterial. The considerations focus on *the novel* transfer matrix method for deriving the dispersion relation of SPPs propagating at the boundary of the novel metamaterials. The scientific publications were published on the topic of the second chapter (Ioannidis et al., 2020; Ioannidis et al., 2021) and findings were presented at META 2021 and META 2021 conferences.

2.1 Analytical models of the investigated systems

This section presents analytical models for investigating the studied systems. The section provides an insight into the study of surface plasmon polaritons propagating at the interface separating nanocomposite and hypercrystal and at the boundary of spiral wire metamaterial.

2.1.1. Surface plasmon polaritons at the interface separating nanocomposite and hypercrystal

The structure under study is presented in Fig. 2.1. It is worthwhile mentioning that a photonic hypercrystal (Fig. 2.1) is a novel type of metamaterial combining the properties of photonic crystal and hyperbolic metamaterials.

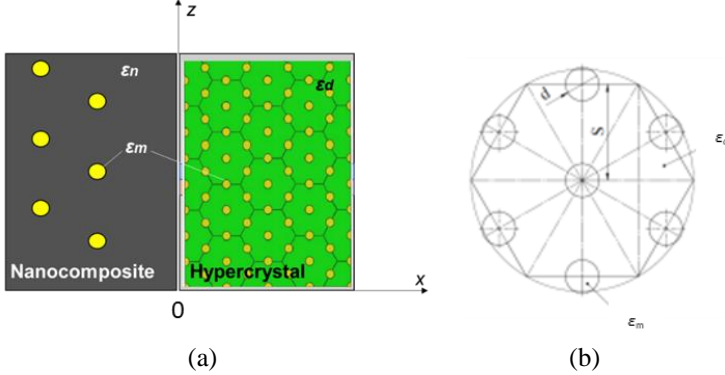


Fig. 2.1. Schematic system under consideration involving a semi-infinite hypercrystal ($x > 0$) and a nanocomposite with semiconductor inclusions ($x < 0$) (a) and metamaterial (hypercrystal) unit cell (b) (made by the author)

The dielectric function of metallic medium in the complex conductivity and frequency domain is written as (Ioannidis et al. 2021):

$$\varepsilon_r(\sigma, \omega) = 1 + \left(\chi + \frac{|\sigma| e^{i\phi}}{\omega \varepsilon_0} \right), \quad (2.1)$$

where χ is the system's susceptibility, $|\sigma|$ is the absolute value of complex conductivity and ϕ is its phase, ω – angular frequency, ε_0 – dielectric constant.

The dispersion relation of SPPs at a planar interface between the dielectric medium and metal forming a simple plasmonic structure in the complex conductivity and frequency domain is written as (Ioannidis et al., 2021):

$$k_{sp}(\sigma, \omega) = \frac{2\pi}{\lambda} \sqrt{\frac{\varepsilon_r(\sigma, \omega) \varepsilon_d}{\varepsilon_r(\sigma, \omega) + \varepsilon_d}}, \quad (2.2)$$

where ε_d is the permittivity of the host material, λ – wavelength. By taking a step towards complex nanostructures, it is assumed that the wavelength and the electromagnetic field penetration depth in the material are much larger than the size of inclusions suspended in a dielectric matrix. It is worthwhile mentioning that an

effective Maxwell Garnett model can be employed aiming to characterise the optical properties of the nanocomposite under consideration. The former approach is possible if the interference effects of the inclusions are neglected and their volume fraction is as small as 1/3. Thus, the homogenisation procedure may be applied, and the effective complex permittivity of the nanocomposite can be expressed as follows:

$$\varepsilon_{nc}(\sigma, \omega) = \varepsilon_n \left[1 + \frac{f}{(1-f)/3 + \varepsilon_n / (\varepsilon_m(\sigma, \omega) - \varepsilon_n)} \right], \quad (2.3)$$

where ε_n is the permittivity of the host material of the nanocomposite and f is the number of nanoparticles in the matrix.

Based on the effective medium approximation, the effective permittivities of the anisotropic nanowire metamaterial (hypercrystal) may be calculated as follows:

$$\varepsilon_{\perp}(\sigma, \omega) = \varepsilon_d \left[\frac{\varepsilon_m(\sigma, \omega)(1+\rho) + \varepsilon_d(1-\rho)}{\varepsilon_m(\sigma, \omega)(1-\rho) + \varepsilon_d(1+\rho)} \right]; \quad (2.4)$$

$$\varepsilon_{\parallel}(\sigma, \omega) = \varepsilon_m(\sigma, \omega)\rho + \varepsilon_d(1-\rho), \quad (2.5)$$

where ε_d is the permittivity of the host material, ε_m is the permittivity of the inclusions embedded into the host material, and ρ is the metal filling fraction ratio, which is calculated as:

$$\rho = \frac{\text{nano wire area}}{\text{unit cell area}}. \quad (2.6)$$

The metal filling fraction (ρ) is calculated based on the values of the pore diameter (d) and spacing (S) (Fig. 2.1b). By considering a perfect hexagonal structure, the equation is applied as follows:

$$\rho = \frac{\pi d^2}{2\sqrt{3}S^2}. \quad (2.7)$$

Based on this assumption, a dispersion relation may be derived for the surface modes propagating at the interface between two anisotropic media. It is particularly important to obtain a single surface mode with the propagation constant by calculating the tangential components of the electric and magnetic fields at the interface

$$\beta(\sigma, \omega) = k \left(\frac{(\varepsilon_{\parallel}(\sigma, \omega) - \varepsilon_{nc}(\sigma, \omega)) \varepsilon_{\perp}(\sigma, \omega) \varepsilon_{nc}(\sigma, \omega)}{\varepsilon_{\perp}(\sigma, \omega) \varepsilon_{\parallel}(\sigma, \omega) - \varepsilon_{nc}^2(\sigma, \omega)} \right)^{1/2}. \quad (2.8)$$

By substituting (2.3)–(2.5) in (2.8), the resulting dispersion relation is as follows:

$$\beta(\sigma, \omega) = k \left[- \frac{\varepsilon_n b(\sigma, \omega) a(\sigma, \omega) (\varepsilon_n a(\sigma, \omega) + \varepsilon_m(\sigma, \omega) \rho - \varepsilon_d(\rho - 1))}{\left(\varepsilon_n^2 a(\sigma, \omega)^2 + \frac{(\varepsilon_m(\sigma, \omega) \rho - \varepsilon_d(\rho - 1)) b(\sigma, \omega)}{\varepsilon_d(\rho + 1) - \varepsilon_m(\sigma, \omega)(\rho - 1)} \right) (\varepsilon_d(\rho + 1) - \varepsilon_m(\sigma, \omega)(\rho - 1))} \right]^{1/2}; \quad (2.9)$$

$$a(\sigma, \omega) = \frac{f}{\frac{f}{3} + \frac{\varepsilon_n}{\varepsilon_n - \varepsilon_m(\sigma, \omega)} - \frac{1}{3}} - 1; \quad (2.10)$$

$$b(\sigma, \omega) = (\rho - 1) \varepsilon_d^2 - \varepsilon_m(\sigma, \omega) \varepsilon_d(\rho + 1). \quad (2.11)$$

It is worthwhile noting that Eq. (2.9) stands for the analytical expression of the dispersion relations investigated in the frame of the present work. The presented model enables the investigation of properties of SPPs propagating at the boundary of nanocomposite and hypercrystal.

2.1.2. Surface plasmon polaritons propagating at the boundary of spiral wire metamaterial

The proposed geometry of the wire composites is shown in Fig. 2.2. Wires with permittivity ε_m^M are embedded in a host material with permittivity ε_d^M .

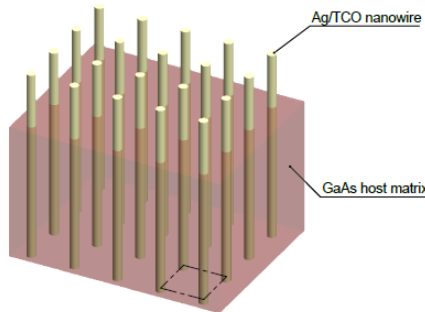


Fig. 2.2. Schematic view of a wire composite (made by the author)

Based on an effective medium approximation, the effective permittivities of the wire metamaterial, according to Ioannidis et al. (2022), can be evaluated as follows:

$$\varepsilon_{\perp}^M = \varepsilon_d^M \left[\frac{\varepsilon_m^M (1 + \rho^M) + \varepsilon_d^M (1 - \rho^M)}{\varepsilon_m^M (1 - \rho^M) + \varepsilon_d^M (1 + \rho^M)} \right]; \quad (2.12)$$

$$\varepsilon_{\parallel}^M = \varepsilon_m^M \rho^M + \varepsilon_d^M (1 - \rho^M). \quad (2.13)$$

Here, subindex M refers to the metamaterial medium, and ρ^M is the metal filling fraction ratio, which is defined as:

$$\rho^M = \frac{\text{nano wire area}}{\text{unit cell area}}. \quad (2.14)$$

To explore and demonstrate the properties of surface waves, a Drude model (Johnson 1972) is adopted to characterise the metal (i.e., silver), expressing the permittivity as $\varepsilon_m^M(\omega) = \varepsilon_{\infty} - \frac{\omega_p^2}{\omega^2 + i\delta\omega}$. The parameters are obtained by fitting this permittivity function to a particular frequency range of bulk material. It is found that for silver, the values of $\varepsilon_{\infty} = 5$, $\omega_p = 2.2971 \cdot 10^{15}$ Hz, $\delta = 2.3866 \cdot 10^{13}$ Hz give a reasonable fit. The metal filling fraction (ρ^M) based on the values of the pore diameter (d^M) and spacing (S^M) is calculated; assuming a perfect rectangular structure, the following equation is applied:

$$\rho^M = \frac{\pi(d^M)^2}{4(S^M)^2}. \quad (2.15)$$

With this assumption, it is possible to derive a dispersion relation for the surface modes localised at the interface between metamaterial and PbS. Evaluating the tangential components of the electric and magnetic fields at the interface, it is then, in turn, possible to obtain a single surface mode with the propagation constant

$$\beta = k \left(\frac{(\varepsilon_{PbS} - \varepsilon_{\parallel}^M) \varepsilon_{PbS} \varepsilon_{\perp}^M}{\varepsilon_{PbS}^2 - \varepsilon_{\perp}^M \varepsilon_{\parallel}^M} \right)^{1/2}, \quad (2.16)$$

where k is the wavenumber (absolute value of the wavevector in vacuum), and β is the component of the wavevector parallel to the interface. The computer algorithm to calculate Eq. 2.16 is presented in Fig. 2.3.

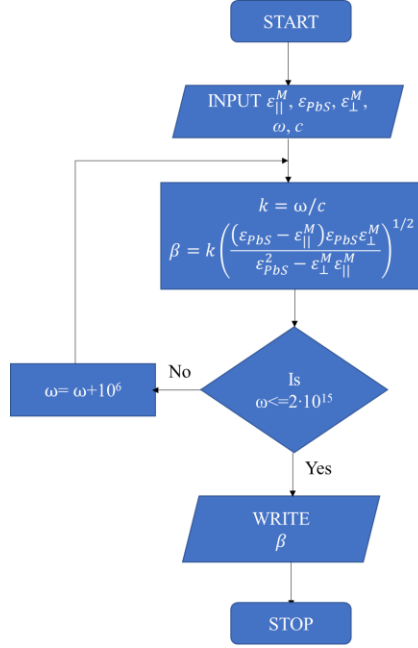


Fig. 2.3. Algorithm allowing the calculation of the dispersion of SPPs at the boundary of the spiral wire metamaterial (made by the author)

Finally, the effective permittivities of the spiral wire metamaterial, as follows (Ioannidis et al., 2022), are obtained:

$$\varepsilon_{\perp}^{SM} = -\varepsilon_d^M \frac{\varepsilon_d^M (\rho^M - 1) + \frac{ad\varepsilon_m^M \sin(2\Theta)(\rho + 1)}{2}}{\varepsilon_d^M (\rho^M + 1) + \frac{ad\varepsilon_m^M \sin(2\Theta)(\rho - 1)}{2}}; \quad (2.17)$$

$$\varepsilon_{\parallel}^{SM} = -\varepsilon_d^M (\rho^M - 1) - \frac{ad\varepsilon_m^M \rho^M (\cos(2\Theta) + 1)}{2}, \quad (2.18)$$

where a – is the groove width of the spiral wire, d – periodicity, and Θ – is the spiral angle. The presented model allows the investigation of the properties of SPPs propagating at the boundary of the spiral wire metamaterial.

2.2. Conclusions of the Second Chapter

This chapter presents the main techniques used to study the properties of SPPs at novel interfaces:

1. The proposed mathematical model allows for treatment permittivities of the anisotropic medium in each chosen direction, enabling its application for complex metamaterial-based anisotropic systems.
2. A model has been presented enabling the investigation of SPP properties propagating at the boundary of nanocomposite and hypercrystal and of the absorption effect.
3. A model has been presented enabling the investigation of SPP properties propagating at the boundary of the spiral wire metamaterial, opening wide avenues for possible applications, such as enhanced photoconductive antennas.

Surface plasmon polaritons: investigation results and conclusions

This chapter presents numerical investigation results on analysing the SPP propagation at the boundaries of novel studied metamaterials. Thus, the doctoral dissertation covers a wide range of investigations, starting from conventional nanowire cases and ending with exotic cases, such as spiral nanowire metamaterials. The scientific publications were published on the topic of the third chapter (Ioannidis et al., 2019; Ioannidis et al., 2020; Ioannidis et al., 2021; Ioannidis et al., 2022) and findings were presented at META 2021, eStream 2022, and “Science – Future of Lithuania” 2021 conferences.

3.1. Theoretical studies of the tunable surface plasmon polaritons

Investigations are presented on tunable SPPs propagating at different interfaces, i.e., nanowire metamaterial interface, corrugated metamaterial interface, spiral nanowire metamaterial interface, acoustic metamaterial interface, nanocomposite and hypercrystal interface.

3.1.1. Propagation of surface plasmon polariton at the interface of nanowire metamaterial

In the first approach to investigate plasmonic nanowires (Gric et al., 2018) from the perspectives of both field enhancement and tunability, two different cases have been suggested for consideration: the first uses a metallic nanowire metamaterial interface, while the other involves a hollow-core metamaterial interface. SPPs act as surface waves propagating along the boundary between a metal and a dielectric while exponentially decaying into both the dielectric and metal. Denoting the dielectric constant of the metal and the dielectric material as ϵ_m and ϵ_d , correspondingly, the dispersion equation of SPPs is expressed as:

$$\beta = \frac{\omega}{c} \sqrt{\frac{\epsilon_m \epsilon_d}{\epsilon_m + \epsilon_d}}, \quad (3.1)$$

where ω is the angular frequency of the SPP modes, c is the speed of light, and β is the wave constant of SPPs along the propagation direction. It is worthwhile noting that the localised SPPs are dramatically influenced by the material properties along with the size and shape of the metallic nanostructures (Fig. 3.1a). By doing so, it is possible to achieve an efficient coupling. Fig. 3.1 displays the geometry of the nanowire structure. It is worthwhile mentioning that in the direction perpendicular to the ZX plane, the material is infinite. Metal wires with permittivity ϵ_m are implanted in a dielectric host material with permittivity $\epsilon_d = 2.4$. The mentioned materials have been chosen because of fabrication matters (Hornyak et al., 1997). In doing so, the optical properties of nanoscopic metallic particles prepared by electrochemically depositing metal within the pores of nanoporous alumina membranes are explored.

The derived dispersion equation for the SPPs is:

$$\beta = k \left(\frac{(\epsilon_{\parallel}^R - \epsilon_{\parallel}^L) \epsilon_{\perp}^R \epsilon_{\perp}^L}{\epsilon_{\perp}^R \epsilon_{\parallel}^R - \epsilon_{\perp}^L \epsilon_{\parallel}^L} \right)^{1/2}, \quad (3.2)$$

with k being the wavenumber and β being the component of the wavevector parallel to the boundary, is obtained after dealing with the tangential components of the electric and magnetic fields.

It is worthwhile mentioning that the proposed model was tested by comparing the results obtained using Eq. 3.2 with the outputs (Pluchery et al., 2011) for the classical case, i.e., Au/air interface. The maximum value of propagation constant in all of the approaches is $15 \cdot 10^7$ 1/m, and the calculations have been performed using the mathematical equations by Pluchery et al. (2011). To apply the model under consideration, it is assumed that the nanowire diameter is $d \rightarrow 0$.

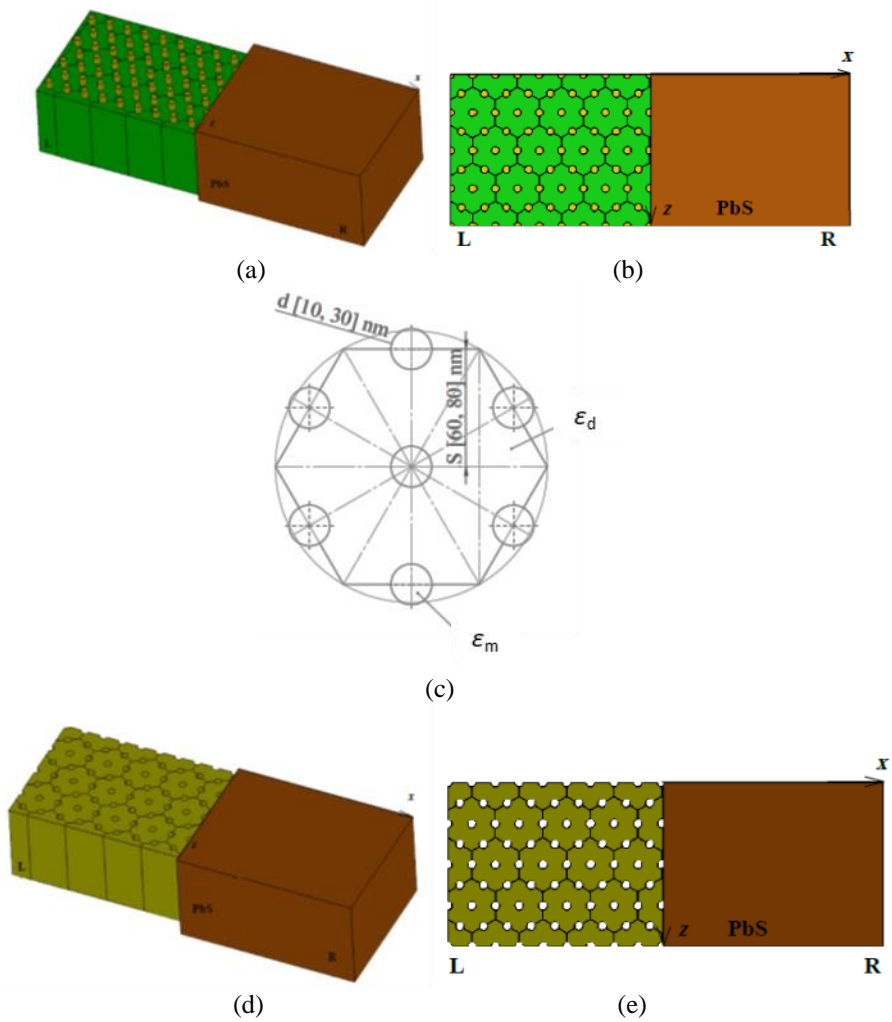


Fig. 3.1. Schematic views of the nanowire (a) and hollow-core (d) structures; view of a boundary of a nanowire (b) and hollow-core (e) composite; metamaterial unit cell (c). Here, PbS is lead sulphide (Gric & Hess, 2017). In the direction perpendicular to the ZX plane, the material is infinite. SPPs propagate along the z-axis (made by the author)

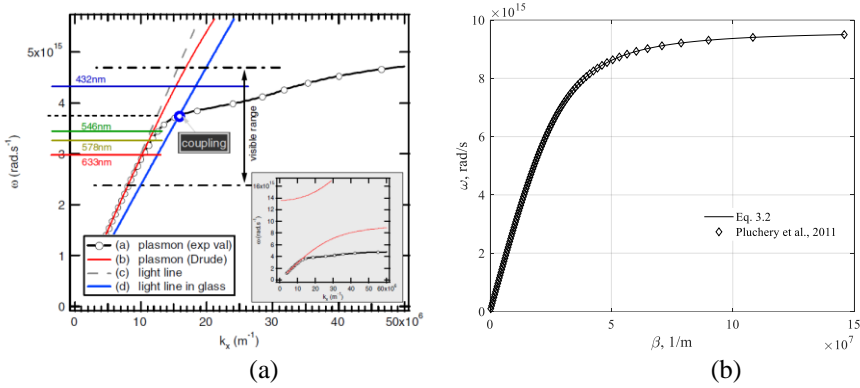


Fig. 3.2. Dispersion relation of the surface plasmon wave at a gold/air interface: (a) the curve obtained by Pluchery et al. (2011), (b) the plot of the dispersion relation (3.2) given in the text (made by the author)

It should be noted from Fig. 3.2 that the agreement of the results is very good, proving the theoretical model of SPP propagation. In the first case of nanowire metamaterial and dielectric, surface modes at the boundary of these two are studied. Fig. 3.3 (a) and (b) display the dispersion diagrams of the surface modes along with the absorption graphs. The spacing is fixed, i.e., $S_L = 60$ nm, and the pore diameter is varying, i.e., $d_L = 10$ nm, 20 nm, 30 nm. To the best of our knowledge, altering either metal or dielectric drastically affects the dispersion diagrams (Gric, 2016). The study focused on the impact of the metamaterial L spacing on the SPPs and found that the spacing varied from 60 to 80 nm. The influence of the spacing parameter on the surface modes' dispersion characteristics is displayed in Fig. 3.3. The increase of spacing S_L causes a shift of the SPPs diagrams to the lower wavelengths. It is worthwhile noting that it is impossible to employ the described tunability mechanisms in the case of the conventional metal–dielectric interface.

In the second case, the hollow-core metamaterial is introduced by replacing the metal nanowires with air holes. On the other hand, metal, i.e., Ag, is used as the host material. Dispersion and absorption in the case of hollow-core metamaterial interface are presented in Fig. 3.3 (c) and (d). It is worthwhile noting that anomalous features of the dispersion diagrams can be observed near the frequency of 10^{15} Hz. The mentioned frequency is particular because it serves as the intersection point of the effective dielectric permittivity perpendicular components obtained by varying the diameter of the nanowires and the distance between the nanowires (Jackson, 1999). It is worthwhile noting that the “jump” point arises $\varepsilon_{\parallel} > 0, \varepsilon_{\perp} < 0$ (Gric & Hess, 2017), providing the possibility to increase the fre-

quency gap region with purely imaginary β prohibiting propagation. The mentioned property does not take place in the case of the conventional metal–dielectric interface.

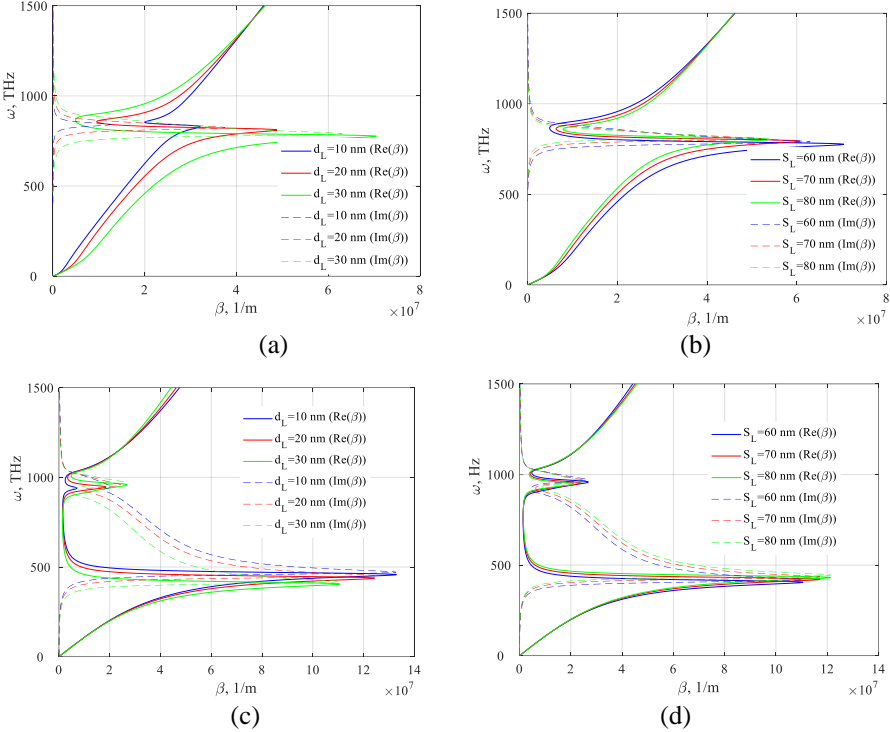


Fig. 3.3. (a) and (b) – the dispersion and absorption for the nanowire metamaterial interface. $S_L = 60$ nm (a), $d_L = 30$ nm (b); (c) and (d) – the dispersion and absorption in case of hollow-core metamaterial interface. $S_L = 60$ nm (c), $d_L = 30$ nm (d) (made by the author)

It is found that both the upper and the lower limits shift to the higher frequencies as d is decreased. However, the movement of the lower limit is quicker than that of the upper one. In doing so, the broader frequency range for surface wave existence arises. This is consistent with the effect of d on the frequency range of negative $\epsilon_{||}$. One can also broaden the frequency range of surface Bloch waves by tuning the distance S (Gric & Hess, 2017). A wide spectrum of possibilities to engineer the SPP is provided due to the impact of the diameter and distance on the frequency range of surface wave existence.

3.1.2. Propagation of surface plasmon polaritons at the interface of the corrugated metamaterial

The second approach studied the SPP wave propagation along the nanostructured graphene-based metamaterial/corrugated metal interface. The considered structure (Fig. 3.4) consists of two building blocks: grating made of Si ($\epsilon = \epsilon_g = 12.25$) and a slab of graphene-dielectric metamaterial. The function of the first building block is the creation of a higher-order transmission channel(s). In such a case, the coupling of the incident waves differs for the two opposite interfaces. Its main function is to attain tunability by changing the state from dielectric to ENZ and then to plasmonic by engineering μ (Khromova et al., 2014).

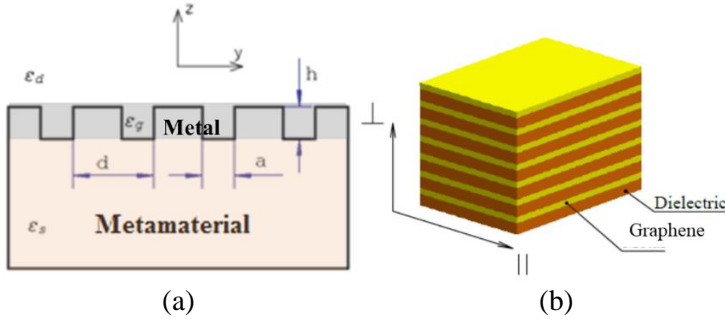


Fig. 3.4. Geometry of structured metamaterial surface:
 (a) interface separating metamaterial and corrugated metal;
 (b) enlarged view of metamaterial structure (made by the author)

The effective-medium approach is applied, aiming to describe the optical response of such a system. The former is justified if the wavelength of the considered radiation is much larger than the thickness of any layer. It is based on averaging the structure parameters. Hence, the effective homogeneous media for the semi-infinite periodic structures is considered next.

Matching the tangential components of the electrical and magnetic fields at the interface implies the dispersion relation for the surface modes localised at the boundary separating two anisotropic media (Iorsh et al., 2011). It is assumed that the permittivity $\epsilon_{mg}(\omega)$ is frequency-dependent as the corresponding layer is represented by graphene. Within the random-phase approximation and without an external magnetic field, graphene may be regarded as isotropic, and the surface conductivity can be written as follows (Falkovsky, 2008; Hanson, 2008), $\sigma = ie^2\mu N / \pi h^2 (\omega + i/\tau)$, where ω , h , e , μ , τ , N is the frequency, Planck constant, a charge of an electron, chemical potential (Fermi energy), and phenomenological scattering rate, number of graphene layers, respectively. The Fermi energy μ can

be straightforwardly obtained from the carrier density n_{2D} in a graphene sheet, $\mu = \hbar v_F \sqrt{\pi n_{2D}}$, v_F is the Fermi velocity of electrons. It should be mentioned that the carrier density n_{2D} can be electrically controlled by an applied gate voltage, thus leading to a voltage-controlled Fermi energy μ . Here, it is assumed that the electronic band structure of a graphene sheet is unaffected by the neighbouring layers. Thus, the effective permittivity ϵ_{mg} of graphene can be calculated as follows (Vakil & Engheta, 2011): $\epsilon_{mg} = 1 + i\sigma / \epsilon_0 \omega d_{mg}$, where ϵ_0 is the permittivity in the vacuum.

The wave vector k (Gric & Hess, 2017) is plotted as a function of the frequency, aiming to illustrate the SPP properties. The research deals with the Ag case (Johnson & Christy, 1972). It is assumed that the structure is surrounded by silicon, i.e., Si ($\epsilon = \epsilon_g = 12.25$). Fig. 3.5(a) depicts the dispersion curves of SPPs at the boundary metamaterial/structured surface with $d = 10$ nm. It is particularly important to investigate the impact of the period on the SPP dispersion curves. Three different groove widths are considered. Based on Fig. 3.5, the asymptotic frequency, i.e., the maximum possible frequency of the propagating modes, decreases with an increase in the groove width.

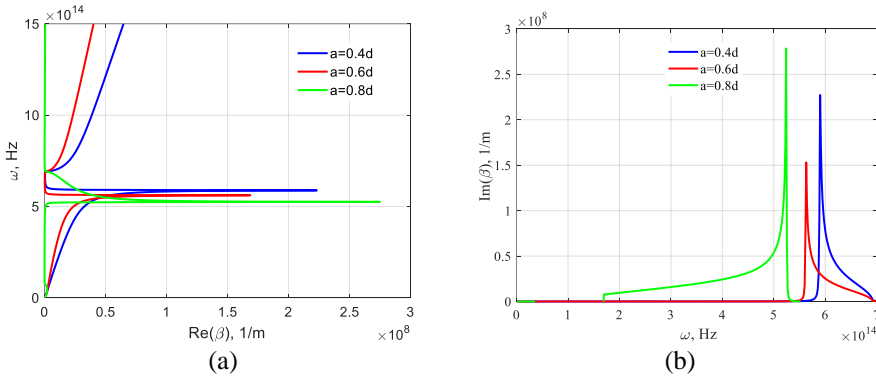


Fig. 3.5. (a) Dispersion curves for SPPs. (b) Attenuation coefficients of SPPs, lattice constant $d = 10$ nm (made by the author)

Fig. 3.5(b) presents the losses of these SPPs as a function of frequency. It is worthwhile noting that the loss of SPPs is dramatically influenced by the increase in frequency. In this relation, it is particularly important to mention that the case $a = 0.8 d$ allows for a significant increase in the absorption peak. The obtained property could be highly relevant while dealing with noise absorption coatings used in the aircraft industry, aiming to reduce the noise level in the aircraft seeking

to increase the passenger's comfort level. The former is possible due to the mimicking nature of SPPs. The observed properties can be translated into the acoustics frequency range. Besides, it is noted that the forbidden region between the modes starts squeezing, as presented in Fig. 3.5(a), and they approach each other with a decrease in the groove width.

It is particularly interesting to analyse the effect of the lattice constant (d) on the dispersion of SPPs. The dispersion curves for SPPs at the boundary metamaterial/corrugated surface with different lattice constants $d = 5, 7, 10$ nm are displayed in Fig. 3.6(a). The groove parameter is $a = 2$ nm for all cases. Fig. 3.6(b) shows the SPP losses for three cases. It can be concluded from Fig. 3.6(b) that a larger loss of SPPs for a given frequency takes place in the case of a smaller lattice constant. Based on Fig. 3.6(b), losses of the SPPs are drastically influenced by the lattice constant. For a given frequency, an increase in the lattice constant may cause a significant reduction in the loss of spoof SPPs. A low-loss THz waveguiding system is essential because of the need for a compact, reliable, and flexible THz system for various applications. The common areas are terahertz medical imaging and sensing, earth sensing, astronomy, pharmaceuticals, screening or non-destructive evolution, quality assurance, material science, telecommunications and many more.

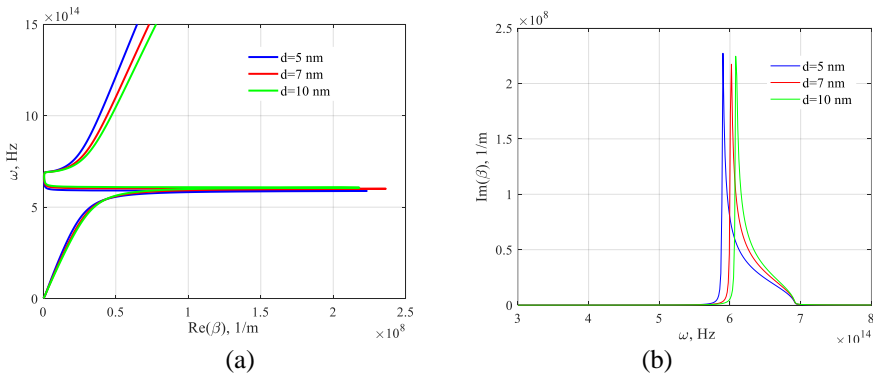


Fig. 3.6. Dispersion curves (a) and attenuation coefficients (b) of SPPs for different lattice constants $d = 5, 7$, and 10 nm, respectively. Parameters of grooves: $a = 2$ nm (made by the author)

The nanostructured metamaterial interface allows for the propagation of the SPP waves. Several schemes have been proposed that include prism configurations, grating, and waveguide geometries to excite the SPPs (Vengurlekar, 2010). The dispersion relationship is computed by implementing the effective medium theory and transfer matrix approach, and the following conclusions can be drawn:

- Surface wave modes propagate along the metamaterial/metal grating interface.
- The bandgap may be tuned corresponding to the non-propagation regime by engineering the groove width or chemical potential of graphene.
- The propagation length is studied as a function of the terahertz frequency range. It has been concluded that under appropriate parameters, the propagation length can be modulated (Ioannidis et al., 2020). The present method of surface wave modulation is quite simple in comparison with the corrugated structures (Anwar et al., 2017).
- The proposed geometry may be applied for noise cancellation systems and wave propagation in the terahertz regime.

3.1.3. Propagation of surface plasmon polaritons at the interface of spiral wire metamaterial

The third case theoretically demonstrates the ability of spiral wire metamaterials to support unique absorption resonances related to radiative bulk plasmon polaritons. These radiative bright modes exhibit properties in stark contrast to conventional dark modes (SPPs). The unique absorption resonances manifested in used metamaterials were originally studied by Ferrell for plasmon-polaritonic thin-films in the ultraviolet (Ferrell, 1958) and by Berreman for phonon-polaritonic thin-films in the mid-infrared spectral region (Berreman, 1963). In this work, an effective medium theoretical model for the analytical description of spiral-shaped spoof devices is developed and used to investigate their spectral properties quantitatively. Seet et al. (2005) demonstrated the fabrication of a 3D spiral architecture. This model allows for a comprehensive understanding of FB modes supported by the structure.

The research focuses on a 2D wire whose surface is decorated by N spiral-shaped grooves, filled with a dielectric material of refractive index n_g . The resulting inner and outer radii, which correspond to the bottom and opening of the grooves, are r and R , respectively, as shown in Fig. 3.7, where d and a indicate the periodicity and groove width along the wire perimeter. The spiral is built so the intersection angle between the tangent to each spiral arm and the radial direction is the same along the spiral length.

The proposed geometry of the wire composites is shown in Fig. 2.2. Wires with permittivity ϵ_m^M are embedded in a host material with permittivity ϵ_d^M .

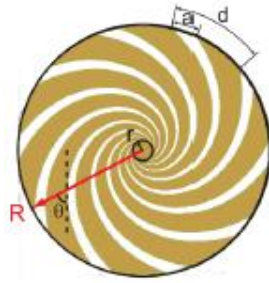


Fig. 3.7. Localised spoof surface plasmons in a 2D subwavelength metal wire corrugated with spiral grooves. Cross-section of the corrugated PEC wire with the inner and outer radii r and R , periodicity d , groove width a , and the spiral angle θ (made by the author)

Fig. 3.8 proved the plotted effective medium constants for the spiral wire and regular wire structures using the homogenisation formulae.

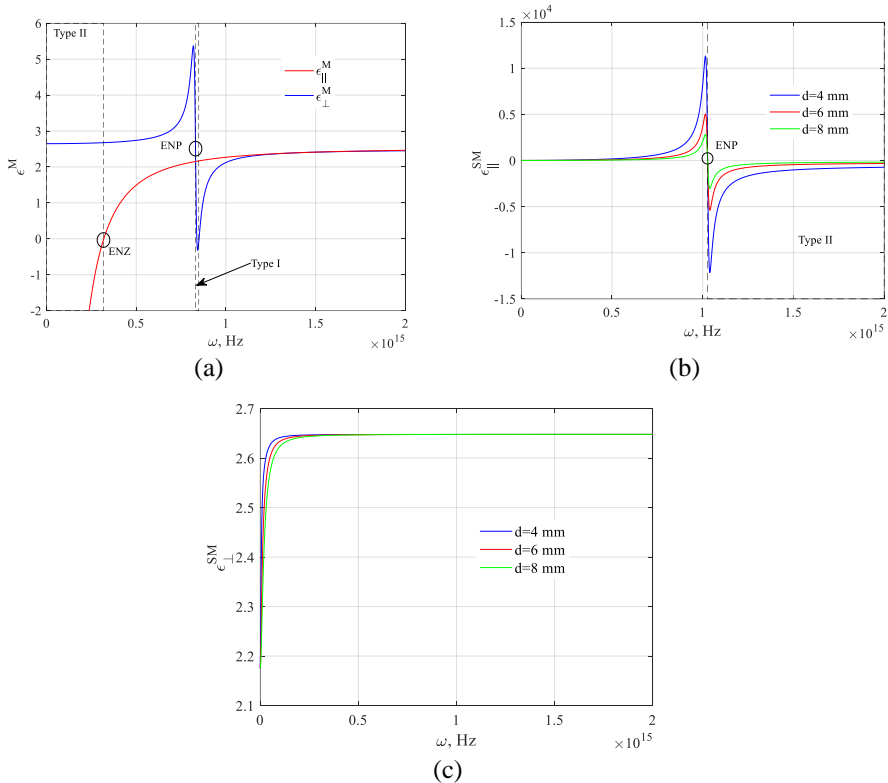


Fig. 3.8. (a) – wire system: real part of the dielectric permittivity for a wire structure (b), (c) – spiral wire system: real part of the dielectric permittivity for a spiral wire structure (made by the author)

The wire metamaterial structure shows an epsilon-near-zero (ENZ) effect as well as epsilon-near-pole (ENP) resonance. An interesting characteristic of multilayer and wire structures is the existence of poles and zeros in the effective medium dielectric constants. This results in an ideal method to first characterise the resonant responses and subsequently infer the hyperbolic characteristics. At these specific wavelengths, a component of the dielectric tensor of the metamaterial either passes through zeros (epsilon-near-zero, ENZ) or has a resonant pole (epsilon-near-pole, ENP). Only the real parts are shown for clarity, and the imaginary parts can be calculated similarly. The wire metamaterial structure consisting of metallic inclusions shows both Type I and Type II hyperbolic behaviour. It is worthwhile mentioning that Type I hyperbolic metamaterials have one component of the dielectric tensor negative ($\epsilon_{zz} \langle 0; \epsilon_{xx}; \epsilon_{yy} \rangle 0$) while Type II hyperbolic metamaterials have two components negative ($\epsilon_{xx}; \epsilon_{yy} \langle 0; \epsilon_{zz} \rangle 0$).

The most important aspect to note about the ENZ and ENP resonances are the directions in which they occur for spiral wire and regular wire samples. The former issue dramatically changes the reflection and transmission spectrum of the two types of hyperbolic media. For the wire design, ENZ occurs along the wire length. This is intuitively expected since the Drude plasma frequency, which determines the ENZ, always occurs in the direction of free electron motion. On the contrary, the resonant ENP behaviour of the two geometries occurs in the direction for which there is no continuous free electron motion. The ENP resonance occurs perpendicular to the wires in the wire geometry (Molesky et al., 2013).

Fig. 3.9 depicts a regime map in a β - ω space, illustrating the regions where FB modes may exist. Fortunately, the frequency range of FB modes' existence can be controlled by the wire periodicity d , spiral angle θ , diameter of the wires d^M and distance between the wires S^M .

The surface polaritons dispersion relations as a function of d are shown in Fig. 3.9(a), where $\theta = 30^\circ$, $d^M = 20$ mm, $S^M = 80$ mm. FB modes exist at the left region of the light line. The polariton dispersions strongly depend on the d parameter, as shown in Fig. 3.9(a), in which dispersion relations are calculated and plotted based on the effective anisotropic permittivity tensor. It should be noted that the frequency range of FB mode's existence increases as d increases, i.e., larger periodicity increases the conductivity of the corrugated wire, thereby increasing the effective plasmonic frequency.

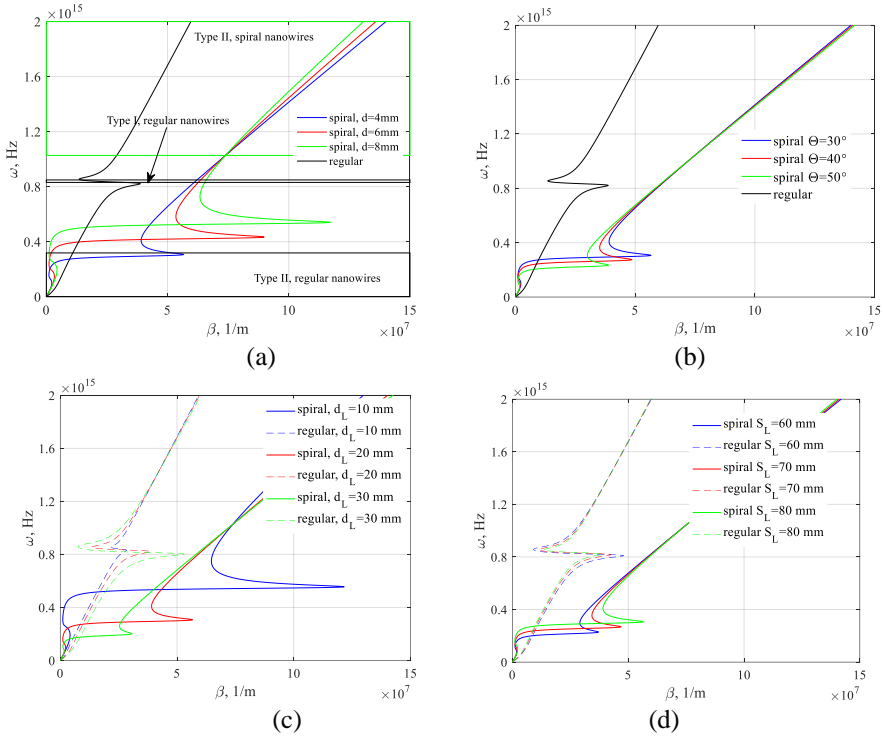


Fig. 3.9. The dependences of dispersion relations of surface polaritons on (a) corrugated wire periodicity d , (b) spiral angle θ , (c) diameter of the wires d^M , and (d) distance between the wires S^M (made by the author)

Except for d , the polariton properties are also dependent on the θ angle. Here, it is assumed that the parameter $d = 4$ mm and θ angle changes. As observed, the existence region increases to a high-frequency band with the decrease of θ angle value. On the whole, the polariton dispersions exhibit an obvious tunability. Apart from passive SPPs, active SPP devices with tunable properties enable applications in real-time controllable subwavelength circuits, such as switches, attenuators, phase and frequency shifters, etc.

3.1.4. Propagation of surface plasmon polaritons at the interface of the acoustic metamaterial

The next approach presents a homogenised acoustic metamaterial for SPP guiding. Acoustic metamaterials are periodic structures with effective properties that can be tuned to engineer wave propagation. Homogenisation of the infinite periodic system is needed to calculate the permittivity of metamaterial. Theoretical

results studying an acoustic metamaterial that possesses negative effective parameters in the optical frequency range are presented. The investigation focused on an acoustic metamaterial with an array of nanowires embedded in a host material. Aiming to achieve propagation of acoustic waves in metamaterials, both density and stiffness should be negative. The goal of this study is to demonstrate the possibilities of constructing a metamaterial exhibiting negative effective parameters and show that acoustic waves can be characterised by unusual behaviour.

A composite consisting of fluid hosts with rods embedded in it is considered. Rods are characterised by a round cylindrical shape and consist of elastic materials. Acoustic waves propagate in a host material with a wave vector perpendicular to the generatrix of the rods. A metamaterial under consideration is quasi-isotropic. In doing so, the wavelength is much longer than the distance between the centres of cylinders and their radii (Caloz & Itoh, 2005). All cylinders are considered to be identical and are placed randomly at approximately equal distances between the cylinders. The aim is to calculate the dynamical effective constitutive parameters of a metamaterial on a given frequency and dispersion of the propagating bulk acoustic wave.

A metamaterial structure under investigation is comprised of arrays of parallel metallic nanowires, such as silver, gold, etc., implanted in a dielectric. Fi. 3.10 is a schematic illustration of the nanowire metamaterial. Nanowires are embedded in a host material. All cylinders are considered to be identical and are placed randomly at approximately equal distances between the cylinders. The aim is to calculate the dynamical effective constitutive parameters of a metamaterial on a given frequency and dispersion of the propagating bulk acoustic wave.

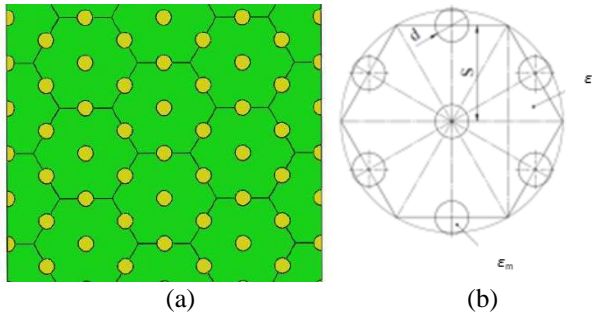


Fig. 3.10. Schematic view of the nanowire composite (a); metamaterial unit cell (b) (made by the author)

The structure can be effectively treated as a homogeneous uniaxial anisotropic material with a density parallel to wires (ρ_{\parallel}) and a density vertical to wires (ρ_{\perp}) (Liu et al., 2008; Podolskiy et al., 2005) if the period of the nanowire array

is much smaller than the wavelength of the propagating wave. Along the boundary between two ideal fluids, any surface wave cannot propagate because the boundary conditions cannot be satisfied. Boundary states can be excited (Ambati et al., 2007) if one of the materials has one negative parameter. This is a direct analogy to surface plasmon states in plasma with $\epsilon < 0$ (Caloz & Itoh, 2005).

Herein, a wave propagating at the interface between a half-space occupied by pure host fluid and a half-space occupied by a fluid with embedded rods in it is considered. The dispersion equation for a surface wave has the following form:

$$\beta = k \left(\frac{(1 - \epsilon_{\parallel}) \epsilon_{\perp}}{1 - \epsilon_{\perp} \epsilon_{\parallel}} \right)^{1/2}, \quad (3.3)$$

where k – is the wavenumber.

Fig. 3.11(a) shows the frequency dependence of the dynamical effective density, allowing for the homogenisation of the system under study. Due to the complex shear and longitudinal field distribution inside inclusion, there are two families of resonances related to shear waves and longitudinal waves. Thus, the dynamical effective density has several frequency ranges where the real part is negative. Fig. 3.11(b) plots the dependence of the permittivity.

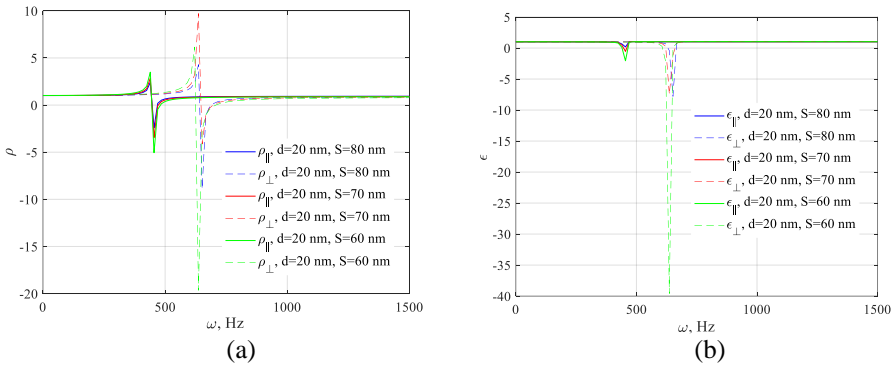


Fig. 3.11. Frequency dependence of effective density (a) and permittivity (b) for the composite under study (made by the author)

Fig. 3.12 shows surface waves propagating on the surface of a semi-infinite elastic metamaterial in a vacuum. As expected, a common surface wave gap exists; in addition, when approaching asymptotic frequency from the low-frequency direction, all the dispersion curves become very flat and asymptotically reach infinity, exhibiting behaviour very similar to that of EM SPPs.

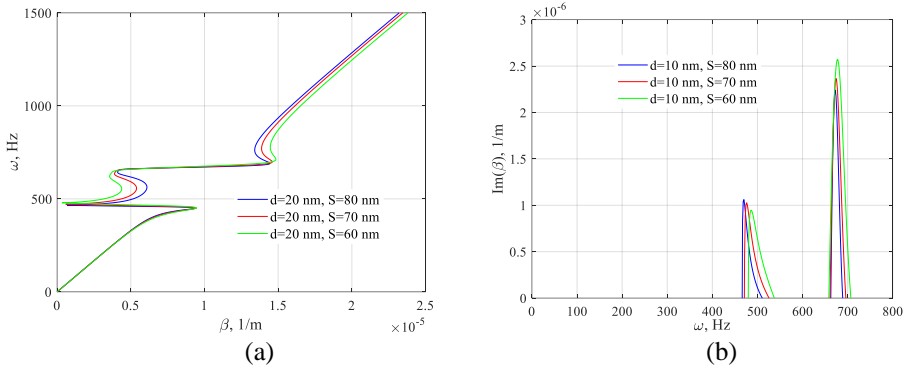


Fig. 3.12. Dispersion curves of SPPs for a system under consideration, (a) $\text{Re}(\beta)$; (b) $\text{Im}(\beta)$ (made by the author)

3.1.5. Propagation of surface plasmon polaritons at the interface of nanocomposite and hypercrystal

The next approach investigates the dispersion properties of surface waves propagating at the interface between a nanocomposite made of semiconductor inclusions systematically distributed in a transparent matrix and low-dimensional acoustic metamaterial constructed by an array of nanowires implanted in a host material. The research observes the SPP propagation. Composite media with metal nanoparticles are of particular interest, aiming to create nanostructured metal-insulator systems and new methods of controlling light. The emergence of transparent conductive oxides (TCOs) has attracted tremendous interest within the scientific community. These stand as the alternative materials for plasmonics (Naik et al., 2013) in the near-infrared region. Contrary to noble metals, such TCOs as indium tin oxide (ITO) (Table 3.1) demonstrate a vast tunability of their optical and electronic properties (Feigenbaum et al., 2010). The former is possible via doping and electric bias.

Hyperbolic materials are a subclass of uniaxial materials. These are characterised by two different values for the permittivity, i.e., parallel and perpendicular to the optical axis (Peragut et al., 2017). The extraordinary wave is characterised by an electric field with components along the optical axis and perpendicular to it. Hyperbolic materials possess this remarkable property. They support propagating waves with arbitrary large wave vectors at a finite frequency (Zhukovsky et al., 2014; Takayama & Lavrinenko, 2019).

Noise has strong penetrating power and dissipates slowly during propagation. In doing so, it is a challenging task to engineer the sound waves. The study of surface waves and plasmonics stands for another inherent part of nanophotonics.

The research deals with the plane interface between a nanocomposite (NC) semi-infinite layer, which fills the half-space $x < 0$, and an adjacent hypercrystal, filling the half-space $x > 0$ (Fig. 3.13). It is worthwhile mentioning that the surface waves under consideration propagate along the z -axis. Nanocomposite is presented as a non-conductive transparent matrix with a permittivity ε_n with regularly distributed semiconductor nanoparticles with permittivity ε_m in its volume.

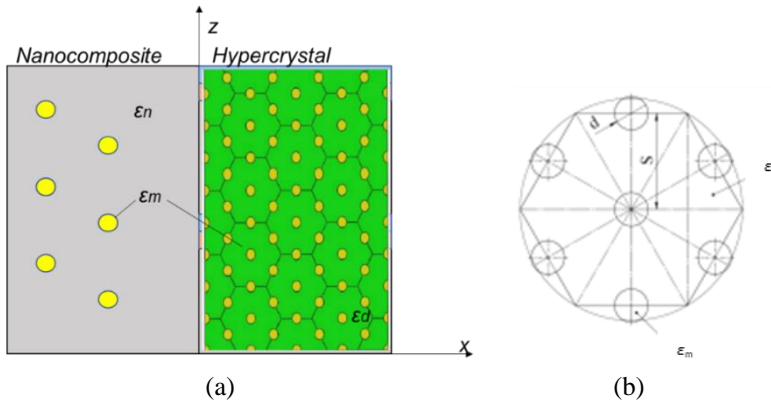


Fig. 3.13. Schematic geometry under study, consisting of a semi-infinite hypercrystal ($x > 0$) and a nanocomposite with semiconductor inclusions ($x < 0$) (a), metamaterial (hypercrystal) unit cell (b) (made by the author)

It is assumed that the wavelength and the electromagnetic field penetration depth in the material are much larger than the size of inclusions suspended in a dielectric matrix.

Table 3.1. Drude–Lorentz parameters of plasmonic materials based on experimental data (Molesky et al., 2013)

	AZO	GZO	ITO	TiN (deposited at 800 °C)	TiN (deposited at 500 °C)	ZrN
ε_b	3.5402	3.2257	3.528	4.855	2.485	3.4656
ω_p [eV]	1.7473	1.9895	1.78	7.9308	5.953	8.018
γ_p [eV]	0.04486	0.1229	0.155	0.1795	0.5142	0.5192
f_1	0.5095	0.3859	0.3884	3.2907	2.0376	2.4509
ω_1 [eV]	4.2942	4.050	4.210	4.2196	3.9545	5.48
γ_1 [eV]	0.1017	0.0924	0.0919	2.0341	2.4852	1.7369

The permittivity components of a hypercrystal and nanocomposite versus frequency are studied numerically, aiming to identify the frequency ranges of Dyakonov surface waves (DSWs) and SPP wave existence (Fig. 3.14).

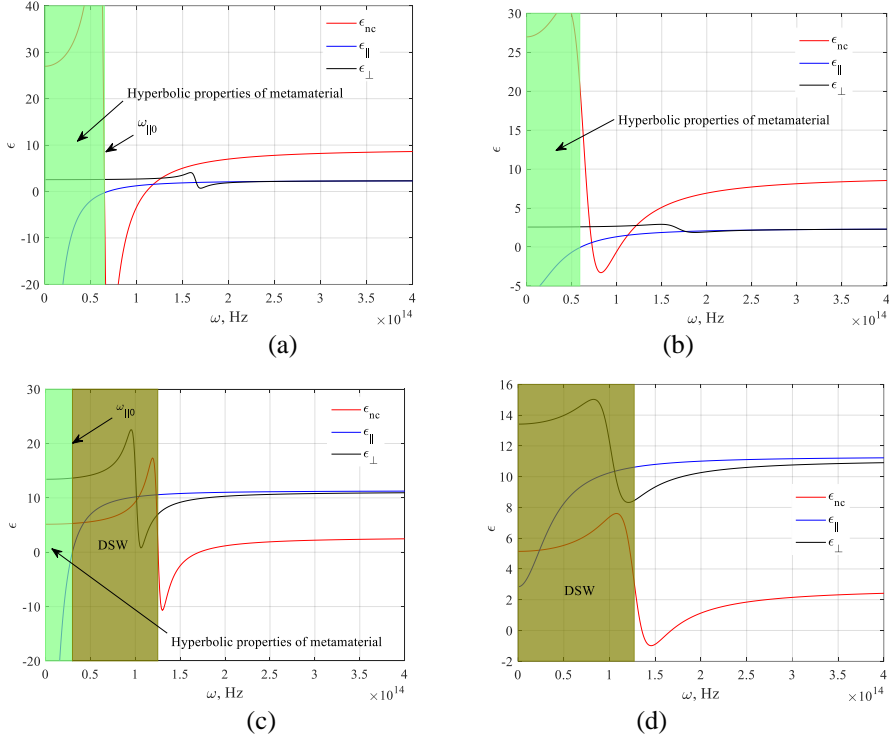


Fig. 3.14. Relative permittivity components of the nanocomposite and hypercrystal versus frequency. Here, $f = 0.3$. (a), (b): $\epsilon_n = 11.8$, $\epsilon_d = 2.25$; (c), (d) $\epsilon_n = 2.25$, $\epsilon_d = 11.8$. Here, AZO (a), (c) and ITO (b), (d) inclusions are employed in nanocomposite and hypercrystal (made by the author)

In the frequency ranges below the frequency $\omega_{\parallel 0}$, the semiconductor-dielectric metamaterial possesses hyperbolic properties. It is worthwhile noting that in this frequency range, the presence of conventional SPP waves with propagation parallel to the optical axis is feasible under specific conditions. The dependence of the transmission characteristics on frequency for different filling ratios was obtained. Moreover, the possibilities to increase frequency ranges of DSW existence have been demonstrated.

It is particularly interesting to analyse two cases, i.e., when $\varepsilon_n > \varepsilon_d$ and $\varepsilon_d > \varepsilon_n$. The case when $\varepsilon_n = 2.25$, $\varepsilon_d = 11.8$ is depicted in Fig. 3.15(a). It is observed that dispersion curves in these cases exhibit an exotic behaviour contrary to the conventional surface plasmons propagating at the metal/dielectric interface (Maier, 2007). The case, when $\varepsilon_n = 11.8$, $\varepsilon_d = 2.25$ is depicted in Fig. 3.15(b). By having a deeper insight into the properties of DSW obtained by changing the filling factor of the nanocrystal as displayed in Fig. 3.15(a), it is possible to observe that in contrast to the case depicted in Fig. 3.15(a), DSW does not propagate if $\varepsilon_n = 11.8$, $\varepsilon_d = 2.25$ (Fig. 3.15(c)).

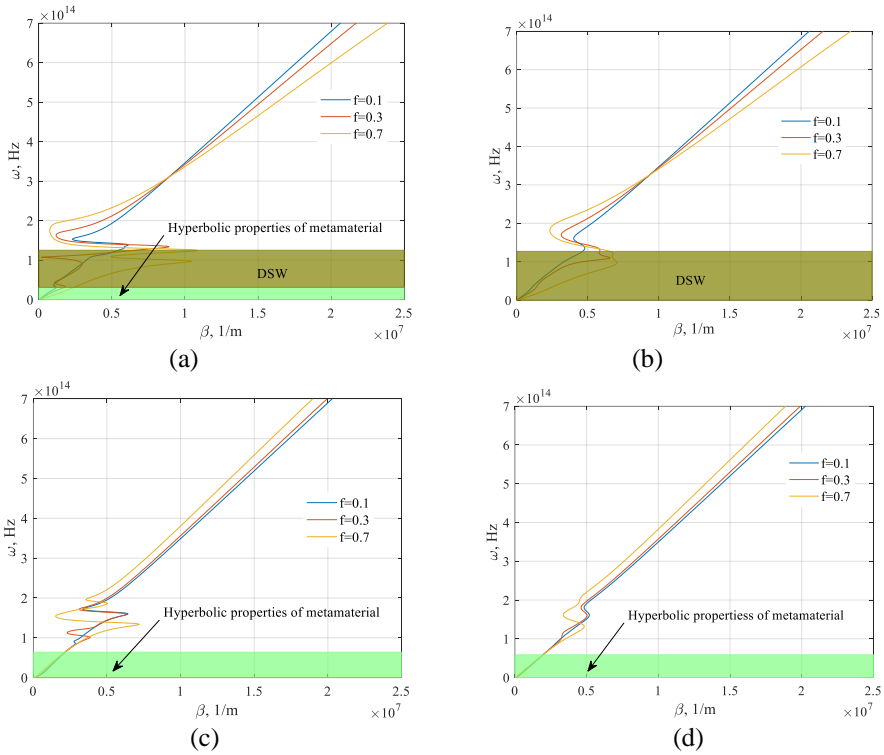


Fig. 3.15. Solution of the wave equation for different filling ratio f :

(a), (b) – $\varepsilon_n = 2.25$, $\varepsilon_d = 11.8$; (c), (d) – $\varepsilon_n = 11.8$, $\varepsilon_d = 2.25$.

Here, AZO (a), (c) and ITO (b), (d) inclusions are employed in nanocomposite and hypercrystal (made by the author)

3.1.6. Conductivity-dependent surface plasmon polaritons propagating at the boundary of nanocomposite and hypercrystal

The main goal of the last investigation is to analyse the dispersion of the SPPs propagating at the boundary separating two different media. It is demonstrated that the SPP dispersive properties are dramatically affected by the material conductivity. Correspondingly, the filling ratio of the nanoparticles in the composite and their dielectric properties also allow for the engineering of the SPP characteristics. The research discusses the complex conductivity of the medium, which dramatically affects the tunability of SPPs. A detailed study is provided on SPP characteristics at the interface separating a nanocomposite and hypercrystal. Engineering properties of the nanocomposite and that of hypercrystal, the SPPs properties are tuned significantly. A complete description of the SPP dispersion relation with different controlling parameters is presented. The study is extended, aiming to examine the complex conductivity-dependent properties. The discussion focuses on the complex conductivity of the medium, which dramatically affects the tunability of SPPs. The geometry is the same as in the previous work.

For a deeper insight into the problem, permittivity components versus conductivity are investigated. So, in Fig. 3.16, the permittivity function is plotted if $\omega = 0.3 \times 10^{14}$ Hz (Fig. 3.16a) and $\omega = 3 \times 10^{14}$ Hz (Fig. 3.17b).

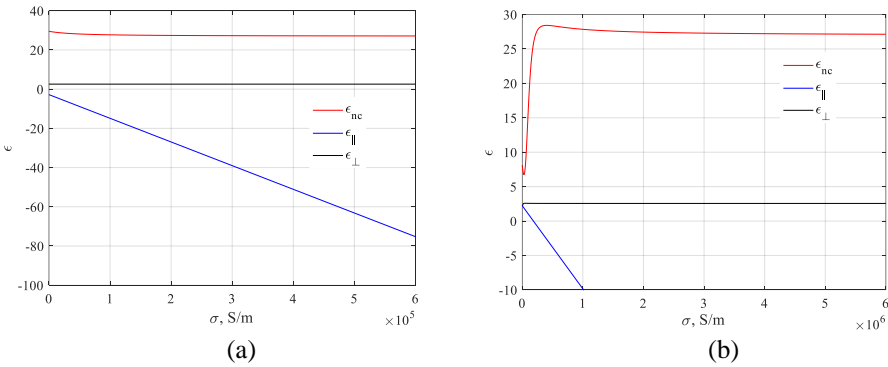


Fig. 3.16. Relative permittivity components of the nanocomposite and hypercrystal versus conductivity. Here, $f = 0.3$, $\epsilon_n = 11.8$, $\epsilon_d = 2.25$.

Here, ITO inclusions are employed in nanocomposite and hypercrystal.

(a) $\omega = 0.3 \times 10^{14}$ Hz; (b) $\omega = 3 \times 10^{14}$ Hz (made by the author)

The former allows for investigating conductivity-dependent permittivity functions for both regimes, i.e., hyperbolic and conventional. Moreover, the phenomenon of conductivity-dependent functions for the DSW regime (Fig. 3.16a) is studied. A comparison of Fig. 3.16a and Fig. 3.18a may lead to a conclusion

$\varepsilon_{nc}(\sigma) > \varepsilon_{\perp}(\sigma)$ in the case of the hyperbolic regime and $\varepsilon_{nc}(\sigma) < \varepsilon_{\perp}(\sigma)$ for DSW waves. Moreover, it is interesting to compare the conditions that are valid in the case of hyperbolic and DSW regimes for both, i.e., frequency and conductivity-dependent functions.

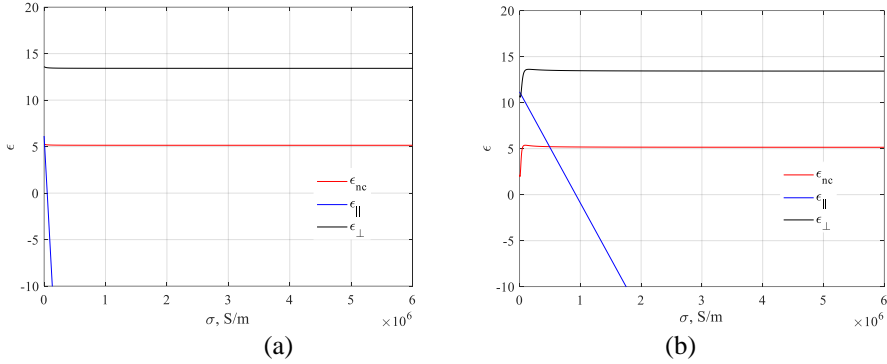


Fig. 3.17. Relative permittivity components of the nanocomposite and hypercrystal versus conductivity. Here, $f = 0.3$, $\varepsilon_n = 2.25$, $\varepsilon_d = 11.8$.

Here, ITO inclusions are employed in nanocomposite and hypercrystal.

(a) $\omega = 0.3 \times 10^{14}$ Hz; (b) $\omega = 3 \times 10^{14}$ Hz (made by the author)

The variations of propagation length L_p of SPPs versus frequency and the absolute value of complex conductivity are shown in the following figures. It is shown that the absolute value of complex conductivity strongly affects the SPP propagation at the interface of two media. Additionally, the propagation length L_p increases with the absolute value of complex conductivity (Fig. 3.19 (b)).

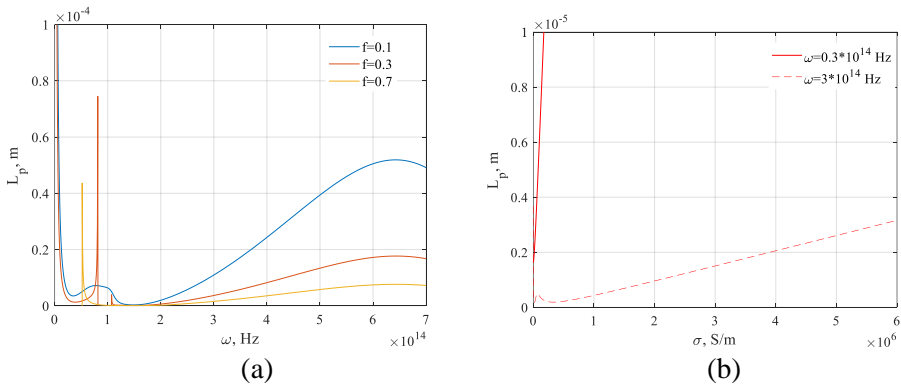


Fig. 3.18. Dependence of propagation length versus frequency for different filling factors (a) and versus conductivity for $f = 0.3$ (b). $\varepsilon_n = 2.25$, $\varepsilon_d = 11.8$

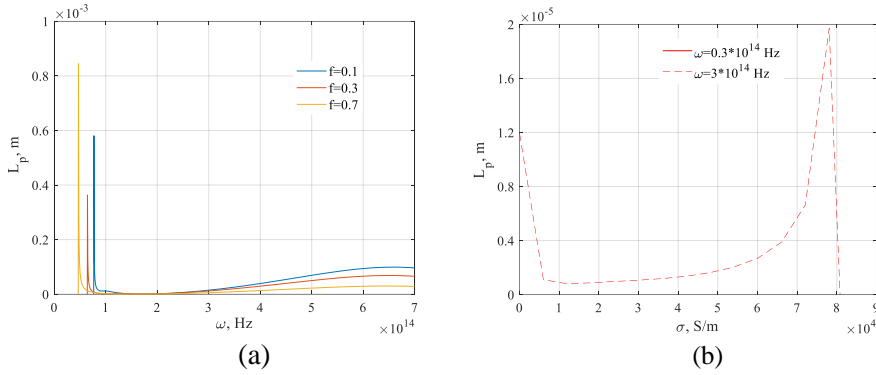


Fig. 3.19. Dependence of propagation length versus frequency for different filling factors (a) and versus conductivity for $f = 0.3$ (b). $\epsilon_n = 11.8$, $\epsilon_d = 2.25$ (made by the author)

All the above-presented results were obtained for the ITO inclusions.

3.2. Conclusions of the Third Chapter

Investigations of the interface separating the metallic nanowire metamaterial interface and the hollow-core metamaterial interface result in the conclusions as follows:

1. The slow wave effect is obtained. At a given frequency range ($0 < \omega < 1500$ THz), free-space wavenumber k_0 is smaller than β .
2. It has been shown that the use of a nanowire metamaterial interface ($d = 10$ nm, $S = 60$ nm) instead of the hollow-core metamaterial allows for the increase in the frequency range of surface wave existence from 500 THz (600 nm) to approximately 1000 THz (300 nm).

Investigations of the SPPs at the metamaterial/corrugated metal interface results in the following conclusions:

3. The groove width drastically affects the asymptotic frequency of SPPs, opening wide avenues for reaching the high tunability regime.
4. The loss of SPPs is sensitive to all parameters of the surface structure, i.e., the groove width (a) and the chemical potential (μ) parameters have a dramatic impact aiming to engineer resonance surface plasmon frequencies of the propagation modes enabling additional degree of freedom for system properties tunability.

5. One can tune the bandgap corresponding to the non-propagation regime by modifying the groove width parameter, enabling an additional degree of freedom for system properties' tunability.
6. The impact of the groove width (a) and the chemical potential (μ) on the propagation length of the SPPs was investigated, enabling an additional degree of freedom for system properties tunability.

Investigations of the spiral wire metamaterials interface result in the following conclusions:

7. The developed model allows for a quantitative study of plasmon polaritons, which can be engineered by the angle of the spiral and the number of grooves corrugating the perfectly conducting wire surface, enabling a high degree of freedom for system properties tunability.
8. It was shown that spiral wire superlattice-based metamaterials exhibit unique microscopic radiative bulk plasmon resonances called Ferrell-Berremann modes that can be excited with free space, allowing for the exploitation of the system in such applications as sensing, imaging and absorption spectroscopy.

Investigations of the SPPs propagating at the boundary of acoustic metamaterials result in the following conclusions:

9. It is shown that frequency regions exist in which dynamic constitutive parameters are instantaneously negative, and the wave under consideration becomes backward ($500 \text{ Hz} < f < 750 \text{ Hz}$), allowing for the exploitation of the system in applications, such as a contra-directional coupler routing the microwave signal to opposite terminals at different operating frequencies.

Investigations of the SPPs propagating at the interface of low-dimensional acoustic metamaterials result in the following conclusions:

10. The obtained increase of the absorption enhancement (the imaginary part of the propagation constant) equals 0.83 dB, making a dramatic impact while dealing with the noise cancellation approach.

General Conclusions

1. Investigations of the interface separating the metallic nanowire metamaterial interface and the hollow-core metamaterial interface result in the slow wave effect
2. Investigations of the SPPs at the metamaterial/corrugated metal interface result in the possibility of tuning the bandgap corresponding to the non-propagation regime by modifying the groove width parameter, enabling an additional degree of freedom for system properties' tunability.
3. Investigations of the spiral wire metamaterials interface resulted in the developed model allowing for a quantitative study of plasmon polaritons, which can be engineered by the angle of the spiral and the number of grooves corrugating the perfectly conducting wire surface, enabling a high degree of freedom for system properties tunability.
4. Investigations of the SPPs propagating at the interface of low-dimensional acoustic metamaterials resulted in the obtained increase of the absorption enhancement (the imaginary part of the propagation constant) equals 0.83 dB, making a dramatic impact while dealing with the noise cancellation approach.

References

- Ali, K., Ullah, M., Bacha, B. A., & Jabar, M. S. A. (2019). Complex conductivity-dependent two-dimensional atom microscopy. *European Physical Journal Plus*, 134, 618. <https://doi.org/10.1140/epjp/i2019-12978-1>
- Ambati, M., Fang, N., Sun, C., & Zhang, X. (2007). Surface resonant states and superlensing in acoustic metamaterials. *Physical Review B* 75, 195447. <https://doi.org/10.1103/PhysRevB.75.195447>
- Anglin, K., Ribaud, T., Adams, D. C., Qian, X., Goodhue, W. D., Dooley, S., Shaner, E. A., Wasserman, D. (2011). Voltage-controlled active mid-infrared plasmonic devices. *Journal of Applied Physics*, 109, 1. <https://doi.org/10.1063/1.3600230>
- Anwar, R. S., Ning, H., & Mao, L. (2017). Recent advancements in surface plasmon polaritons-plasmonics in subwavelength structures at microwave and terahertz regime. *Digital Communications and Networks*, 4(4), 244–257. <https://doi.org/10.1016/j.dcan.2017.08.004>
- Berreman, D. W. (1963). Infrared absorption at longitudinal optic frequency in cubic crystal films. *Physical Review*, 130, 2193–2198. <https://doi.org/10.1103/PhysRev.130.2193>
- Balili, R. B. (2012). Transfer matrix method in nanophotonics. *6th Jagna International Workshop International Journal of Modern Physics: Conference Series*, 17, 159–168. <https://doi.org/10.1142/S2010194512008057>

Bliokh, K. Y., & Nori, F. (2019). Klein-Gordon representation of acoustic waves and topological origin of surface acoustic modes. *Physical Review Letters*, 123, 054301. <https://doi.org/10.1103/PhysRevLett.123.054301>

Born, M., & Wolf, E. (1999). *Principles of Optics*. Cambridge University Press. <https://doi.org/10.1017/CBO9781139644181>

Byun, J., Lee, Y., Yoon, J., Lee, B., Oh, E., Chung, S., Lee, T., Cho, K.-J., Kim, J., & Hong, Y. (2018). Electronic Skins for Soft, Compact, Reversible Assembly of Wirelessly Activated Fully Soft Robots. *Science Robotics* 3, eaas9020. <https://doi.org/10.1126/scirobotics.aas9020>

Caloz, C., & Itoh, T. (2005). *Electromagnetic Metamaterials: Transmission Line Theory and Microwave Applications*. Wiley-IEEE Press. <https://doi.org/10.1002/0471754323>

Chen, H. T., Yang, H., Singh, R., O'Hara, J. F., Azad, A. K., Trugman, S. A., Jia, Q. X. and Taylor, A. J. (2010). Tuning the resonance in high-temperature super-conducting terahertz metamaterials. *Physical Review Letters*, 105, 247402. <https://doi.org/10.1103/PhysRevLett.105.247402>

Chen, X., Rogers, J. A., Lacour, S. P., Hu, W., & Kim, D.-H. (2019). Materials chemistry in flexible electronics. *Chemical Society Reviews*, 48, 1431. <https://doi.org/10.1039/C9CS90019E>

Dani, K. M., Ku, Z., Upadhyay, P. C., Prasankumar, R. P., Brueck, S. R. J., Taylor, A. J. (2009). Subpicosecond optical switching with a negative index metamaterial. *Nano Letters*, 9, 3565. <https://doi.org/10.1021/nl9017644>

Falkovsky, L. A. (2008). Optical properties of graphene. *Journal of Physics: Conference Series*, 129(1), 012004. <https://doi.org/10.1088/1742-6596/129/1/012004>

Feigenbaum, E., Diest, K., & Atwater, H. A. (2010). Unity-order index change in transparent conducting oxides at visible frequencies. *Nano Letters*, 10, 2111. <https://doi.org/10.1021/nl1006307>

Ferrari, L., Wu, C., Lepage, D., Zhang, X., & Liu, Z. (2015). Hyperbolic metamaterials and their applications. *Progress in Quantum Electronics*, 40, 1–40. <https://doi.org/10.1016/j.pquantelec.2014.10.001>

Ferrell, R. (1958). Predicted radiation of plasma oscillations in metal films. *Physical Review* 111, 1214–1222. <https://doi.org/10.1103/PhysRev.111.1214>

Garcia-Vidal, F. J., Martin-Moreno, L., & Pendry, J. B. (2005). Surfaces with holes in them: New plasmonic metamaterials. *Journal of Optics A: Pure and Applied Optics*, 7, S97. <https://doi.org/10.1088/1464-4258/7/2/013>

Goubau, G. (1950). Surface waves and their application to transmission lines. *Journal of Applied Physics*, 21, 1119–1128. <https://doi.org/10.1063/1.1699553>

Gric, T. (2016). Surface Plasmon polaritons at the interface of nanostructured metamaterials. *Progress in Electromagnetic Research M* 46, 165–172. <https://doi.org/10.2528/PIERM15121605>

- Gric, T., Gorodetsky, A., Trofimov, A., Rafailov, E. (2018). Tunable plasmonic properties and absorption enhancement in terahertz photoconductive antenna based on optimized plasmonic nanostructures. *Journal of Infrared Millimeter and Terahertz Waves*, 39(10), 1028–1038. <https://doi.org/10.1007/s10762-018-0516-0>
- Gric, T., & Hess, O. (2017a). Surface plasmon polaritons at the interface of two nanowire metamaterials. *Journal of Optics*, 19(8), 085101. <https://doi.org/10.1088/2040-8986/aa75fd>
- Gric, T., & Hess, O. (2017b). Controlling hybrid-polarization surface plasmon polaritons in dielectric-transparent conducting oxides metamaterials via their effective properties. *Journal of Applied Physics*, 122, 193105. <https://doi.org/10.1063/1.5001167>
- Hajiaghajani, A., Afandizadeh Zargari, A. H., Dautta, M., Jimenez, A., Kurdahi, F., & Tseng, P. (2021). Textile-integrated metamaterials for near-field multibody area networks. *Nature Electronics*, 4, 808. <https://doi.org/10.1038/s41928-021-00663-0>
- Han, J., Lakhtakia, A., & Qiu, C. W. (2008). Terahertz metamaterials with semi-conductor split-ring resonators for magnetostatic tunability. *Optics Express*, 16, 14390. <https://doi.org/10.1364/OE.16.014390>
- Hanson, G. W. (2008). Dyadic Green's functions and guided surface waves for a surface conductivity model of graphene. *Journal of Applied Physics*, 103(6), 064302. <https://doi.org/10.1063/1.2891452>
- Harvey, A. F. (1960). Periodic and guiding structures at microwave frequencies. *IEEE Transactions on Microwave Theory and Techniques*, 8, 30–61. <https://doi.org/10.1109/TMTT.1960.1124658>
- Hoffman, A. J., Alekseyev, L., Howard, S. S., Franz, K. J., Wasserman, D., Podolskiy, V. A., Narimanov, E. E., Sivco, D. L., Gmachl, C. (2007). Negative refraction in semiconductor metamaterials. *Nature Materials*, 6(12), 946–950. <https://doi.org/10.1038/nmat2033>
- Hornyak, L., Patrissi, C. J., & Martin, C. R. (1997). Fabrication, characterization and optical properties of gold nanoparticle/porous alumina composites: the nonscattering Maxwell-Garnett limit. *The Journal of Physical Chemistry B*, 101, 1548–1555. <https://doi.org/10.1021/jp962685o>
- Iorsh, I., Orlov, A., Belov, P., & Kivshar, Y. (2011). Interface modes in nanostructured metal-dielectric metamaterials. *Applied Physics Letters*, 99, 151914. <https://doi.org/10.1063/1.3643152>
- Jackson, J. D. (1999). *Classical Electrodynamics*. New York, USA: Wiley & Sons.
- Jiang, T., Shen, L., Zhang, X., & Ran, L.-X. (2009). High-order modes of spoof surface plasmon polaritons on periodically corrugated metal surfaces. *Progress in Electromagnetic Research M*, 8, 91–102.
- Johnson, P. B., & Christy, R. W. (1972). Optical constants of the noble metals. *Physical Review B* 6, 4370.

- Kadic, M., Milton, G. W., van Hecke, M., & Wegener, M. (2019). 3D metamaterials. *Nature Reviews Physics*, 1, 198–210. <https://doi.org/10.1038/s42254-018-0018-y>
- Kielczyński, P. (2022). New surface-plasmon-polariton-like Acoustic surface waves at the interface between two semi-infinite media. *Archives of Acoustics*, 47(3), 363–371.
- Khan, N., Bacha, N. B. A., Iqba, A., Rahman, A. U., & Afaq, A. (2017). Gain-assisted superluminal propagation and rotary drag of photon and surface plasmon polaritons. *Physical Review A* 96, 013848. <https://doi.org/10.1103/PhysRevA.96.013848>
- Khromova, I., Andryeuskii, A., & Lavrinenko, A. (2014). Ultrasensitive terahertz/infrared waveguide modulators based on multilayer graphene metamaterials. *Laser & Photonics Reviews*, 8(6), 916–923. <https://doi.org/10.1002/lpor.201400075>
- Klotz, G., Mallejac, N., Guenneau, S., & Enoch, S. (2019). Controlling frequency dispersion in electromagnetic invisibility cloaks. *Scientific reports*, 9, 6022. <https://doi.org/10.1038/s41598-019-42481-7>
- Kneipp, K. (2007). Surface-enhanced Raman scattering. *Physics Today*, 60, 40–45. <https://doi.org/10.1063/1.2812122>
- Lepeshov, S., Gorodetsky, A., Krasnok, A., Toropov, N., Vartanyan, T. A., Belov, P., Alú, A., Rafailov, E. U. (2018). Boosting the terahertz photoconductive antenna performance with optimized plasmonic nanostructures. *Scientific Reports*, 8, 6624. <https://doi.org/10.1038/s41598-018-25013-7>
- Kong, X., Xu, J., Mo, J. J., & Liu, S. (2017). Broadband and conformal metamaterial absorber. *Frontiers of Optoelectronics*, 10, 124. <https://doi.org/10.1007/s12200-017-0682-z>
- Liu, Y., Bartal, G., & Zhang, X. (2008). All-angle negative refraction and imaging in a bulk medium made of metallic nanowires in the visible region. *Optics Express*, 16, 15439–15448. <https://doi.org/10.1364/OE.16.015439>
- Maier, S. A. (2007). *Plasmonics: fundamentals and applications*. Springer Science + Business Media. <https://doi.org/10.1007/0-387-37825-1>
- Maier, S. A. (2007). *Surface plasmon polaritons at Metal / Insulator Interfaces*. In *Plasmonics: Fundamentals and Applications*. Springer. https://doi.org/10.1007/0-387-37825-1_2
- Maxwell, J. C. (1865). A dynamical theory of the electromagnetic field. *Philosophical Transactions of the Royal Society of London*, 155, 459–512. <https://doi.org/10.1098/rstl.1865.0008>
- Min, L., & Huang, L. (2015). All-semiconductor metamaterial-based optical circuit board at the microscale. *Journal of Applied Physics*, 118, 013104. <https://doi.org/10.1063/1.4923298>
- Min, L., Huang, L., Sun, R., & Xi, M. (2015). Dual Metamaterial With Large Birefringence. *IEEE Photonics Journal*, 7, 1. <https://doi.org/10.1109/JPHOT.2015.2497228>

- Molesky, S., Dewalt, C. J., & Jacob, Z. (2013). High temperature epsilon-near-zero and epsilon-near-pole metamaterial emitters for thermophotovoltaics. *Optics Express*, 21(S1), A96–A110. https://doi.org/10.1364/CLEO_QELS.2013.QTu1A.6
- Naik, G. V., Shalae, V. M., & Boltasseva, A. (2013). Alternative plasmonic materials: Beyond gold and silver. *Advanced Materials*, 25, 3264–3294. <https://doi.org/10.1002/adma.201205076>
- Pendry, J. B., Martin-Moreno, L., & Garcia-Vidal, F. J. (2004). Mimicking surface plasmons with structured surfaces. *Science*, 305, 847–848. <https://doi.org/10.1126/science.1098999>
- Peragut, F., Cerutti, L., Baranov, A., Hugonin, J. P., Taliercio, T., de Wilde, Y., & Greffet, J. J. (2017). Hyperbolic metamaterials and surface plasmon polaritons. *Optica*, 4(11), 1409–1415. <https://doi.org/10.1364/OPTICA.4.001409>
- Pluchery, O., Vayron, R., & Van, K.-M. (2011). Laboratory experiments for exploring the surface plasmon resonance. *European Journal of Physics*, 32, 585–599. <https://doi.org/10.1088/0143-0807/32/2/028>
- Poddubny, A., Iorsh, I., Belov, P., & Kivshar, Y. (2013). Hyperbolic metamaterials. *Nature Photonics*, 7(12), 948–957. <https://doi.org/10.1038/nphoton.2013.243>
- Podolskiy, V. A., & Narimanov, E. E. (2005). Strongly anisotropic waveguide as a non-magnetic left-handed system. *Physical Review B* 71, 201101. <https://doi.org/10.1103/PhysRevB.71.201101>
- Raether, B. H. (1988). *Surface plasmons*. Springer-Verlag Berlin. <https://doi.org/10.1007/BFb0048323>
- Ratni, B., Lustrac, A. D., Piau, G. P., & Burokur, S. N. (2018). Active metasurface for reconfigurable reflectors. *Applied Physics A*, 124, 104. <https://doi.org/10.1007/s00339-017-1502-4>
- Seet, K. K., Mizeikis, V., Matsuo, S., Juodkazis, S., & Misawa, H. (2005). Three-Dimensional Spiral-Architecture Photonic Crystals Obtained By Direct Laser Writing. *Advanced Materials*, 17, 541. <https://doi.org/10.1002/adma.200401527>
- Shi, X., Zuo, Y., Zhai, P., Shen, J., Yang, Y., Gao, Z., Liao, M., Wu, J., Wang, J., Xu, X., Tong, Q., Zhang, B., Wang, B., Sun, X., Zhang, L., Pei, Q., Jin, D., Chen, P., & Peng, H. (2021). Large-area display textiles integrated with functional systems. *Nature*, 591, 240. <https://doi.org/10.1038/s41586-021-03295-8>
- Singh, M. R. (2021). A Review of many-body interactions in linear and nonlinear plasmonic nanohybrids. *Symmetry*, 13, 445. <https://doi.org/10.3390/sym13030445>
- Singh, M. R., Brassem, G., & Yastrebov, S. (2021). Enhancement of radiative and nonradiative emission in random lasing plasmonic nanofibers. *Annalen Physik*, 533, 2000558. <https://doi.org/10.1002/andp.202000558>
- Singh, M. R., & Racknor, C. (2015). Nonlinear energy transfer in quantum dot and metallic nanorod nanocomposites. *Journal of the Optical Society of America B* 32, 2216–2222. <https://doi.org/10.1364/JOSAB.32.002216>

- Song, Y., Min, J., & Gao, W. (2019). Wearable and Implantable Electronics: Moving toward Precision Therapy. *ACS Nano*, 13, 12280. <https://doi.org/10.1021/acsnano.9b08323>
- Starko-Bowes, R., Atkinson, J., Newman, W., Hu, H., Kallos, T., Palikaras, G., Fedosejevs, R., Pramanik, S., & Jacob, Z. (2015). Optical characterization of Epsilon Near Zero, Epsilon Near Pole and hyperbolic response in nanowire metamaterials. *Journal of the Optical Society of America B*, 32(10), 2074–2080. <https://doi.org/10.1364/JOSAB.32.002074>
- Stiens, J., Vounckx, R., & Veretennicoff, I. (1997). Slab plasmon polaritons and waveguide modes in four-layer resonant semiconductor waveguides. *Journal of Applied Physics*, 81, 1–4. <https://doi.org/10.1063/1.363842>
- Takayama, O., & Lavrinenko, A. V. (2019). Optics with hyperbolic materials. *Journal of the Optical Society of America B* 36, F38. <https://doi.org/10.1364/JOSAB.36.000F38>
- Vakil, A., & Engheta, N. (2011). Transformation optics using graphene. *Science*, 332(6035), 1291–294. <https://doi.org/10.1126/science.1202691>
- Vengurlekar, A. S. (2010). Extraordinary optical transmission through metal films with subwavelength holes and slits. *Current Science*, 98, 1020–1032.
- Zhukovsky, S. V., Andryieuski, A., Sipe, J. E., & Lavrinenko, A. V. (2014). From surface to volume plasmons in hyperbolic metamaterials: General existence conditions for bulk high-k waves in metal-dielectric and graphene-dielectric multilayers. *Physical Review B* 90, 155429. <https://doi.org/10.1103/PhysRevB.90.155429>
- Yang, G.-Z., Bellingham, J., Dupont, P. E., Fischer, P., Floridi, L., Full, R., Jacobstein, N., Kumar, V., McNutt, M., Merrifield, R., Nelson, B. J., Scassellati, B., Taddeo, M., Taylor, R., Veloso, M., Wang, Z. L., & Wood, R. (2018). The grand challenges of science robotics. *Science Robotics*, 3, eaar 7650. <https://doi.org/10.1126/scirobotics.aar7650>

Author's publications collection

Papers in the reviewed scientific journals

*Ioannidis, T., Gric, T., & Rafailov, E. (2022). Tunable polaritons of spiral nanowire metamaterials. *Waves in random and complex media*, 32(1), 381–389, DOI: 10.1080/17455030.2020.1774095

* Ioannidis, T., Gric, T., & Rafailov, E. (2021). Controlling surface plasmon polaritons propagating at the boundary of low-dimensional acoustic metamaterials. *Applied sciences: Special Issue Functional Metamaterials*, 11(14), 1–8, DOI: <https://doi.org/10.3390/app11146302>

* Ioannidis, T., Gric, T., & Rafailov, E. (2021). Looking into surface plasmon polaritons guided by the acoustic metamaterials. *Plasmonics*, 16(2), 1835–1839, DOI: <https://doi.org/10.1007/s11468-021-01377-x>

* Ioannidis, T., Gric, T., & Rafailov, E. (2021). The study of the surface plasmon polaritons at the interface separating nanocomposite and hypercrystal. *Applied sciences: Special issue: The newest research in novel materials*, 11(11), 1–13, DOI: <https://doi.org/10.3390/app11115255>

* The dissertation is defended on the basis of these articles. Full-text articles are available at the end of the chapter “Author’s Publications Collection”. Articles published with the consent of the publisher /-s.

* Ioannidis, T., Gric, T., & Rafailov, E. (2020). Surface plasmon polariton waves propagation at the boundary of graphene based metamaterial and corrugated metal in THz range. *Optical and quantum electronics*, 52, 1–12, DOI: <https://doi.org/10.1007/s11082-019-2128-x>

* Ioannidis, T., Gric, T., Gorodetsky, A., Trofimov, A., & Rafailov, E. (2019). Enhancing the properties of plasmonic nanowires. *Materials research express*, 6, 1–8, DOI: <https://doi.org/10.1088/2053-1591/ab0a1b>

Papers in other editions

Ioannidis, T., Gric, T., & Rafailov, E. (2021). Tunable polaritons enhanced by the spiral nanowire metamaterials. META 2021 Warsaw – Poland. *The 11th international conference on metamaterials, photonic crystals and plasmonics, July 20–23, 2021: proceedings*. University of Warsaw, 841–842, DOI: https://metaconferences.org/META/files/meta21_proceedings.pdf

Article 1. Ioannidis et al. (2022). Tunable polaritons of spiral nanowire metamaterials

(https://doi.org/10.1080/17455030.2020.1774095)

WAVES IN RANDOM AND COMPLEX MEDIA
2022, VOL. 32, NO. 1, 381–389
<https://doi.org/10.1080/17455030.2020.1774095>



Taylor & Francis
Taylor & Francis Group



Tunable polaritons of spiral nanowire metamaterials

Thanos Ioannidis^a, Tatjana Gric^{a,b,c} and Edik Rafailov^{b,d}

^aDepartment of Electronic Systems, Vilnius Gediminas Technical University, Vilnius, Lithuania; ^bAston Institute of Photonic Technologies, Aston University, Birmingham, UK; ^cSemiconductor Physics Institute, Center for Physical Sciences and Technology, Vilnius, Lithuania; ^dPeter the Great St. Petersburg Polytechnic University, St. Petersburg, Russia

ABSTRACT

The tunable spiral nanowire metamaterial design at optical frequency is presented, and the surface polaritons are theoretically studied. It was found that the dispersions of the polaritons could be tuned by varying physical dimensions of the spiral nanowire metamaterial. This geometry is unique. Doing so, one may dynamically control the properties of surface polaritons. In addition, the Ferrell–Berreman modes can be excited that is impossible with the regular nanowire metamaterials having the circular cross-section of the nanowires. Herein, the presence of Ferrell–Berreman branches is confirmed by the performed analysis of the metamaterial band structure. It is worthwhile noting, that existence of Ferrell–Berreman modes is possible without epsilon-near-zero (ENZ) regime. The design of devices where Ferrell–Berreman modes can be exploited for practical applications ranging from plasmonic sensing to imaging and absorption enhancement is possible because of the propagation constant revealing subtle microscopic resonances.

ARTICLE HISTORY

Received 7 October 2019
Accepted 20 May 2020

KEYWORDS

Metamaterials

1. Introduction

Surface plasmons (SPs) are known as the collective oscillations of the delocalized electrons existing at metal–dielectric interfaces. Owing to their ability to confine light in subwavelength dimensions with high efficiency, SPs offer a route to overcome the diffraction limit of classical optics [1,2]. This enables a wide range of applications including surface-enhanced spectroscopy [3,4], biomedical sensing [5,6], solar cell photovoltaics [7,8], and optical antennas [9,10] since surface-plasmon-based circuits are known to merge the fields of photonics and electronics at the nanoscale, thereby enabling them to overcome the existing difficulties related to the large size mismatch between the micrometer-scale bulky components of photonics and the nanometer-scale electronic chips. These applications, however, are generally limited to high electromagnetic (EM) frequencies (the UV, visible, and near-infrared ranges). This is because metals behave akin to perfect electric conductors (PECs) at lower frequency regimes and do not support SP modes. Early works showed that by corrugating metal surfaces, this limitation can be overcome, and they reported the excitation of highly confined SP-like EM modes at microwave frequencies [11,12]. In 2004, Pendry et al.

CONTACT Tatjana Gric  tatjana.gric@vgtu.lt, tatjana.gric@dal.ca

© 2020 Informa UK Limited, trading as Taylor & Francis Group

introduced the concept of spoof SPs and demonstrated that plasmonic metamaterials constructed by patterning metal surfaces with subwavelength periodic features can mimic, at low frequencies (far IR, terahertz, or microwave regimes), the EM guiding characteristics of optical SPs [13,14]. It should be mentioned that the exceptional properties of SPPs, such as subwavelength confinement and strong field enhancement give rise to a wide range of innovative applications [15–17].

Since most of the conventional nanowire metamaterials can be controlled by the limited number of geometrical parameters, the focus of research has been moved to the possibility of tunable SPs by dealing with spiral nanowire metamaterial. Herein, the ability of spiral nanowire metamaterials to support unique absorption resonances related to radiative bulk plasmon-polaritons is theoretically demonstrated. The properties of these radiative bright modes significantly differ from the ones of the conventional dark modes (SP polaritons). The unique absorption resonances manifested in our metamaterials were originally studied by Ferrell in 1958 for plasmon-polaritonic thin-films in the ultraviolet [18], and by Berreman in 1963 for phonon-polaritonic thin-films in the mid-infrared spectral region [19]. One key for reaching the broadened SPs existence region is the tunability of the spiral angle.

In this work, we develop an effective medium theoretical model for the analytical description of spiral-shaped spoof devices and use it to investigate quantitatively their spectral properties. This model allows for a comprehensive understanding of FB modes supported by the structure.

2. Theoretical model

Herein, we focus on a 2D wire whose surface is decorated by N spiral-shaped grooves filled with a dielectric material of refractive index n_g . The resulting inner and outer radii, which correspond to the bottom and opening of the grooves, are r and R , respectively, as shown in Figure 1. The period and width of the grooves along the wire perimeter are d and a . The spiral is built in such a way that the intersection angle between the tangent to each spiral arm and the radial direction is the same along the spiral length; see Figure 1. These are the so-called logarithmic spirals, characterized by a spiral angle θ , and can be parametrized as

$$x(t) = re^{t/\cos\theta} \cos t \quad (1)$$

$$y(t) = re^{t/\cos\theta} \sin t \quad (2)$$

In the limit $a < d \ll \lambda$, a metamaterial approximation, in which the textured PEC is treated as a homogeneous effective medium, can be applied. In this homogeneous metamaterial picture, the effective permittivity and permeability in the region between the inner and outer radii acquire a diagonal, spatially independent tensor form. The component of the permittivity normal to the spiral arms (z-direction) is given by $\varepsilon_n = n_g^2 d/a$, while the parallel components diverge. The permeability components are set so that the EM radiation propagates at the speed of light inside the spiral grooves. This procedure yields the following effective permittivity and permeability tensors for TM waves expressed in cylindrical coordinates:

$$\bar{\varepsilon}^{-1} = \frac{a}{2n_g^2 d} \begin{bmatrix} 1 - \cos 2\theta & -\sin 2\theta \\ -\sin 2\theta & 1 + \cos 2\theta \end{bmatrix} \quad (3)$$

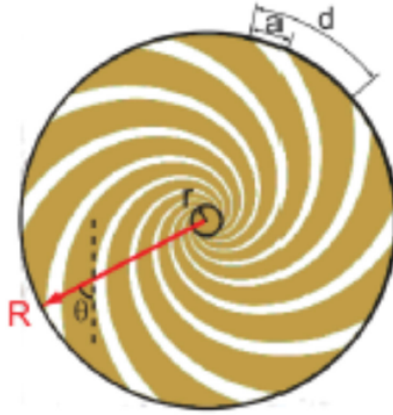


Figure 1. Localized spoof SPs in a 2D subwavelength PEC wire corrugated with spiral grooves. Cross-section of the corrugated PEC wire with the inner and outer radii r and R , periodicity d , groove width a , and the spiral angle θ .

$$\mu_z^{-1} = \frac{d}{a} \quad (4)$$

where the permittivity tensor is restricted to the xy -plane.

3. Modeling and the analytical solution

The proposed geometry of the nanowire composites is shown in Figure 2. Nanowires with permittivity ϵ_m^M are embedded in a dielectric host material with permittivity $\epsilon_d^M = 2.4$.

On the basis of an effective medium approximation, we evaluate the effective permittivities of the nanowire metamaterial according to:

$$\epsilon_{\perp}^M = \epsilon_d^M \left[\frac{\epsilon_m^M(1 + \rho^M) + \epsilon_d^M(1 - \rho^M)}{\epsilon_m^M(1 - \rho^M) + \epsilon_d^M(1 + \rho^M)} \right] \quad (5)$$

$$\epsilon_{\parallel}^M = \epsilon_m^M \rho^M + \epsilon_d^M(1 - \rho^M) \quad (6)$$

Here, subindex M refers to the metamaterial medium, and ρ^M is the metal filling fraction ratio which is defined as

$$\rho^M = \frac{\text{nanowire area}}{\text{unit cell area}} \quad (7)$$

To explore and demonstrate the properties of surface waves we adopt a Drude model to characterize the metal (i.e. silver), expressing the permittivity as $\epsilon_m^M(\omega) = \epsilon_{\infty} - \frac{\omega_p^2}{\omega^2 + i\delta\omega}$. The parameters are obtained by fitting this permittivity function to a particular frequency range of bulk material [20]. It is found [21] that for silver, the values of $\epsilon_{\infty} = 5$, $\omega_p = 2.2971 \cdot 10^{15}$ Hz, $\delta = 2.3866 \cdot 10^{13}$ Hz give a reasonable fit. We calculate the metal filling fraction (ρ^M) based on the values of the pore diameter (d^M) and spacing (S^M) and, assuming

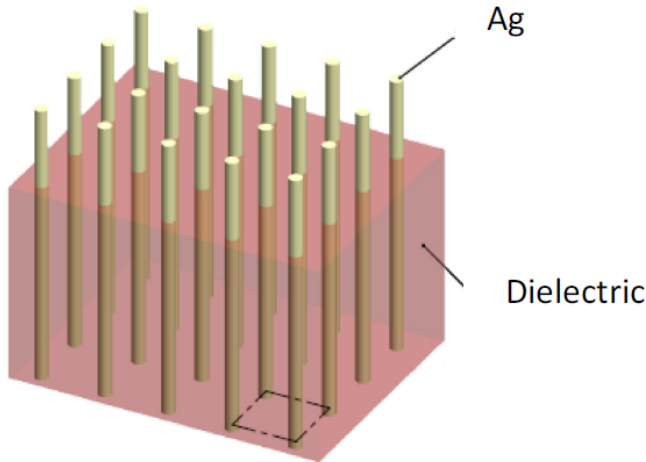


Figure 2. Schematic view of a nanowire composite.

a perfect rectangular structure, we apply the following equation [22]:

$$\rho^M = \frac{\pi (d^M)^2}{4(S^M)^2} \quad (8)$$

With this assumption, it is possible to derive a dispersion relation for the surface modes localized at the interface between metamaterial and PbS. Evaluating the tangential components of the electric and magnetic fields at the interface it is then, in turn, possible to obtain a single surface mode with the propagation constant [23]

$$\beta = k \left(\frac{(\varepsilon_{PbS} - \varepsilon_{||}^M) \varepsilon_{PbS} \varepsilon_{\perp}^M}{\varepsilon_{PbS}^2 - \varepsilon_{\perp}^M \varepsilon_{||}^M} \right)^{1/2}, \quad (9)$$

where k is the wavenumber (absolute value of the wavevector in vacuum) and β is the component of the wavevector parallel to the interface.

By substituting effective permittivity in different direction from Equation (3) in Equations (5) and (6), we arrive at the effective permittivities of the spiral nanowire metamaterial as follows:

$$\varepsilon_{\perp}^{SM} = -\varepsilon_d^M \frac{\varepsilon_d^M (\rho^M - 1) + \frac{ad\varepsilon_m^M \sin(2\theta)(\rho+1)}{2}}{\varepsilon_d^M (\rho^M + 1) + \frac{ad\varepsilon_m^M \sin(2\theta)(\rho-1)}{2}} \quad (10)$$

$$\varepsilon_{||}^{SM} = -\varepsilon_d^M (\rho^M - 1) - \frac{ad\varepsilon_m^M \rho^M (\cos(2\theta) + 1)}{2} \quad (11)$$

In Figure 3, we plot the effective medium constants for the spiral nanowire and regular nanowire structures using the homogenization formulae. The nanowire metamaterial structure shows an ENZ effect as well as epsilon-near-pole (ENP) resonance. Only the

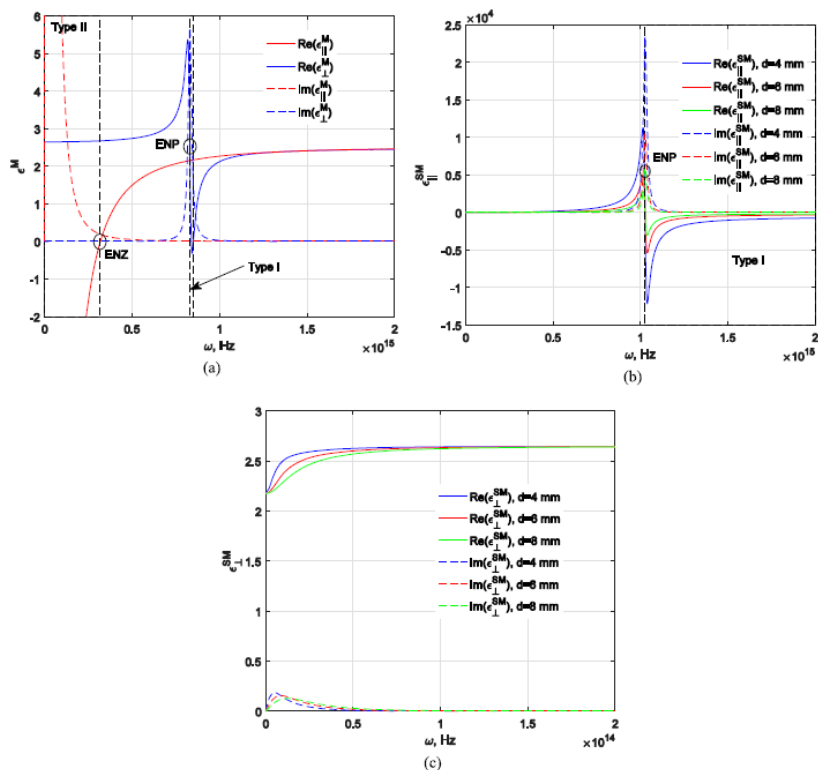


Figure 3. (a) Nanowire system: Real part of the dielectric permittivity for a nanowire structure. (b), (c) Spiral nanowire system: Real part of the dielectric permittivity for a spiral nanowire structure.

real parts are shown for clarity and the imaginary parts can be calculated similarly. The nanowire metamaterial structure consisting of metallic inclusions shows both Type I and Type II hyperbolic behavior. The spiral nanowire effective medium theory parameters are shown in Figure 3(b), (c). Type II behavior, which is difficult to achieve with spiral nanowire metamaterial structures, is observed. It also shows the characteristic ENP resonance.

The most important aspect to note about the ENZ and ENP resonances are the directions in which they occur for spiral nanowire and regular nanowire samples. The former issue dramatically changes the reflection and transmission spectrum of the two types of hyperbolic media. For the nanowire design, ENZ occurs along the nanowire length. This is intuitively expected since the Drude plasma frequency which determines the ENZ always occurs in the direction of free electron motion. On the contrary, the resonant ENP behavior of the two geometries occurs in the direction for which there is no continuous free electron motion. The ENP resonance occurs perpendicular to the wires in the nanowire geometry [24].

By presenting a modal analysis, we now show that the physical origin of the bulk absorption in metamaterials is due to the excitation of leaky bulk polaritons called Ferrell–Berreman modes [25–27]. Actually, the bulk metal forms volume charge oscillations at the ENZ of the metal (bulk or volume plasmons). It is worthwhile noting that these excitations are in the form of a completely longitudinal wave. Doing so, they cannot be excited with free-space light (which a transverse wave). In case of films of metal with thicknesses less than the metal skin depth, the top and bottom interface couple. The former issue allows for collective charge oscillations across the film. Thus, the bulk plasmon is no longer purely longitudinal and interaction with free-space light at frequencies near the metal ENZ [28] is possible. Ferrell addressed this approach for metallic foils in [29], Berreman – for polar dielectric films in [19]. Nanowire metamaterials support radiative excitations called FB modes. It is should be mentioned, that these FB modes differ from SP polaritons supported by metal foils. In case of SP modes, energy propagates along the surfaces of

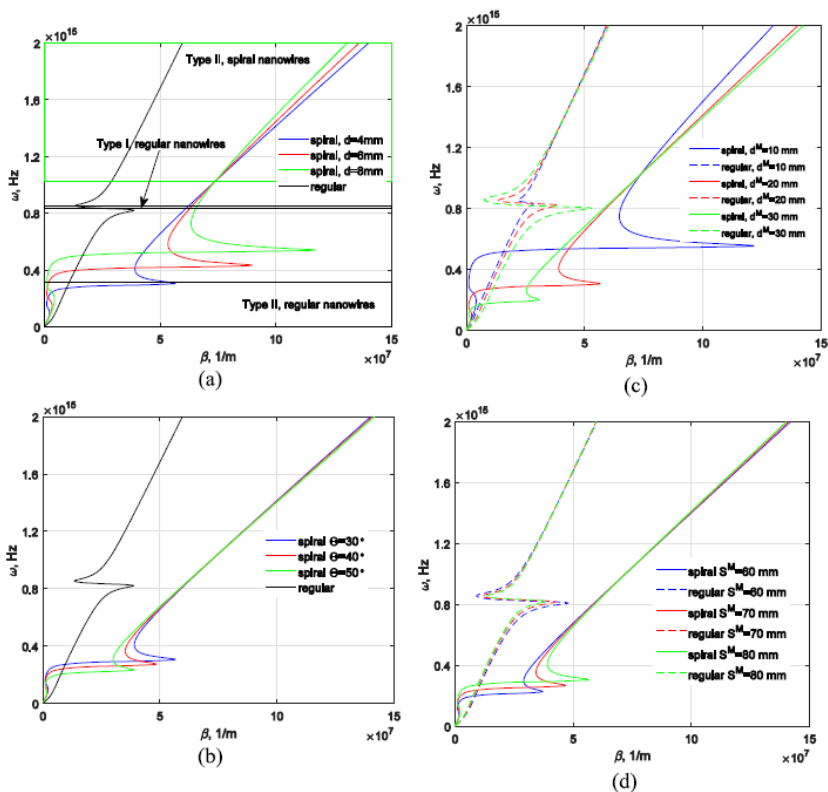


Figure 4. The dependences of dispersion relations of surface polaritons on (a) corrugated wire periodicity d , (b) spiral angle θ , (c) diameter of the nanowires d^M , and (d) distance between the nanowires S^M .

the metal, whereas in FB modes volume charge oscillations are setup across the foil and energy propagates within the bulk of the metal. The bulk polaritons under consideration have transverse wavevectors similar to free-space light and exist to the left of the light line. Thus, in Figure 4, it is interesting to observe the FB modes which usually exist at energies near the ENZ of the hyperbolic metamaterial to the left of the light line [30]. It is worthwhile noting, that in case of spiral nanowire metamaterials, FB modes exist with the absence of ENZ.


From Equations (5), (6), (10), and (11), the effective permittivity is one important parameter which determines the existence of polaritons in the structure under consideration. Figure 4 depicts a regime map in a β - f space, illustrating the regions where FB modes may exist. Fortunately, the frequency range of FB modes existence can be controlled by the wire periodicity d , spiral angle θ , diameter of the nanowires d^M , and distance between the nanowires S^M . Figure 4 depicts a regime map in a β - f space, illustrating the regions where FB polaritons may exist.

The surface polaritons dispersion relations as a function of d is shown in Figure 4(a), where $\theta = 30^\circ$, $d^M = 20$ nm, $S^M = 80$ nm. It is clear that FB modes exist at the left region of the light line. The polariton dispersions strongly depend on d parameter, as it can be clearly seen in Figure 4(a), in which we calculate and plot dispersion relations based on the effective anisotropic permittivity tensor. It should be noted that the frequency range of FB modes existence increases as d increases, i.e. larger periodicity increases the conductivity of the corrugated wire, thereby increasing the effective plasmonic frequency. Furthermore, dramatic tuning of the existence of the polariton spectrum is possible through the modification of the spiral metamaterial structure. The dashed lines are also drawn to facilitate discussion and to compare the spiral metamaterial properties with the regular nanowire metamaterial properties.

Except for d , the polariton properties are also dependent on the θ angle. Here we keep the parameter d of $d = 4$ nm, and change θ angle. As observed, the existence region obviously increases to high-frequency band with the decrease of θ angle value. On the whole, the polariton dispersions exhibit an obvious tunability.

4. Conclusion

In conclusion, we have theoretically studied the EM properties of spiral nanowire metamaterials based on the permittivity homogenization model. The developed theoretical model allows to design and investigate spoof plasmon devices with spiral textures in the optical frequency range. This model allows the quantitative study of plasmon polaritons, which can be engineered by the angle of spiral and the number of grooves corrugating the perfectly conducting wire surface. It has been shown that spiral nanowire superlattice-based metamaterials exhibit unique microscopic radiative bulk plasmon resonances called Ferrell-Berberman modes that can be excited with free-space light. In the metamaterial, effective medium picture the excitation of these modes is captured in the propagation constant, not in the effective dielectric permittivity constants. We observe these modes as anomalous transmission minima, which lie within the transparency window of the metamaterials. These radiative volume polaritonic modes could be exploited in applications such as sensing, imaging, and absorption spectroscopy.

388  T. IOANNIDIS ET AL.

Disclosure statement

No potential conflict of interest was reported by the author(s).

Funding

This project has received funding from the European Union's Horizon 2020 research and innovation program under the Marie Skłodowska Curie [grant agreement number 713694] and from Engineering and Physical Sciences Research Council (EPSRC) [grant number EP/R024898/1]. E.U.R. also acknowledges partial support from the Academic Excellence Project 5-100 proposed by Peter the Great St. Petersburg Polytechnic University.

References

- [1] Pendry JB. Negative refraction makes a perfect lens. *Phys Rev Lett*. 2000;85:3966–3969.
- [2] Barnes WL, Dereux A, Ebbesen TW. Surface plasmon subwavelength optics. *Nature*. 2003;424:824–830.
- [3] García-Vidal FJ, Pendry JB. Collective theory for surface enhanced Raman scattering. *Phys Rev Lett*. 1996;77:1163–1166.
- [4] Luo Y, Aubry A, Pendry JB. Electromagnetic contribution to surface-enhanced Raman scattering from rough metal surfaces: a transformation optics approach. *Phys Rev B Condens Matter Mater Phys*. 2011;83:155422.
- [5] Anker JN, Hall WP, Lyandres O, et al. Biosensing with plasmonic nanosensors. *Nat Mater*. 2008;7:442–453.
- [6] Li J, Ye J, Chen C, et al. Biosensing using diffractively coupled plasmonic crystals: the figure of merit revisited. *Adv Opt Mater*. 2015;3:176–181.
- [7] Ferry VE, Munday JN, Atwater HA. Design considerations for plasmonic photovoltaics. *Adv Mater*. 2010;22:4794–4808.
- [8] Li X, Ren X, Xie F, et al. High-performance organic solar cells with broadband absorption enhancement and reliable reproducibility enabled by collective plasmonic effects. *Adv Opt Mater*. 2015;3:1220–1231.
- [9] Halas NJ, Lal S, Chang W-S, et al. Plasmons in strongly coupled metallic nanostructures. *Chem Rev*. 2011;111:3913–3961.
- [10] Giannini V, Fernández-Domínguez AI, Heck SC, et al. Plasmonic nanoantennas: fundamentals and their use in controlling the radiative properties of nanoemitters. *Chem Rev*. 2011;111:3888–3912.
- [11] Goubau G. Surface waves and their application to transmission lines. *J Appl Phys*. 1950;21:1119–1128.
- [12] Harvey AF. Periodic and guiding structures at microwave frequencies. *IEEE Trans Microwave Theory Tech*. 1960;8:30–61.
- [13] Pendry JB, Martín-Moreno L, García-Vidal FJ. Mimicking surface plasmons with structured surfaces. *Science*. 2004;305:847–848.
- [14] García-Vidal FJ, Martín-Moreno L, Pendry JB. Surfaces with holes in them: new plasmonic metamaterials. *J Opt A Pure Appl Opt*. 2005;7:S97.
- [15] Ioannidis T, Gric T, Gorodetsky A, et al. Enhancing the properties of plasmonic nanowires. *Mater Res Express*. 2019;6:065014.
- [16] Gric T, Gorodetsky A, Trofimov A, et al. Tunable plasmonic properties and absorption enhancement in terahertz photoconductive antenna based on optimized plasmonic nanostructures. *J Infrared Millimeter Terahertz Waves*. 2018;39(10):1028–1038.
- [17] Lepeshov S, Gorodetsky A, Krasnok A, et al. Boosting the terahertz photoconductive antenna performance with optimized plasmonic nanostructures. *Sci Rep*. 2018;8:6624.
- [18] Ferrell R. Predicted radiation of plasma oscillations in metal films. *Phys Rev*. 1958;111:1214–1222.
- [19] Berreman DW. Infrared absorption at longitudinal optic frequency in cubic crystal films. *Phys Rev*. 1963;130:2193–2198.
- [20] Johnson PB, Christy RW. Optical constants of the noble metals. *Phys Rev B*. 1972;6:4370–4379.

- [21] Oubre C, Nordlander P. Finite-difference time-domain studies of the optical properties of nanoshell dimers. *J Phys Chem B*. 2005;109(20):10042–10051.
- [22] Starko-Bowes R, Atkinson J, Newman W, et al. Optical characterization of epsilon near zero, epsilon near pole and hyperbolic response in nanowire metamaterials. *J Opt Soc Am B*. 2015;32(10):2074–2080.
- [23] Iorsh I, Orlov A, Belov P, et al. Interface modes in nanostructured metal-dielectric metamaterials. *Appl Phys Lett*. 2011;99:151914.
- [24] Molesky S, Dewalt CJ, Jacob Z. High temperature epsilon-near-zero and epsilon-near-pole metamaterial emitters for thermophotovoltaics. *Opt Express*. 2013;21(51):A96–A110.
- [25] Vassant S, Hugonin J-P, Marquier F, et al. Berreman mode and epsilon near zero mode. *Opt Express*. 2012;20:23971–23977.
- [26] Vassant S, Archambault A, Marquier F, et al. Epsilon-near-zero mode for active optoelectronic devices. *Phys Rev Lett*. 2012;109:237401.
- [27] Campione S, Brener I, Marquier F. Theory of epsilon-near-zero modes in ultrathin films. *Phys Rev B*. 2015;91:121408.
- [28] Kliever K, Fuchs R. Collective electronic motion in a metallic slab. *Phys Rev*. 1967;153:498–512.
- [29] McAlister A, Stern E. Plasma resonance absorption in thin metal films. *Phys Rev*. 1963;132:1599–1602.
- [30] Newman WD, Cortes CL, Atkinson J, et al. Ferrell-Berreman modes in plasmonic epsilon-near-zero media. *ACS Photonics*. 2015;2(1):2–7.

Article 2. Ioannidis et al. (2021). Controlling surface plasmon polaritons propagating at the boundary of low-dimensional acoustic metamaterials (<https://doi.org/10.3390/app11146302>)



Article

Controlling Surface Plasmon Polaritons Propagating at the Boundary of Low-Dimensional Acoustic Metamaterials

Thanos Ioannidis ¹, Tatjana Gric ^{1,2,3,*} and Edik Rafailov ^{2,4}

¹ Department of Electronic Systems, VILNIUS TECH, 10223 Vilnius, Lithuania; athanasios.ioannidis@vgtu.lt
² Aston Institute of Photonic Technologies, Aston University, Birmingham B4 7ET, UK; e.rafaelov@aston.ac.uk
³ Center for Physical Sciences and Technology, Semiconductor Physics Institute, 10222 Vilnius, Lithuania
⁴ Peter the Great St. Petersburg Polytechnic University, 195251 St. Petersburg, Russia
 * Correspondence: Tatjana.gric@vilniustech.lt

Abstract: As a novel type of artificial media created recently, metamaterials demonstrate novel performance and consequently pave the way for potential applications in the area of functional engineering in comparison to the conventional substances. Acoustic metamaterials and plasmonic structures possess a wide variety of exceptional physical features. These include effective negative properties, band gaps, negative refraction, etc. In doing so, the acoustic behaviour of conventional substances is extended. Acoustic metamaterials are considered as the periodic composites with effective parameters that might be engineered with the aim to dramatically control the propagation of supported waves. Homogenization of the system under consideration should be performed to seek the calculation of metamaterial permittivity. The dispersion behaviour of surface waves propagating from the boundary of a nanocomposite composed of semiconductor enclosures that are systematically distributed in a transparent matrix and low-dimensional acoustic metamaterial and constructed by an array of nanowires implanted in a host material are studied. We observed the propagation of surface plasmon polaritons. It is demonstrated that one may dramatically modify the properties of the system by tuning the geometry of inclusions.

Keywords: surface plasmon polaritons; low-dimensional; acoustic; metamaterial



Citation: Ioannidis, T.; Gric, T.; Rafailov, E. Controlling Surface Plasmon Polaritons Propagating at the Boundary of Low-Dimensional Acoustic Metamaterials. *Appl. Sci.* **2021**, *11*, 6302. <https://doi.org/10.3390/app11146302>

Academic Editor: Luigi La Spada

Received: 25 May 2021

Accepted: 6 July 2021

Published: 8 July 2021

Publisher's Note: MDPI stays neutral with regard to jurisdictional claims in published maps and institutional affiliations.



Copyright: © 2021 by the authors. Licensee MDPI, Basel, Switzerland. This article is an open access article distributed under the terms and conditions of the Creative Commons Attribution (CC BY) license (<https://creativecommons.org/licenses/by/4.0/>).

1. Introduction

Over the past few years, interest in creating materials allowing for the control the flow of electromagnetic waves (e.g., light) in exceptional ways has increased dramatically. Novel engineering tools have opened wide avenues to construct artificial materials possessing properties that are not possible in the case of the naturally existing materials. These new designs are possible due to the wide variety of inclusions. Moreover, the novel response appears to be because of their specific interactions with electromagnetic fields. These designs can be scaled down and constructed thanks to nanotechnology.

Hyperbolic metamaterials represent a multi-functional platform providing a fertile ground for the realization of waveguiding, imaging, sensing, quantum, and thermal engineering outside the scope of conventional devices. These novel composites utilize the notion of tuning the fundamental dispersion relation of surface plasmon polaritons aiming to generate exceptional electromagnetic modes with a wide spectrum of applications. The hyperbolic metamaterial can be considered from the perspective of polaritonic crystal.

The unique positioning of nanomaterials bridging atoms and bulk solids, along with their interesting features and potential applications [1] has provided a fertile ground for the growing scientific interest in them. The capability to create such nanoscale-sized materials advances many fields of modern science and technology.

Transparent conductive oxides (TCOs) are of particular interest within the scientific community. These might be utilized as the optional materials for plasmonic applications [2] in the near-infrared region. It should be mentioned that TCOs such as indium tin oxide

(ITO) show a wide spectrum of engineerable features [3]. The former is possible via doping and electric bias. The modelling and fulfillment of ultra-compact electro-absorption modulators [4–8], including the application of novel multimode modulator architectures, [9] has profited from the chance of actively switching between two different regimes.

The unique properties of SP-based nanostructures and their applications in waveguides, sources, near-field optics, nonlinear optics, surface enhanced Raman spectroscopy (SERS), data storage, solar cells (or photovoltaic devices), chemical sensors, biosensors, etc. [10,11], have stimulated a tremendous interest in their properties.

Hyperbolic materials belong to a class of uniaxial materials. These are characterized by two different values for permittivity, i.e., parallel and perpendicular to the optical axis [12]. The exceptional wave is characterized by an electric field with components along the optical axis and perpendicular to it. Hyperbolic materials possess a remarkable property. They support propagating waves possessing arbitrary large wave vectors at a finite frequency [13–15]. Consequently, the corresponding local density of states is exceptionally large. In doing so, hyperbolic substances open wide avenues for many applications such as superresolution, enhanced spontaneous emission, and large energy density [16].

Based on the frequency range, one may divide sound waves into the types that follow: low frequency, intermediate frequency, and high frequency. Noise has a strong penetrating power and dissipates slowly during propagation. In doing so, it is a challenging task to engineer the sound waves. Hence, it is of particular importance to focus on the investigation of sound waves and vibration control. The investigations of surface waves and plasmonics represent an additional inherent part of nanophotonics. The former provide a fertile ground aiming to lower the length scales and dimensionality of a wide range of electromagnetic phenomena. Not remarkably, nonreciprocity and unidirectional propagation of surface plasmon-polaritons (SPPs) have stimulated a tremendous interest. Magneto-optical nonreciprocity in the transverse Voigt geometry is mostly dealt with in these studies, comprising topological quantum-Hall-effect states. Herein we consider a novel approach allowing for the propagation of SPPs at the acoustic metamaterial interface. It is worthwhile to note that inclusions of the composites are fulfilled by the TCOs, making a stronger case towards implementation the properties of possible devices. It should be mentioned, that in the present work we, deal with the spoof SPPs. Natural SPPs only exist at optical frequencies. To realize SPPs at lower frequencies, spoof SPPs are proposed. In doing so, we end up with the concept of “designer” surface modes.

2. Theoretical Approach

In the frame of the present study, we investigate the plane interface separating a nanocomposite (NC) semi-infinite layer and a hypercrystal that is adjacent to it (Figure 1). It is of particular importance to mention that the surface waves propagate along z axis. It is possible to construct the system under investigation by means of molecular beam epitaxy [17], chemical vapor deposition, atomic layer deposition and sacrificial etching [18]. Nanocomposite is understood as a non-conductive transparent matrix with a permittivity ϵ_H . Semiconductor nanoparticles with permittivity ϵ_m are regularly distributed in its host material. The dielectric function of the TCO based nanoparticles is of special importance to the academic community. The topic has become one of significance due to the metal being opaque to light. The parameters of the Drude–Lorentz approach for AZO, GZO, and ITO are obtained from experimental data [2].

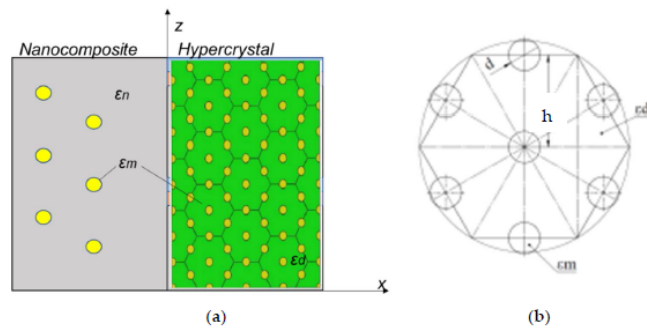


Figure 1. Schematic design under consideration, comprising a semi-infinite hypercrystal ($x > 0$) and a nanocomposite with semiconductor inclusions ($x < 0$) (a), metamaterial (hypercrystal) unit cell (b).

We have made an assumption that the size of the inclusions suspended in a dielectric matrix is much smaller than the wavelength and the electromagnetic field penetration depth in the material. It is worthwhile to mention that an effective Maxwell Garnett model can be employed, aiming to characterize the optical parameters of the nanocomposite under consideration. The former approach is possible if the interference impacts of the inclusions are neglected. In this relation, the homogenization of the system should be performed, and the effective dielectric permittivity of the nanocomposite can be expressed as follows:

$$\varepsilon_{nc} = \varepsilon_n \left[1 + \frac{f}{(1-f)/3 + \varepsilon_n/(\varepsilon_m - \varepsilon_n)} \right] \quad (1)$$

where f is the filling factor, i.e., the fraction of nanoparticles in the matrix.

Based on the effective medium approximation, the effective permittivities of the nanowire metamaterial (hypercrystal) can be obtained according to [19]:

$$\varepsilon_{\perp} = \varepsilon_d \left[\frac{\varepsilon_m(1+\rho) + \varepsilon_d(1-\rho)}{\varepsilon_m(1-\rho) + \varepsilon_d(1+\rho)} \right] \quad (2)$$

$$\varepsilon_{\parallel} = \varepsilon_m \rho + \varepsilon_d(1-\rho) \quad (3)$$

Here, ρ is the metal filling fraction ratio which is defined as:

$$\rho = \frac{\text{nanowire area}}{\text{unit cell area}} \quad (4)$$

The calculation of the metal filling fraction (ρ) taking into account the data sheet of the pore diameter (d) and spacing (h) (Figure 1b). The following equation [20,21] is applied, taking into consideration a perfect hexagonal structure:

$$\rho = \frac{\pi d^2}{2\sqrt{3}h^2} \quad (5)$$

One may attain a surface mode with the propagation constant [22] by evaluating the tangential components of the electric and magnetic fields at the interface.

$$\beta = k \left(\frac{(\varepsilon_{\parallel} - \varepsilon_{nc})\varepsilon_{\perp}\varepsilon_{nc}}{\varepsilon_{\perp}\varepsilon_{\parallel} - \varepsilon_{nc}^2} \right)^{1/2} \quad (6)$$

By substituting (1)–(3) in (6), the resulted dispersion relation is as follows:

$$\beta = k \left(-\frac{\varepsilon_n b a (\varepsilon_n a + \varepsilon_m \rho - \varepsilon_d (\rho - 1))}{\left(\varepsilon_n^2 a^2 + \frac{(\varepsilon_m \rho - \varepsilon_d (\rho - 1)) b}{\varepsilon_d (\rho + 1) - \varepsilon_m (\rho - 1)} \right) (\varepsilon_d (\rho + 1) - \varepsilon_m (\rho - 1))} \right)^{1/2} \quad (7)$$

$$a = \frac{f}{\frac{1}{\varepsilon_n} + \frac{1}{\varepsilon_m} - \frac{1}{\varepsilon_d}} - 1, b = (\rho - 1) \varepsilon_d^2 - \varepsilon_m \varepsilon_d (\rho + 1).$$

3. Results and Discussions

Herein, the dependencies of the permittivity components of a hypercrystal and nanocomposite upon frequency are modelled aiming to detect the frequency ranges of Dyakonov surface waves (DSWs) and the existence of SPP waves (Figure 2).

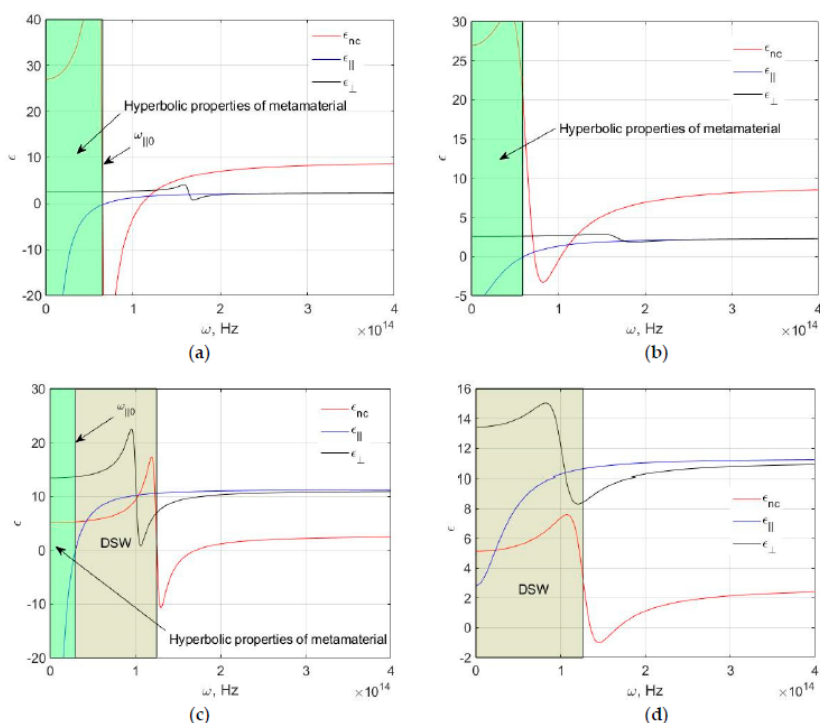


Figure 2. Relative permittivity components of the nanocomposite and hypercrystal versus frequency. Herein, $f = 0.3$. (a,b) $\varepsilon_n = 11.8$, $\varepsilon_d = 2.25$; (c,d) $\varepsilon_n = 2.25$, $\varepsilon_d = 11.8$. Herein AZO (a,c) and ITO (b,d) inclusions are employed in nanocomposite and hypercrystal.

In the range the frequency $\omega_{||0}$ the semiconductor-dielectric metamaterial possesses hyperbolic properties. It can be seen from Figure 2, that the propagation of DSW is possible in the case of $\varepsilon_n = 2.25$, $\varepsilon_d = 11.8$. It is worthwhile to note that the regime of DSW

propagation is possible in the case of $\varepsilon_{||}$, $\varepsilon_{nc} > 0$. Moreover, it is possible to increase the frequency range of DSW existence by changing the nature of inclusions, i.e., by replacing AZO with ITO.

It is of particular interest to analyze two cases, i.e., when $\varepsilon_n > \varepsilon_d$ and $\varepsilon_d > \varepsilon_n$. The case when $\varepsilon_n = 2.25$, $\varepsilon_d = 11.8$ is depicted in Figure 3a. It can be observed that dispersion curves in these cases exhibit an exotic behavior in contrary to the conventional surface plasmons propagating at the metal/dielectric interface [23]. The case when $\varepsilon_n = 11.8$, $\varepsilon_d = 2.25$ is depicted in Figure 3b. By having a glance into the properties of DSW obtained by changing the filling factor of the nanocrystal as displayed in Figure 3a, one may observe that in contrast to the case depicted in Figure 3a, DSW does not propagate if $\varepsilon_n = 11.8$, $\varepsilon_d = 2.25$ (Figure 3c).

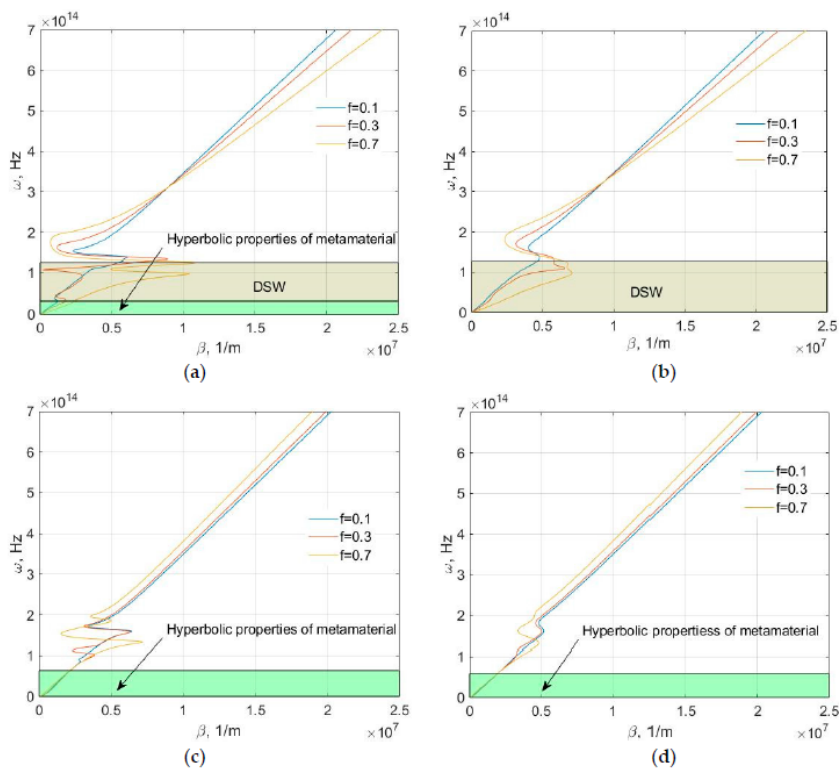


Figure 3. Solution of the wave equation for different filling ratio f : (a,b)— $\varepsilon_n = 2.25$, $\varepsilon_d = 11.8$; (c,d)— $\varepsilon_n = 11.8$, $\varepsilon_d = 2.25$. Herein AZO (a,c) and ITO (b,d) inclusions are employed in nanocomposite and hypercrystal.

Figure 4 demonstrates the transmission characteristics on frequency for various filling ratios. It can be seen in Figure 4a,c that with the increase of frequency, the imaginary part of β decreases at certain intervals, and the transmission distance increases. The former reveals the reduction of transmission loss with increasing frequency. Figure 4 shows that the filling ratio has a dramatic impact on the transmission characteristics of

the SPPs. In this relationship, the realization of dimension-tunable SPPs is enabled. It is worth noting that the results presented in Figure 4a,c are very important for practical application. The increase of the absorption enhancement (imaginary part of the propagation constant) makes a dramatic impact while creating photoconductive antennas with this enhanced performance [24].

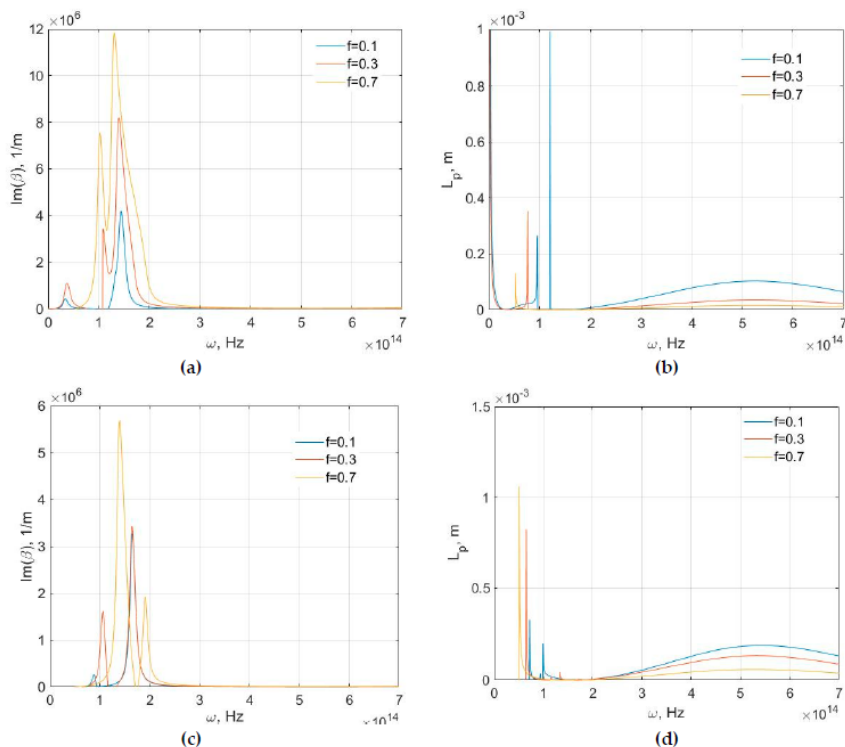


Figure 4. Dependence of transmission characteristics versus frequency for different filling factors: (a,c) the imaginary part of β ; (b,d) the propagation length L_p . The case $\epsilon_n = 2.25$, $\epsilon_d = 11.8$ is presented in (a,b); $\epsilon_n = 11.8$, $\epsilon_d = 2.25$ —(c,d). All of the presented results were obtained for the AZO inclusions.

4. Conclusions

Thorough theoretical derivation the excellent transmission characteristics of SPPs were analyzed and verified effectively in this paper. The dependence of the transmission characteristics on frequency for different filling ratios was obtained in this paper. Moreover, the possibilities to increase the frequency ranges where DSW can exist have been demonstrated. It has been concluded that with the increase of frequency, the imaginary part of β decreases at certain intervals, and the transmission distance increases. The former reveals the reduction of transmission loss with increasing frequency. The filling ratio has a dramatic impact on the transmission characteristics of SPPs. From this relationship, the

realization of dimension tunable SPPs is enabled. This work is of great significance to the further research of optical devices based on SPPs.

Author Contributions: Conceptualization, T.I. and T.G.; methodology, T.I.; software, T.G.; validation, T.G. and E.R.; formal analysis, E.R.; investigation, T.I.; resources, E.R.; data curation, T.G.; writing—original draft preparation, T.I.; writing—review and editing, T.G. and E.R.; visualization, T.I.; supervision, T.G.; project administration, E.R.; funding acquisition, T.G. and E.R. All authors have read and agreed to the published version of the manuscript.

Funding: This project has received funding from the European Union's Horizon 2020 research and innovation programme under the Marie Skłodowska Curie grant agreement No 713694 and from Engineering and Physical Sciences Research Council (EPSRC) (Grant No. EP/R024898/1). The work of E.U. Rafailov was partially funded by the Ministry of Science and Higher Education of the Russian Federation as part of World-class Research Center program: Advanced Digital Technologies (contract No. 075-15-2020-934 dated 17.11.2020).

Institutional Review Board Statement: Not applicable.

Informed Consent Statement: Not applicable.

Data Availability Statement: The data presented in this study are available on request from the corresponding author.

Conflicts of Interest: The authors declare no conflict of interest.

References

- Halperin, W.P. Quantum size effects in metal particles. *Rev. Mod. Phys.* **1986**, *58*, 533–606. [\[CrossRef\]](#)
- Naik, G.V.; Shalae, V.M.; Boltasseva, A. Alternative plasmonic materials: Beyond gold and silver. *Adv. Mater.* **2013**, *25*, 3264–3294. [\[CrossRef\]](#) [\[PubMed\]](#)
- Feigenbaum, E.; Diest, K.; Atwater, H.A. Unity-Order Index Change in Transparent Conducting Oxides at Visible Frequencies. *Nano Lett.* **2010**, *10*, 2111–2116. [\[CrossRef\]](#)
- Sorger, V.J.; Lanzillotti-Kimura, N.D.; Ma, R.-M.; Zhang, X. Ultracompact silicon nanophotonic modulator with broadband response. *Nanophotonics* **2012**, *1*, 17. [\[CrossRef\]](#)
- Cai, W.; White, J.S.; Brongersma, M.L. Compact, High-Speed and Power-Efficient Electrooptic Plasmonic Modulators. *Nano Lett.* **2009**, *9*, 4403–4411. [\[CrossRef\]](#) [\[PubMed\]](#)
- Das, S.; Salandrino, A.; Wu, J.Z.; Hui, R. Near-infrared electro-optic modulator based on plasmonic graphene. *Opt. Lett.* **2015**, *40*, 1516–1519. [\[CrossRef\]](#)
- Ye, C.; Khan, S.; Li, Z.R.; Simsek, E.; Sorger, V.J. λ -size ITO and graphene-based electro-optic modulators on SOI. *IEEE J. Sel. Top. Quantum Electron.* **2014**, *20*, 40.
- Vasudev, A.P.; Kang, J.-H.; Park, J.; Liu, X.; Brongersma, M.L. Electro-optical modulation of a silicon waveguide with an “epsilon-near-zero” material. *Opt. Express* **2013**, *21*, 26387. [\[CrossRef\]](#)
- Das, S.; Fardad, S.; Kim, I.; Rho, J.; Hui, R.; Salandrino, A. Nanophotonic modal dichroism: Mode-multiplexed modulators. *Opt. Lett.* **2016**, *41*, 4394–4397. [\[CrossRef\]](#)
- Barnes, W.L.; Dereux, A.; Ebbesen, T.W. Surface plasmon subwavelength optics. *Nature* **2003**, *424*, 824–830. [\[CrossRef\]](#) [\[PubMed\]](#)
- Zhang, J.; Zhang, L.; Xu, W. Surface plasmon polaritons: Physics and applications. *J. Phys. D Appl. Phys.* **2012**, *45*, 113001. [\[CrossRef\]](#)
- Peragut, F.; Cerruti, L.; Baranov, A.; Hugonin, J.P.; Taliencio, T.; De Wilde, Y.; Greffet, J.J. Hyperbolic metamaterials and surface plasmon polaritons. *Optica* **2017**, *4*, 1409–1415. [\[CrossRef\]](#)
- Zhukovsky, S.V.; Andryieuski, A.; Sipe, J.E.; Lavrinenko, A.V. From surface to volume plasmons in hyperbolic metamaterials: General existence conditions for bulk high-k waves in metal-dielectric and graphene-dielectric multilayers. *Phys. Rev. B* **2014**, *90*, 155429. [\[CrossRef\]](#)
- Mahmoodi, M.; Tavassoli, S.H.; Takayama, O.; Sukham, J.; Malureanu, R.; Lavrinenko, A.V. Existence Conditions of High-k Modes in Finite Hyperbolic Metamaterials. *Laser Photon Rev.* **2019**, *13*, 1800253. [\[CrossRef\]](#)
- Takayama, O.; Lavrinenko, A. Optics with hyperbolic materials. *J. Opt. Soc. Am. B* **2019**, *36*, F38–F48. [\[CrossRef\]](#)
- Ferrari, L.; Lu, D.; Lepage, D.; Liu, Z. Enhanced spontaneous emission inside hyperbolic metamaterials. *Opt. Express* **2014**, *22*, 4301–4306. [\[CrossRef\]](#)
- Hoffman, A.; Alekseyev, L.; Howard, S.; Franz, K.; Wasserman, D.; Podolskiy, V.; Narimanov, E.; Sivco, D.; Gmachl, C. Negative refraction in semiconductor metamaterials. *Nat. Mater.* **2007**, *6*, 946–950. [\[CrossRef\]](#)
- Feng, J.; Chen, Y.; Blair, J.; Kurt, H.; Hao, R.; Citrin, D.S.; Summers, C.J.; Zhou, Z. Fabrication of annular photonic crystals by atomic layer deposition and sacrificial etching. *J. Vac. Sci. Technol. B Microelectron. Nanometer Struct.* **2009**, *27*, 568. [\[CrossRef\]](#)

19. Shekhar, P.; Atkinson, J.; Jacob, Z. Hyperbolic metamaterials: Fundamentals and applications. *Nano Converg.* **2014**, *1*, 1–17. [[CrossRef](#)] [[PubMed](#)]
20. Starko-Bowes, R.; Atkinson, J.; Newman, W.; Hu, H.; Kallos, T.; Palikaras, G.; Fedosejevs, R.; Pramanik, S.; Jacob, Z. Optical characterization of epsilon-near-zero, epsilon-near-pole, and hyperbolic response in nanowire metamaterials. *J. Opt. Soc. Am. B* **2015**, *32*, 2074–2080. [[CrossRef](#)]
21. Gric, T.; Hess, O. Surface plasmon polaritons at the interface of two nanowire metamaterials. *J. Opt.* **2017**, *19*, 085101. [[CrossRef](#)]
22. Iorsh, I.; Orlov, A.; Belov, P.; Kivshar, Y. Interface modes in nanostructured metal-dielectric metamaterials. *Appl. Phys. Lett.* **2011**, *99*, 151914. [[CrossRef](#)]
23. Maier, S. Surface Plasmon Polaritons at Metal/Insulator Interfaces. In *Plasmonics: Fundamentals and Applications*; Springer: New York, NY, USA, 2007.
24. Gric, T.; Gorodetsky, A.; Trofimov, A.; Rafailov, E.U. Tunable Plasmonic Properties and Absorption Enhancement in Terahertz Photoconductive Antenna Based on Optimized Plasmonic Nanostructures. *J. Infrared Millim. Terahertz Waves* **2018**, *39*, 1028–1038. [[CrossRef](#)]

Article 3. Ioannidis et al. (2021). Looking into surface plasmon polaritons guided by the acoustic metamaterials (<https://doi.org/10.1007/s11468-021-01377-x>)

Plasmonics (2021) 16:1835–1839
<https://doi.org/10.1007/s11468-021-01377-x>



Looking Into Surface Plasmon Polaritons Guided by the Acoustic Metamaterials

Thanos Ioannidis¹ · Tatjana Gric^{1,2,3} · Edik Rafailov^{2,4,5}

Received: 20 August 2020 / Accepted: 20 January 2021 / Published online: 14 April 2021
 © The Author(s), under exclusive licence to Springer Science+Business Media, LLC, part of Springer Nature 2021

Abstract

Acoustic metamaterials are introduced as the structures with the alternating elements possessing effective properties that can be tuned seeking for the dramatic control on wave propagation. Homogenization of the structure under consideration is needed aiming to calculate permittivity of metamaterial. We present theoretical outcomes studying an acoustic composite possessing negative effective parameters in the acoustic frequency range. An acoustic metamaterial with an the alternating nanowires arranged in a building block and embedded in a host material was investigated. Propagation of surface plasmon polaritons at the metamaterial interface was predicted.

Keywords Surface plasmon polaritons · Acoustic · Metamaterial

Introduction

Acoustic metamaterials give rise to novel properties of the propagation of mechanical waves. The former are impossible in case of conventional materials. Recently, acoustic artificial structured materials possessing properties not found previously and opening the wide avenues for the diverse potential applications with remarkable functionalities [1–4] have been widely studied. Aiming to have a deeper insight into the properties of the structure under investigation the geometric parameters along with the effective permittivity can be tailored according to the elastic features of the scatterers. These might include either the medium preference

[5, 6], or an some external factors, i.e., either electric field [7] or temperature [8].

Aiming to achieve propagation of acoustic waves in metamaterials, both density and stiffness should be negative. Recently, scientists made several suggestions and experiments aiming to attain negative effective parameters for acoustic metamaterials. To do so, different procedures, for instance, implanting soft inclusions in fluids [9], using Helmholtz resonators [10] and pipe-membrane compounds [11], have been employed.

The goal of this study is to demonstrate possibilities to construct a metamaterial exhibiting negative effective parameters and show that acoustic waves can be characterized by unusual behavior. Aiming to achieve this goal, we have chosen the structures that are composites of a hexagonal array of metal nanowires in a dielectric medium. An indefinite medium with a metallic nanowire array embedded in a dielectric matrix is not affected by the magnetic resonance and operates over a broad range of frequency with much lower material loss [12]. Such an anisotropic material possesses a negative electric permittivity along the nanowires and a positive permittivity perpendicular to the wires, i.e., indefinite permittivity, resulting in a hyperbolic dispersion. A great number of existing effective-medium theories [13] are limited to the optical response of nanowires that are isotropically distributed in the host material. The predicted response of these systems is not influenced by nanowire distribution and is characterized by the nanowire concentration

✉ Tatjana Gric
tatjana.gric@vgtu.lt

¹ Department of Electronic Systems, Vilnius Gediminas Technical University, Vilnius, Lithuania

² Aston Institute of Photonic Technologies, Aston University, Birmingham B4 7ET, UK

³ Semiconductor Physics Institute, Center for Physical Sciences and Technology, Vilnius, Lithuania

⁴ Interdisciplinary Center of Critical Technologies in Medicine, Saratov State University, 83 Astrakhanskaya Street, Saratov 410012, Russia

⁵ Peter the Great St. Petersburg Polytechnic University, St. Petersburg 195251, Russia

only. These existing techniques are therefore not applicable for practical composites where the geometry is anisotropic due to fabrication process or as a result of a controlled mechanical deformation. Herein, we deal with a practical homogenized acoustic metamaterial for surface plasmon polariton guiding. It should be mentioned that the hyperbolic structures under investigation have already attracted interest before [14, 15]. Similar approaches have already been conducted for the optical frequency ranges [16–18]. However, to the best of our knowledge, the enhanced structure based on the hexagonal distribution of the nanowires has not been used for acoustic SPP propagation before.

Homogenization of Periodic Phononic Crystals

Mathematical Model

A metamaterial structure under investigation is comprised of the building blocks composed of periodically arranged metallic cylinders made either of silver or gold implanted in a dielectric. These metals are chosen as the metallic nanowire materials for their lowest loss at the investigated frequency range. Figure 1 is a schematic illustration of the nanowire metamaterial. Figure 1 presents the anticipated geometrical drawing of the nanowire structures. Nanowires are implanted in a host material.

Nanowire filling fraction is described as:

$$f = \frac{\text{nanowire area}}{\text{unit cell area}} \quad (1)$$

The nanowire filling ratio is calculated on the basis of the evaluation of the nanowire diameter (d) and spacing (S). It is assumed that the structure under consideration possesses a perfect hexagonal distribution. Doing so, we employ the equation as follows [18]:

$$f = \frac{\pi d^2}{2\sqrt{3}S^2} \quad (2)$$

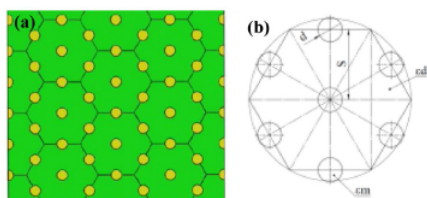


Fig. 1 Schematic illustration of the nanowire composite (a) metamaterial unit cell (b)

By proceeding further with this assumption, one may obtain a dispersion equation to characterize the modes propagating at the acoustic metamaterial interface.

Effective Constitutive Parameters

Herein, we study a composite containing rods with a perfect hexagonal distribution embedded in a fluid host. Nanowires are characterized by a round cylindrical shape and are made of elastic materials. Host material supports propagation of acoustic waves. It is worthwhile mentioning that in this case, wave number is perpendicular to the generatrix of the rods. A composite under consideration is quasi-isotropic. Doing so, geometrical dimensions of the inclusions needed to form the building blocks [19] are much smaller than the wavelength. We have made an assumption that all cylinders are identical. Moreover, they are distributed in a random order. It is worthwhile mentioning that distance between them is approximately equal. Our goal is to calculate the values of the effective parameters of a composite at a frequency range under consideration. Dispersion of the supported acoustic wave is also of particular interest.

Sonic or phononic crystals have provided a fertile ground for dealing with the composites for guiding acoustic or elastic waves. It is worthwhile noting, that in the low-frequency limit, an anisotropic compound exhibits behavior of a homogeneous composite described by outstanding effective features. The plane wave expansion method stands for as an alternative approach to multiple scattering aiming to perform homogenization of highly anisotropic medium consisting of periodic building blocks. The former methodology was for the first time considered by Krokhin [20] for sonic crystals and generalized for non-local phononic crystals in [21].

The system can be efficiently treated as a homogeneous uniaxial anisotropic material with a density parallel to wires ($\rho_{||}$) and a density vertical to wires (ρ_{\perp}) [22, 23] if the wavelength of supported wave is much longer than the period of the array containing distributed nanorods. The derived expressions can be used in the low-frequency limit to get the effective parameters as follows:

$$\rho_{||} = (1-f)\rho_d + f\rho_m \quad (3)$$

$$\rho_{\perp} = \rho_d \left[\frac{\rho_m(1+f) + \rho_d(1-f)}{\rho_m(1-f) + \rho_d(1+f)} \right] \quad (4)$$

In a conventional case of a two-dimensional distribution of nanowire enclosures (parameters labeled with “m”) in a fluid background (parameters labeled “d”), f is the filling ratio of the crystal calculated by dividing area of the enclosures by the area of the unit cells. Aiming to modify the frequency range under consideration, one may apply the

effective-medium theory designed for the specific frequency range [24].

It is possible to drastically alter the parameters under investigation by the dispersive corrections. For instance, the resonant Lorentz-type dispersion of the density [25] might be considered:

$$\rho(\omega) = \rho_0 \omega_0^2 / (\omega_0^2 - \omega^2) \quad (5)$$

Herein, $\rho_0 > 0$ is a constant and ω_0 is the resonant frequency of microresonators in the compound.

Some important relationship between the permittivity and the bulk density of the air-particle mixture is needed if the dielectric features of granular or powdered solid materials are taken into consideration. Fundamentally, linearly dependent functions of the real and imaginary parts of the complex permittivity characterizing the specific materials such as pulverized coal, wheat, and whole-wheat flour and their bulk densities have already been found before [26, 27]. The former formalism is based on earlier studies. The linearity of $\sqrt{\epsilon'}$ was observed by Klein [28]. Quadratic nature of ϵ' and ϵ'' was found by Kent [29] as follows:

$$\epsilon' = a\rho^2 + b\rho + 1 \quad (6)$$

$$\epsilon'' = c\rho^2 + d\rho \quad (7)$$

Herein, ρ characterizes the density of the air-particle mixture and a , b , c , and d are constant values for a given particular material. It is worthwhile mentioning that ϵ' and ϵ'' have values of 1 and 0, respectively, for air alone ($\rho = 0$).

Surface Acoustic Wave

It is worthwhile mentioning that surface waves cannot propagate at the boundary between two ideal fluids. The main reason lies in the fact of impossibility to satisfy boundary conditions in this case. Boundary states can be excited [25] if one of the materials possesses a parameter with negative values. The former provides a fertile ground for a direct analogy to surface plasmon states in plasma with $\epsilon < 0$ [19].

Herein, we investigate a wave supported at the boundary separating a pure host fluid and a fluid containing nanowires implanted in a host material. The dispersion relation aiming to have a deeper insight into the properties of a surface wave is calculated as follows:

$$\beta = k \left[\frac{(1 - \epsilon_{||})\epsilon_{\perp}}{1 - \epsilon_{\perp}\epsilon_{||}} \right]^{1/2} \quad (8)$$

where k is the wavenumber.

Results

In the model employed for calculations, the nanowires are considered to be conventional cylinders. Host material is air. Calculations in case of a bulk wave in the composite are presented in Fig. 2. At low frequencies effective constitutive parameters have a tendency to approach “classic” values for composites [30]. However, at frequencies close to resonances inside the inclusions, the values of dynamical effective parameters are significantly altered.

Figure 2a demonstrates frequency dependence of the dynamical effective density. Because of the complex shear and longitudinal field distribution inside inclusion, resonances of different nature related to shear waves and longitudinal waves might be observed. Thus, there is a significant amount of the frequency ranges where the real part of the dynamical effective density is negative. In Fig. 2b

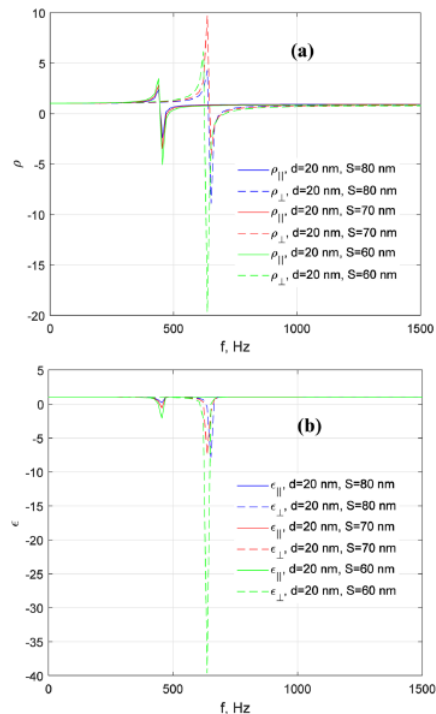


Fig. 2 Effective density (a) and permittivity (b) versus frequency for the composite under study

1838

Plasmonics (2021) 16:1835–1839

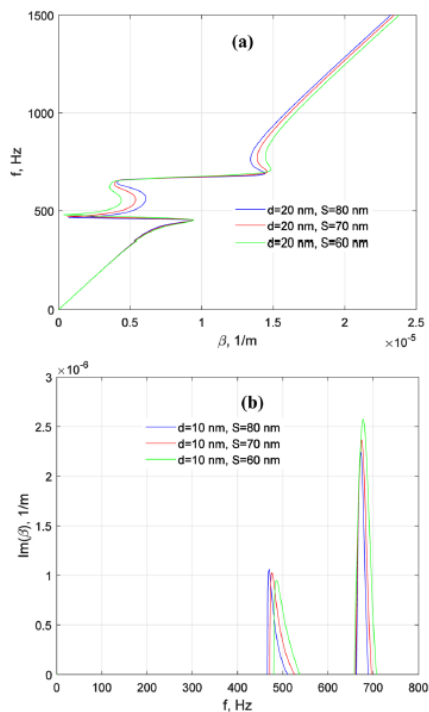


Fig. 3 The dispersion pattern of modes of surface plasmon polaritons supported by a structure under consideration demonstrated in Fig. 1: **a** $\text{Re}(\beta)$ and **b** $\text{Im}(\beta)$

permittivity versus frequency is depicted. It is worthwhile mentioning that dimensions of the nanowires along with the distances between them have been chosen in order to meet the manufacturing requirements [31].

In what follows (Fig. 3), we have studied acoustic surface waves of the Rayleigh type, i.e., surface waves supported by the surface of a semi-infinite elastic metamaterial in vacuum. It is worthwhile mentioning that the frequency for SPP propagation is determined by negative permittivity. As expected, there exists a common surface waves gap; in addition, when approaching asymptotic frequency from the low frequency direction, all the dispersion curves become very flat and asymptotically reach infinity, exhibiting behavior very similar to that of EM surface plasmon polaritons.

Conclusions

Herein, effective dynamic density of composite consisting of nanowires embedded in a host material in terms of coherent potential approximations is calculated. It is demonstrated that there are frequency regions in which dynamic constitutive parameters are instantaneously negative. In this relation, the wave under consideration becomes backward.

Dispersion pattern of the acoustic wave propagating at the boundary separating metamaterial and conventional medium is studied. It is demonstrated that there are frequency ranges in which the surface states are bounded to the interface. Moreover, the exotic behavior of surface plasmon polaritons has been investigated.

In summary, we presented modeling of the acoustic metamaterial. The wide spectral width of the present research for acoustic double negative metamaterials is expected. Moreover, anticipated applications including acoustic superlensing and cloaking [25, 32–34] might be possible.

Author Contributions Conceptualization, data curation, and methodology, T.I.; investigation, formal analysis, software, visualization, writing—original draft preparation, writing—review, and editing, T.I.; T.G.; E.R.; supervision and revision of the manuscript and validation, T.G.; E.R. All authors have read and agreed to the published version of the manuscript.

Funding This project has received funding from the European Union's Horizon 2020 research and innovation program under the Marie Skłodowska Curie grant agreement No 713694 and from Engineering and Physical Sciences Research Council (EPSRC) (Grant No. EP/R024898/1). The work of E.U. Rafailov was partially funded by the Ministry of Science and Higher Education of the Russian Federation as part of World-class Research Center program: Advanced Digital Technologies (contract No. 075-15-2020-934 dated 17.11.2020).

Data Availability The data that support the findings of this study are available from the corresponding author upon reasonable request.

Code Availability All simulation parameters of this study are included in this manuscript.

Declarations

Conflict of Interest The authors declare that they have no conflict of interest.

References

- Pennec Y, Vasseur JO, Djafari-Rouhani B, Dobrzyński L, Deymier PA (2010) Two-dimensional phononic crystals: Examples and Applications. *Surf Sci Rep* 65:229–291
- Ge H, Yang M, Ma C et al (2017) Breaking the barriers: advances in acoustic functional materials. *Nat Sci Review* 5:159–182

3. Khelif A, Adibi A (2015) Phononic crystals: fundamentals and applications. Springer, Berlin
4. Ma G, Sheng P (2016) Acoustic metamaterials: from local resonances to broad horizons. *Sci Adv* 2:e1501595
5. Lin S-CS, Huang TJ, Sun J-H, Wu T-T (2009) Gradient-index phononic crystals. *Phys Rev B* 79:094302
6. Titovich AS, Norris AN, Haberman MR (2016) A high transmission broadband gradient index lens using elastic shell acoustic metamaterial elements. *J Acoust Soc Am* 139:3357–3364
7. Yi K, Collet M, Ichchou M, Li L (2016) Flexural waves focusing through shunted piezoelectric patches. *Smart Mater Struct* 25:075007
8. Yong G, Hong-Xiang S, Chen L et al (2016) Acoustic focusing by an array of heat sources in air. *Appl Phys Express* 9:066701
9. Li J, Chan CT (2004) Double-negative acoustic metamaterial. *Phys Rev E* 70:055602
10. Fang N, Xi D, Xu J, Ambati M, Sritravanich W, Sun C, Zhang X (2006) Ultrasonic metamaterials with negative modulus. *Nat Mater* 5:452–456
11. Lee SH, Park CM, Seo YM, Wang ZG, Kim CK (2010) Composite acoustic medium with simultaneously negative density and modulus. *Phys Rev Lett* 104:054301
12. Liu Y, Bartal G, Zhang X (2008a) All-angle negative refraction and imaging in a bulk medium made of metallic nanowires in the visible region. *Opt Exp* 16(15):439–448
13. Milton GW (2002) The theory of composites. Cambridge University Press, Cambridge
14. Wong ZJ, Wang Y, O'Brien K, Rho J, Yin X, Zhang S, Fang N, Yen T-J, Zhang X (2017) Optical and acoustic metamaterials: superlens, negative refractive index and invisibility cloak. *J Opt* 19:084007
15. Fan B, Filonov D, Ginzburg P, Podolskiy VA (2018) Low-frequency nonlocal and hyperbolic modes in corrugated wire metamaterials. *Opt Express* 26:17541–17548
16. Ioannidis T, Gric T, Gorodetsky A, Trofimov A, Rafailov E (2019) Enhancing the properties of plasmonic nanowires. *Materials research express* 6:1–8
17. Ioannidis T, Gric T, Rafailov E (2020) Surface plasmon polariton waves propagation at the boundary of graphene based metamaterial and corrugated metal in THz range. *Opt Quant Electron* 52:1–12
18. Starko-Bowes R, Atkinson J, Newman W, Hu H, Kallos T, Palikaras G, Fedosejevs R, Pramanik S, Jacob Z (2015) Optical characterization of epsilon near zero, epsilon near pole and hyperbolic response in nanowire metamaterials. *J Opt Soc Am B* 32:2074–2080
19. Caloz C, Itoh T (2005) Electromagnetic metamaterials: transmission line theory and microwave applications. Wiley-IEEE Press, Hoboken/New Jersey
20. Krokhin AA, Arriaga J, Gumen LN (2003) Speed of sound in periodic elastic composites. *Phys Rev Lett* 91:264302
21. Norris AN, Shuvalov AL, Kutsenko AA (2012) Analytical formulation of three-dimensional dynamic homogenization for periodic elastic systems. *Proc Roy Soc A-Math Phys Eng Sci* 468:1629–1651
22. Liu Y, Bartal G, Zhang X (2008b) All-angle negative refraction and imaging in a bulk medium made of metallic nanowires in the visible region. *Opt Exp* 16:15439–15448
23. Podolskiy VA, Narimanov EE (2005) Strongly anisotropic waveguide as a nonmagnetic left-handed system. *Phys Rev B* 71:201101
24. Gric T, Hess O (2017) Surface plasmon polaritons at the interface of two nanowire metamaterials. *J Opt* 19:085101
25. Ambati M, Fang N, Sun C, Zhang X (2007) Surface resonant states and superlensing in acoustic metamaterials. *Phys Rev B* 75:195447
26. Nelson SO (1983) Observations on the density dependence of the dielectric properties of particulate materials. *J Microw Power* 18(2):143–152
27. Nelson SO (1984) Density dependence of the dielectric properties of wheat and whole-wheat flour. *J Microw Power* 19(1):55–64
28. Klein A (1981) Microwave determination of moisture in coal—comparison of attenuation and phase measurement. *J Microw Power* 16(3&4):289–304
29. Kent M (1977) Complex permittivity of fish meal: a general discussion of temperature, density, and moisture dependence. *J Microw Power* 12(4):341–345
30. Berryman G (1809) Long-wavelength propagation in composite elastic media I. Spherical inclusions. *J Acoust Soc Am* 1980:68
31. Yao BJ, Wang Y, Tsai K-T, Liu Z, Yin X, Bartal G, Stacy AM, Wang Y-L, Zhang X (2011) Design, fabrication and characterization of indefinite metamaterials of nanowires. *Phil Trans R Soc A* 369:3434–3446
32. Guenneau S, Movchan A, P'etursson G, Ramakrishna SA, (2007) Acoustic metamaterials for sound focusing and confinement. *New J Phys* 9:399
33. Chen H, Chan CT (2007) Acoustic cloaking in three dimensions using acoustic metamaterials. *Appl Phys Lett* 91:183518
34. Torrent D, Sanchez-Dehesa J, (2008) Acoustic cloaking in two dimensions: A feasible approach. *New J Phys* 10:063015

Publisher's Note Springer Nature remains neutral with regard to jurisdictional claims in published maps and institutional affiliations.

Article 4. Ioannidis et al. (2021). The study of the surface plasmon polaritons at the interface separating nanocomposite and hypercrystal (<https://doi.org/10.3390/app11115255>)



Article

The Study of the Surface Plasmon Polaritons at the Interface Separating Nanocomposite and Hypercrystal

Thanos Ioannidis ¹, Tatjana Gric ^{1,2,3,*} and Edik Rafailov ^{2,4}

¹ Department of Electronic Systems, VILNIUS TECH, 10223 Vilnius, Lithuania; athanasios.ioannidis@vgtu.lt

² Aston Institute of Photonic Technologies, Aston University, Birmingham B4 7ET, UK; e.rafailov@aston.ac.uk

³ Semiconductor Physics Institute, Center for Physical Sciences and Technology, 02300 Vilnius, Lithuania

⁴ Peter the Great St. Petersburg Polytechnic University, 195251 St. Petersburg, Russia

* Correspondence: tatjana.gric@vilniustech.lt

Abstract: Surface plasmon polaritons (SPPs) propagating at the interfaces of composite media possess a number of fascinating properties not emerging in case of conventional SPPs, i.e., at metal-dielectric boundaries. We propose here a helpful algorithm giving rise for investigation of basic features of complex conductivity dependent SPPs at the interface separating nanocomposite and hypercrystal. The main goal of the work is to investigate dispersion of the SPPs propagating at the boundary separating two different media. Aiming to achieve the aforementioned goal that the effective Maxwell Garnett model is used. It is demonstrated that the SPPs dispersive properties are dramatically affected by the material conductivity. Correspondingly, the filling ratio of the nanoparticles in the composite and their dielectric properties also allow one to engineer characteristics of the SPPs. Having a deep insight into the conductivity dependent functions, we concluded, on their behavior for the case of hyperbolic regime and Dyakonov surface waves case. Our model gives rise for studying features of surface waves in the complex conductivity plane and provides more options to tune the fundamental features of SPPs at the boundaries correlated with composite media.

Keywords: conductivity; surface plasmon polaritons; metamaterial



Citation: Ioannidis, T.; Gric, T.; Rafailov, E. The Study of the Surface Plasmon Polaritons at the Interface Separating Nanocomposite and Hypercrystal. *Appl. Sci.* **2021**, *11*, 5255. <https://doi.org/10.3390/app11115255>

Academic Editor:
Dimitrios Zografopoulos

Received: 7 May 2021
Accepted: 3 June 2021
Published: 5 June 2021

Publisher's Note: MDPI stays neutral with regard to jurisdictional claims in published maps and institutional affiliations.



Copyright © 2021 by the authors. Licensee MDPI, Basel, Switzerland. This article is an open access article distributed under the terms and conditions of the Creative Commons Attribution (CC BY) license (<https://creativecommons.org/licenses/by/4.0/>).

1. Introduction

During the last decades plasmonics attracted significant attention as the novel field pivoting the way for modern technologies, such as spectroscopy and sensing [1] and optical tweezers [2]. Surface plasmons (SPs) are introduced as the collective oscillations of the delocalized electrons presenting at metal-dielectric interfaces. SPs open the wide avenues to escape the diffraction limit of conventional optics [3] because of their capability to confine light in subwavelength dimensions with high efficiency. Doing so, the previous provides a fertile ground for a broad spectrum of applications ranging from surface enhanced spectroscopy [4], biomedical sensing [5] and solar cell photovoltaics [6] to optical antennas [7]. It is worthwhile noting that surface-plasmon-based circuits are established to bridge the disciplines of photonics and electronics at the nanoscale. The former allows to escape the current problems associated with the large size difference between the micrometer-scale bulky components of photonics and the nanometer-scale electronic chips.

The resonant oscillations of free electrons at the interface of nanocomposite media due to optical radiations give rise to surface plasmon polaritons (SPPs) [8]. The propagation of SPPs in nanocomposites has been extensively studied in [9–11]. Composite media with metal nanoparticles are of particular importance aiming to create nanostructured metal-insulator systems and novel approaches of manipulating light based on them. The emerge of transparent conductive oxides (TCOs) has attracted tremendous interest within the scientific community. These stand for as the alternative approach for plasmonics [12] in the near-infrared region. In contrary to noble metals, TCOs such as indium tin oxide (ITO) demonstrate a great tunability of their optical and electronic properties [13]. The former is

possible via doping and electric bias. The construction and fabrication of ultra-compact electroabsorption modulators [14] and for the proposal of new multimode modulator architectures [15] has benefited from the option of actively switching between a low-loss dielectric regime and a high-absorption plasmonic regime.

In the present work, we discuss complex conductivity of the medium, which dramatically affects tunability of SPPs. The obtained results may have significant applications in storage and sensing devices. Herein, we provide a detailed study of SPPs characteristics at the interface separating a nanocomposite and hypercrystal. Engineering properties of the nanocomposite and that of hypercrystal, the SPPs properties are tuned significantly. We present a complete description of the SPPs dispersion relation with different controlling parameters. Our study is extended aiming to examine the complex conductivity dependent properties.

2. Materials and Methods

Herein, we deal with the plane boundary separating a nanocomposite (NC) semi-infinite layer, which fills the half-space $x < 0$ and adjacent to it, hypercrystal filling the half-space $x > 0$ (Figure 1). It should be stressed that the surface waves under consideration propagate along z axis. It is worthwhile noting that the structure under the study can be constructed by means of molecular beam epitaxy [16], chemical vapor deposition, atomic layer deposition and sacrificial etching [17]. The nanocomposite is presented as a non-conductive transparent matrix with a permittivity ϵ_n , in the volume of which regularly distributed semiconductor nanoparticles with permittivity ϵ_m . The frequency dependent dielectric function of the TCO based nanoparticles is of particular interest. An emergence of high-conducting metal being transparent has opened wide avenues recently. The issue has attracted lots of interest within the scientific community because of the metal being opaque for light. From the perspectives of the potential applications, transparent conducting metals described by high DC conductivity (σ_{DC}) are anticipated for optoelectronic devices, ranging from solar cells to electronic paper, touch screens and displays. Though, since $\sigma_{DC} = n_e e^2 \tau / m$ (with τ being relaxation time of the electron and m —electron mass) of a metal is associated with plasmon frequency $\omega_p^2 = n_e e^2 / \epsilon_0 m$ through the free-electron density n_e , a high-conducting metal (with a high n_e) is certainly opaque for light because of its permittivity ϵ being typically very negatively affected by its high ω_p . Conventional techniques to produce transparent conducting metals include the decrease of the n_e , by utilizing transparent conducting oxides (TCOs). The parameters of the Drude–Lorentz approach for aluminum-doped zinc oxide (AZO), Ga-doped ZnO (GZO) and indium tin oxide (ITO) gained from experimental data [12] are presented in Table 1.

Table 1. Drude–Lorentz parameters of plasmonic materials obtained from experimental data. One may approximate the materials dielectric function by the complex dielectric function: $\epsilon_{TCO} = \epsilon_b - \frac{\omega_p^2}{\omega(\omega + i\gamma_p)} + \frac{f_l \omega_l^2}{(\omega_l^2 - \omega^2 - i\omega\gamma_l)}$, with the values of the parameters outlined in the table [18]. Here ϵ_b is the polarization response from the core electrons (background permittivity), ω_p is the plasma frequency, γ_p is the Drude relaxation rate.

	AZO	GZO	ITO	TiN (Deposited at 800 °C)	TiN (Deposited at 500 °C)	ZrN
ϵ_b	3.54	3.23	3.53	4.86	2.49	3.47
ω_p (eV)	1.75	1.99	1.78	7.93	5.95	8.02
γ_p (eV)	0.04	0.12	0.16	0.18	0.51	0.52
f_l	0.51	0.39	0.39	3.29	2.04	2.45
ω_l (eV)	4.29	4.05	4.21	4.22	3.95	5.48
γ_l (eV)	0.10	0.09	0.09	2.03	2.49	1.74

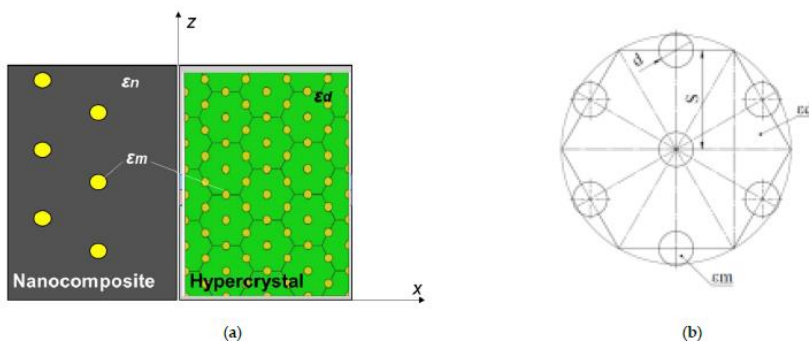


Figure 1. Schematic system under consideration, involving a semi-infinite hypercrystal ($x > 0$) and a nanocomposite with semiconductor inclusions ($x < 0$) (a) and metamaterial (hypercrystal) unit cell (b).

The dielectric function of metallic medium in the complex conductivity and frequency domain is written as [19]:

$$\varepsilon_r(\sigma, \omega) = 1 + \left(\chi + \frac{|\sigma|e^{i\phi}}{\omega\varepsilon_0} \right) \quad (1)$$

where χ is the susceptibility of the system, $|\sigma|$ is absolute value of complex conductivity and ϕ is its phase.

The dispersion relation of SPPs at a planar interface between the dielectric medium and metal forming a simple plasmonic structure in the complex conductivity and frequency domain is written as [20]:

$$k_{sp}(\sigma, \omega) = \frac{2\pi}{\lambda} \sqrt{\frac{\varepsilon_r(\sigma, \omega)\varepsilon_d}{\varepsilon_r(\sigma, \omega) + \varepsilon_d}} \quad (2)$$

where ε_d is the permittivity of the host material. By making a step forward towards complex nanostructures, we made an assumption that the wavelength and the electromagnetic field penetration depth in the material are much larger than the size of inclusions suspended in a dielectric matrix. It is worthwhile mentioning that effective Maxwell Garnett model can be employed aiming to characterize the optical properties of the nanocomposite under consideration. The former approach is possible, if the interference effects of the inclusions are neglected and their volume fraction is as small as $1/3$. Thus, one may apply the homogenization procedure and the effective complex permittivity of the nanocomposite can be expressed as follows

$$\varepsilon_{nc}(\sigma, \omega) = \varepsilon_n \left[1 + \frac{f}{(1-f)/3 + \varepsilon_n/(\varepsilon_m(\sigma, \omega) - \varepsilon_n)} \right] \quad (3)$$

where ε_n is the permittivity of the host material of the nanocomposite and f is the number of nanoparticles in the matrix.

Based on the effective medium approximation one may calculate the effective permittivities of the anisotropic nanowire metamaterial (hypercrystal) according to [21]:

$$\varepsilon_{\perp}(\sigma, \omega) = \varepsilon_d \left[\frac{\varepsilon_m(\sigma, \omega)(1+\rho) + \varepsilon_d(1-\rho)}{\varepsilon_m(\sigma, \omega)(1-\rho) + \varepsilon_d(1+\rho)} \right] \quad (4)$$

$$\varepsilon_{\parallel}(\sigma, \omega) = \varepsilon_m(\sigma, \omega)\rho + \varepsilon_d(1-\rho) \quad (5)$$

where ϵ_d is the permittivity of the host material, ϵ_m is the permittivity of the inclusions embedded into the host material and ρ is the metal filling fraction ratio, which is calculated as:

$$\rho = \frac{\text{nanowire area}}{\text{unit cell area}} \quad (6)$$

The metal filling fraction (ρ) is calculated based on the values of the pore diameter (d) and spacing (S) (Figure 1b). By taking into account a perfect hexagonal structure, the equation [22,23] is applied as follows:

$$\rho = \frac{\pi d^2}{2\sqrt{3}S^2} \quad (7)$$

Based on this assumption one may derive a dispersion relation for the surface modes propagating at the interface between two anisotropic media. It is of particular importance to obtain a single surface mode with the propagation constant [24] by calculating the tangential components of the electric and magnetic fields at the interface

$$\beta(\sigma, \omega) = k \left(\frac{(\epsilon_{||}(\sigma, \omega) - \epsilon_{nc}(\sigma, \omega)) \epsilon_{\perp}(\sigma, \omega) \epsilon_{nc}(\sigma, \omega)}{\epsilon_{\perp}(\sigma, \omega) \epsilon_{||}(\sigma, \omega) - \epsilon_{nc}^2(\sigma, \omega)} \right)^{1/2} \quad (8)$$

By substituting (3)–(5) in (8), one may result in the dispersion relation as follows:

$$\beta(\sigma, \omega) = k \left(- \frac{\epsilon_n b(\sigma, \omega) a(\sigma, \omega) (\epsilon_n a(\sigma, \omega) + \epsilon_m(\sigma, \omega) \rho - \epsilon_d(\rho - 1))}{\left(\epsilon_n^2 a(\sigma, \omega)^2 + \frac{\epsilon_m(\sigma, \omega) \rho - \epsilon_d(\rho - 1)}{\epsilon_d(\rho + 1) - \epsilon_m(\sigma, \omega)(\rho - 1)} b(\sigma, \omega) \right) (\epsilon_d(\rho + 1) - \epsilon_m(\sigma, \omega)(\rho - 1))} \right)^{1/2} \quad (9)$$

$$a(\sigma, \omega) = \frac{f}{5 + \frac{\epsilon_m}{\epsilon_n - \epsilon_m(\sigma, \omega)} - 3} - 1, \quad b(\sigma, \omega) = (\rho - 1) \epsilon_d^2 - \epsilon_m(\sigma, \omega) \epsilon_d(\rho + 1).$$

It is worthwhile noting, that Equation (9) stand for as the analytical expression of the dispersion relations investigated in the frame of the present work.

3. Results

The propagation of SPPs at the boundary of nanocomposite and hypercrystal is investigated. The absolute value of complex conductivity $|\sigma|$ varies from 0 to 6×10^7 S/m. Herein, the permittivity components of a hypercrystal and nanocomposite versus frequency are studied numerically aiming to identify the frequency ranges of Dyakonov surface waves (DSWs) and SPP waves existence (Figure 2). In the frequency ranges below the frequency ω_{110} [25] the semiconductor-dielectric metamaterial possesses hyperbolic properties. It is worthwhile noting that in this frequency range the presence of conventional surface plasmon polaritons waves with propagation parallel to the optical axis is feasible under specific conditions. One may conclude from Figure 2 that propagation of DSW is possible in case of $\epsilon_n = 2.25$, $\epsilon_d = 11.8$. It is worthwhile noting that the regime of DSW propagation takes place if $\epsilon_{||}(\omega)$, $\epsilon_{nc}(\omega) > 0$. To have a deeper insight into the problem, we investigated permittivity components versus conductivity. Doing so, in Figure 3 permittivity function is plotted if $\omega = 0.3 \times 10^{14}$ Hz (Figure 3a) and $\omega = 3 \times 10^{14}$ Hz (Figure 3b). The former allows us to investigate conductivity dependent permittivity functions for both regimes, i.e., hyperbolic and conventional. Moreover, we studied the phenomenon of conductivity dependent functions for the DSW regime (Figure 4a). Comparing Figures 3a and 4a, one may conclude that $\epsilon_{nc}(\sigma) > \epsilon_{\perp}(\sigma)$ in case of the hyperbolic regime and $\epsilon_{nc}(\sigma) < \epsilon_{\perp}(\sigma)$ for DSW waves. Moreover, it is interesting to compare the conditions that are valid in case of hyperbolic and DSW regimes for both, i.e., frequency and conductivity dependent functions. Thus, it is seen in Figure 2a that hyperbolic properties of metamaterial are possible if $\epsilon_{nc}(\omega)$, $\epsilon_{\perp}(\omega) > 0$ and $\epsilon_{||}(\omega) < 0$. Dealing with the conductivity dependent functions, one may conclude that the same conditions are needed in other to obtain hyperbolic

regime. On the contrary to the described case conditions for existence of DSW regime are different in two different planes, i.e., DSW is obtainable if $\epsilon_{nc}(\omega)$, $\epsilon_{\perp}(\omega)$, $\epsilon_{\parallel}(\omega) > 0$ and if $\epsilon_{nc}(\sigma)$, $\epsilon_{\perp}(\sigma) > 0$, $\epsilon_{\parallel}(\sigma) < 0$.

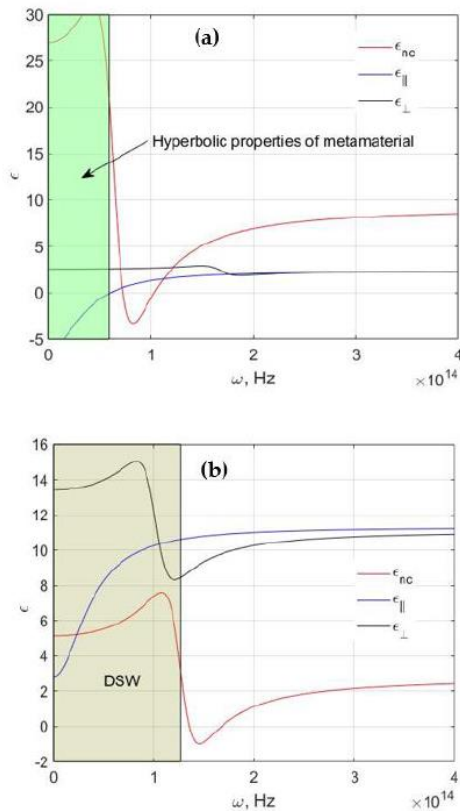


Figure 2. Relative permittivity components of the nanocomposite and hypercrystal versus frequency. Herein, $f = 0.3$. (a) $\epsilon_n = 11.8$, $\epsilon_d = 2.25$; (b) $\epsilon_n = 2.25$, $\epsilon_d = 11.8$. Herein ITO inclusions are employed in nanocomposite and hypercrystal.

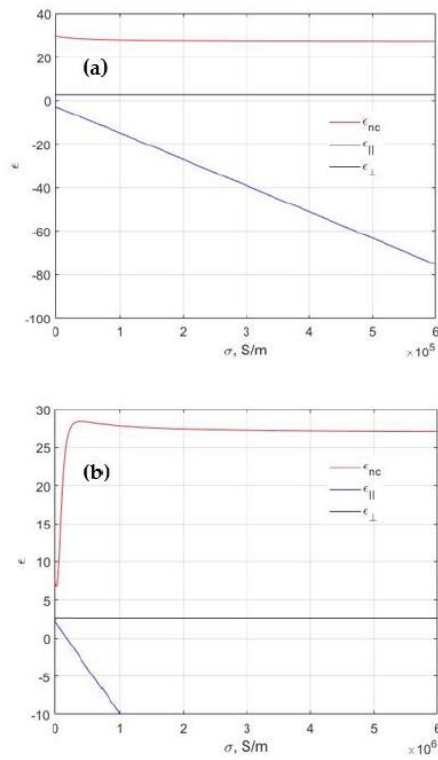


Figure 3. Relative permittivity components of the nanocomposite and hypercrystal versus conductivity. Herein, $f = 0.3$, $\epsilon_H = 11.8$, $\epsilon_d = 2.25$. Herein ITO inclusions are employed in nanocomposite and hypercrystal. (a) $\omega = 0.3 \times 10^{14}$ Hz; (b) $\omega = 3 \times 10^{14}$ Hz.

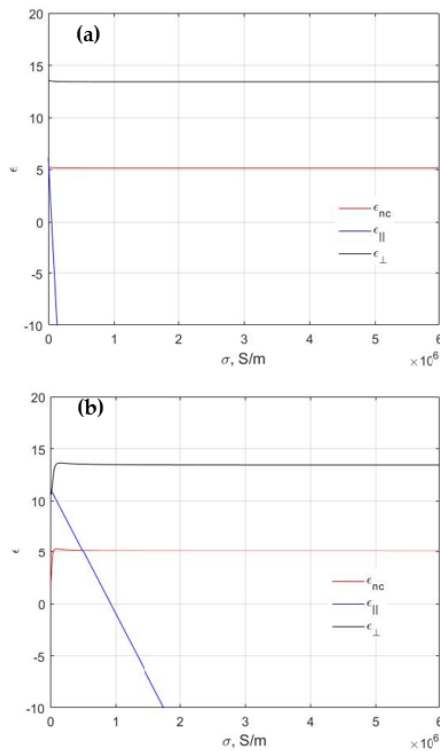


Figure 4. Relative permittivity components of the nanocomposite and hypercrystal versus conductivity. Herein, $f = 0.3$, $\epsilon_n = 2.25$, $\epsilon_d = 11.8$. Herein ITO inclusions are employed in nanocomposite and hypercrystal. (a) $\omega = 0.3 \times 10^{14} \text{ Hz}$; (b) $\omega = 3 \times 10^{14} \text{ Hz}$.

In Figures 5–10 the plots are obtained for real and imaginary parts of the dispersion relation along with the transmittance characteristics. The real part of propagation constant is related to group velocity and the imaginary part is related to damping of SPPs. If $\text{Re}(\beta) > k_0$ then SPPs propagate at the interface and if $\text{Re}(\beta) < k_0$ then SPPs cannot propagate at the interface of two media. $k_0 = 2\pi\omega/c$ is the wave vector of the electromagnetic wave in free space. Here $\omega_1 = 0.3 \times 10^{14} \text{ Hz}$, $\omega_2 = 0.3 \times 10^{14} \text{ Hz}$ and $c = 3 \times 10^8 \text{ m/s}$, which gives $k_{01} = 6.28 \times 10^5 \text{ 1/m}$ and $k_{02} = 6.28 \times 10^6 \text{ 1/m}$. The value of $\text{Re}(\beta)$ varies from 0 to $15 \times 10^6 \text{ 1/m}$ versus conductivity. The variations of $\text{Re}(\beta)$ and $\text{Im}(\beta)$ versus conductivity are shown in Figures 5–10. The absolute value of complex conductivity strongly affects the SPPs propagation at the interface of two media. The real part of dispersion relation of SPPs increases with the absolute value of complex conductivity.

In Figures 9 and 10 plots are obtained for the propagation length L_p of SPPs versus the absolute value of complex conductivity. The $\text{Im}(\beta)$ is related to the propagation length L_p .

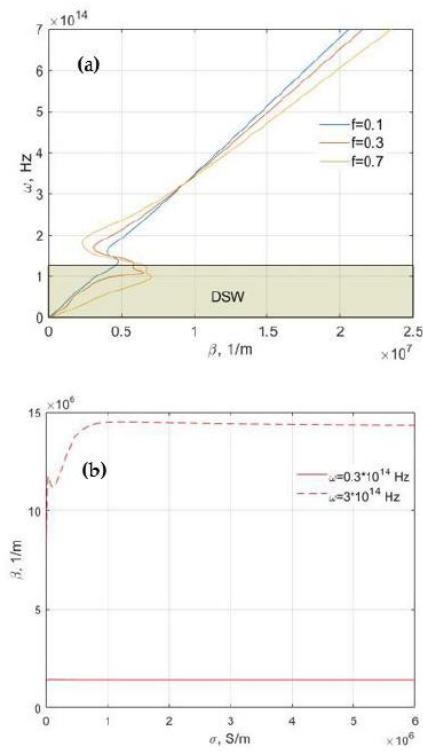


Figure 5. Solution of the dispersion equation versus frequency (a) and versus conductivity (b). $\epsilon_n = 2.25$, $\epsilon_d = 11.8$. Herein ITO inclusions are employed in nanocomposite and hypercrystal, $f = 0.3$ in (b).

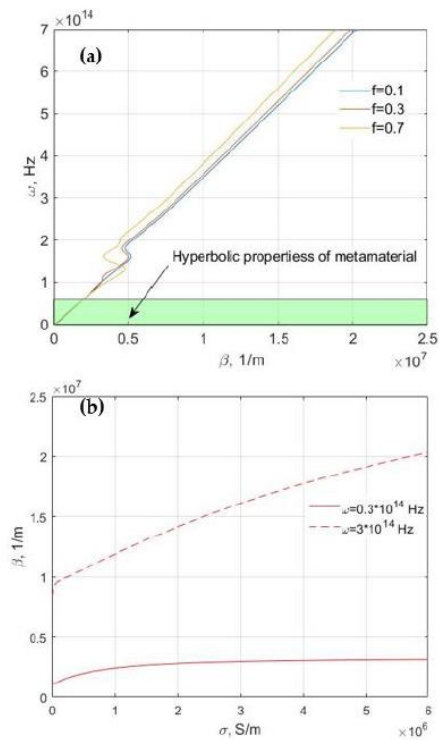


Figure 6. Solution of the dispersion equation versus frequency (a) and versus conductivity (b). $\epsilon_H = 11.8$, $\epsilon_d = 2.25$. Herein ITO inclusions are employed in nanocomposite and hypercrystal, $f = 0.3$ in (b).

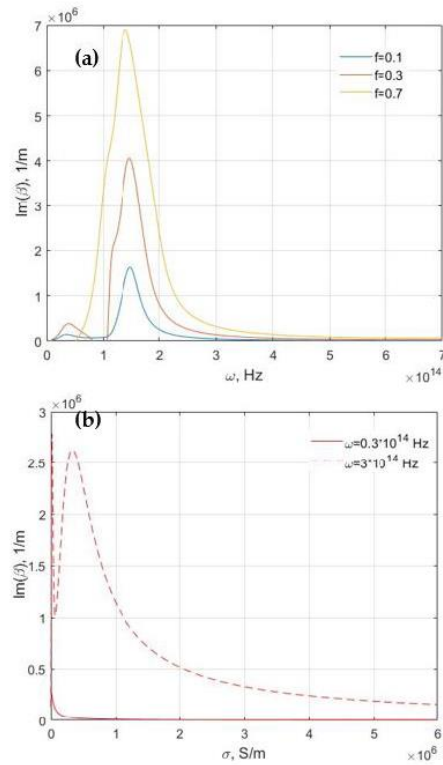


Figure 7. Dependence of imaginary part of propagation constant versus frequency for different filling factors (a) and versus conductivity for $f = 0.3$ (b). $\epsilon_n = 2.25$, $\epsilon_d = 11.8$. All the presented results are obtained for the ITO inclusions.

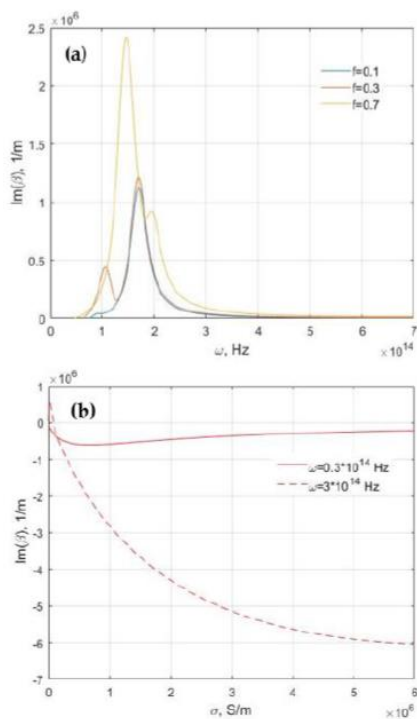


Figure 8. Dependence of imaginary part of propagation constant versus frequency for different filling factors (a) and versus conductivity for $f = 0.3$ (b). $\epsilon_n = 11.8$, $\epsilon_d = 2.25$. All the presented results are obtained for the ITO inclusions.

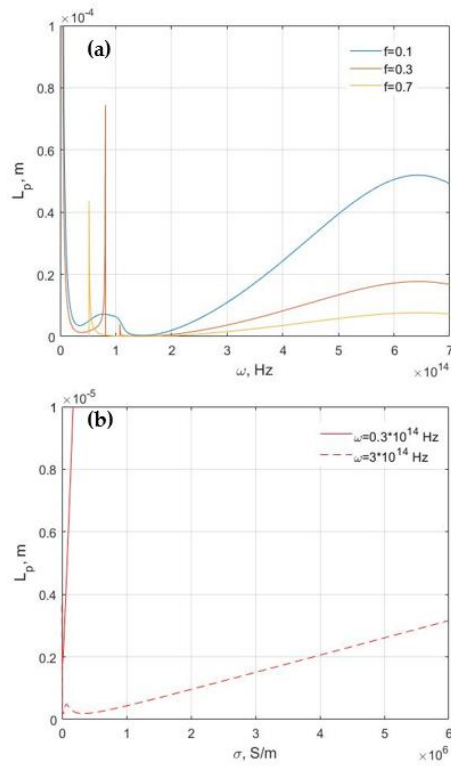


Figure 9. Dependence of propagation length versus frequency for different filling factors (a) and versus conductivity for $f = 0.3$ (b). $\epsilon_H = 2.25$, $\epsilon_d = 11.8$. All the presented results are obtained for the ITO inclusions.

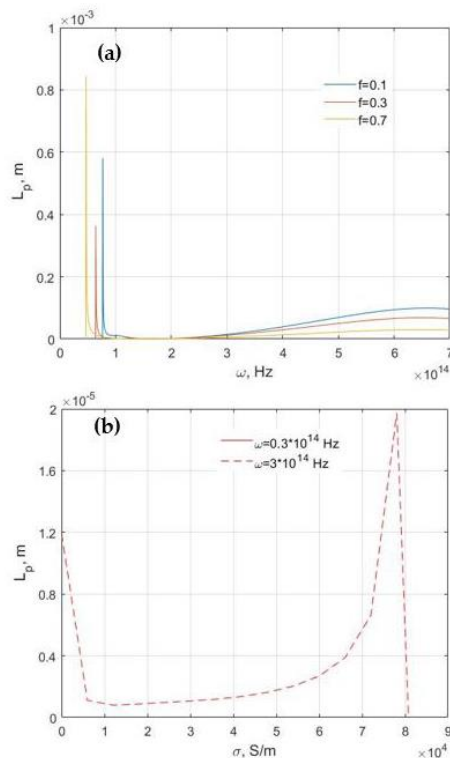


Figure 10. Dependence of propagation length versus frequency for different filling factors (a) and versus conductivity for $f = 0.3$ (b). $\epsilon_H = 11.8$, $\epsilon_d = 2.25$. All the presented results are obtained for the ITO inclusions.

4. Conclusions

In conclusion, the SPPs properties were investigated versus conductivity at the interface of nanocomposite and hypercrystal. The amplitude of complex conductivity significantly influenced the SPPs propagation. The real part of SPPs dispersion relation was very large in comparison with the value of the free space wave-vector $\text{Re}(\beta) > k_0$. It is worthwhile mentioning that propagation of SPPs was achieved at the interface with variation of complex conductivity. The conducted study allows one to conclude on the conditions of surface waves propagation in the complex conductivity plane. Thus, $\epsilon_{nc}(\sigma)$, $\epsilon_{\perp}(\sigma) > 0$ and $\epsilon_{\parallel}(\sigma) < 0$ in the case of hyperbolic regime and $\epsilon_{nc}(\sigma)$, $\epsilon_{\perp}(\sigma) > 0$, $\epsilon_{\parallel}(\sigma) < 0$ for Dyakonov surface waves. The potential applications of this works are in the fields of the development of waveguides sources, near-field optics, surface-enhanced Raman spectroscopy, data storage, solar cells, chemical sensors and biosensors.

Author Contributions: Conceptualization, T.I. and T.G.; methodology, T.I.; software, T.G.; validation, T.G. and E.R.; formal analysis, E.R.; investigation, T.I.; resources, E.R.; data curation, T.G.; writing—original draft preparation, T.I.; writing—review and editing, T.G. and E.R.; visualization, T.I.; supervision, T.G.; project administration, E.R.; funding acquisition, T.G. and E.R. All authors have read and agreed to the published version of the manuscript.

Funding: This project has received funding from the European Union's Horizon 2020 research and innovation program under the Marie Skłodowska Curie grant agreement No 713694 and from Engineering and Physical Sciences Research Council (EPSRC) (Grant No. EP/R024898/1). The work of E.U. Rafailov was partially funded by the Ministry of Science and Higher Education of the Russian Federation as part of World-class Research Center program: Advanced Digital Technologies (contract No. 075-15-2020-934 dated 17.11.2020).

Institutional Review Board Statement: Not applicable.

Informed Consent Statement: Not applicable.

Conflicts of Interest: The authors declare no conflict of interest.

References

- Kneipp, K. Surface-enhanced Raman scattering. *Phys. Today* **2007**, *60*, 40–45. [\[CrossRef\]](#)
- Juan, M.L.; Righini, M.; Quidant, R. Plasmon nano-optical tweezers. *Nat. Photonics* **2011**, *5*, 349. [\[CrossRef\]](#)
- Pendry, J.B. Negative refraction makes a perfect lens. *Phys. Rev. Lett.* **2000**, *85*, 3966–3969. [\[CrossRef\]](#) [\[PubMed\]](#)
- Luo, Y.; Aubry, A.; Pendry, J.B. Electromagnetic contribution to surface-enhanced Raman scattering from rough metal surfaces: A transformation optics approach. *Phys. Rev. B Condens. Matter Mater. Phys.* **2011**, *83*, 155422. [\[CrossRef\]](#)
- Li, J.; Ye, J.; Chen, C.; Hermans, L.; Verellen, N.; Ryken, J.; Jans, H.; Van Roy, W.; Moshchalkov, V.V.; Lagae, L.; et al. Biosensing using diffractively coupled plasmonic crystals: The figure of merit revisited. *Adv. Opt. Mater.* **2015**, *3*, 176–181. [\[CrossRef\]](#)
- Li, X.; Ren, X.; Xie, F.; Zhang, Y.; Xu, T.; Wei, B.; Choy, W.C.H. High-performance organic solar cells with broadband absorption enhancement and reliable reproducibility enabled by collective plasmonic effects. *Adv. Opt. Mater.* **2015**, *3*, 1220–1231. [\[CrossRef\]](#)
- Giannini, V.; Fernández-Domínguez, A.I.; Heck, S.C.; Maier, S.A. Plasmonic nanoantennas: Fundamentals and their use in controlling the radiative properties of nanoemitters. *Chem. Rev.* **2011**, *111*, 3888–3912. [\[CrossRef\]](#)
- Stiens, J.; Vounckx, R.; Veretennicoff, I. Slab plasmon polaritons and waveguide modes in four-layer resonant semiconductor waveguides. *J. Appl. Phys.* **1997**, *81*, 1–4. [\[CrossRef\]](#)
- Singh, M.R.; Racknor, C. Nonlinear energy transfer in quantum dot and metallic nanorod nanocomposites. *J. Opt. Soc. Am. B* **2015**, *32*, 2216–2222. [\[CrossRef\]](#)
- Singh, M.R.; Brasse, G.; Yastrebov, S. Enhancement of Radiative and Nonradiative Emission in Random Lasing Plasmonic Nanofibers. *Annalen Physik* **2021**, *533*, 2000558. [\[CrossRef\]](#)
- Singh, M.R. A Review of Many-Body Interactions in Linear and Nonlinear Plasmonic Nanohybrids. *Symmetry* **2021**, *13*, 445. [\[CrossRef\]](#)
- Naik, G.V.; Shalae, V.M.; Boltasseva, A. Alternative plasmonic materials: Beyond gold and silver. *Adv. Mater.* **2013**, *25*, 3264–3294. [\[CrossRef\]](#)
- Feigenbaum, E.; Diest, K.; Atwater, H.A. Unity-Order Index Change in Transparent Conducting Oxides at Visible Frequencies. *Nano Lett.* **2010**, *10*, 2111. [\[CrossRef\]](#)
- Das, S.; Salandrino, A.; Wu, J.Z.; Hui, R. Near-infrared electro-optic modulator based on plasmonic graphene. *Opt. Lett.* **2015**, *40*, 1516. [\[CrossRef\]](#)
- Das, S.; Fardad, S.; Kim, I.; Rho, J.; Hui, R.; Salandrino, A. Nanophotonic modal dichroism: Mode-multiplexed modulators. *Opt. Lett.* **2016**, *41*, 4394. [\[CrossRef\]](#) [\[PubMed\]](#)
- Hoffman, A.; Alekseyev, L.; Howard, S.; Franz, K.; Wasserman, D.; Podolskiy, V.; Narimanov, E.; Sivco, D.; Gmachl, C. Negative refraction in semiconductor metamaterials. *Nat. Mater.* **2007**, *6*, 946–950. [\[CrossRef\]](#)
- Feng, J.; Chen, Y.; Blair, J.; Kurt, H.; Hao, R.; Citrin, D.S.; Summers, C.J.; Zhou, Z. Fabrication of annular photonic crystals by atomic layer deposition and sacrificial etching. *J. Vac. Sci. Technol. B Microelectron. Nanometer Struct.* **2009**, *27*, 568. [\[CrossRef\]](#)
- Peragut, E.; Cerutti, L.; Baranov, A.; Hugonin, J.P.; Taliercio, T.; de Wilde, Y.; Grefet, J.J. Hyperbolic metamaterials and surface plasmon polaritons. *Optica* **2017**, *4*, 1409–1415. [\[CrossRef\]](#)
- Ali, K.; Ullah, M.; Bacha, B.A.; Jabar, M.S.A. Complex conductivity-dependent two-dimensional atom microscopy. *Eur. Phys. J. Plus* **2019**, *134*, 618. [\[CrossRef\]](#)
- Khan, N.; Bacha, N.B.A.; Iqbal, A.; Rahman, A.U.; Afaq, A. Gain-assisted superluminal propagation and rotary drag of photon and surface plasmon polaritons. *Phys. Rev. A* **2017**, *96*, 013848. [\[CrossRef\]](#)
- Shekhar, P.; Atkinson, J.; Jacob, Z. Hyperbolic metamaterials: Fundamentals and applications. *Nano Converg.* **2014**, *1*, 14. [\[CrossRef\]](#) [\[PubMed\]](#)

-
22. Starko-Bowes, R.; Atkinson, J.; Newman, W.; Hu, H.; Kallos, T.; Palikaras, G.; Fedosejevs, R.; Pramanik, S.; Jacob, Z. Optical characterization of Epsilon Near Zero, Epsilon Near Pole and hyperbolic response in nanowire metamaterials. *J. Opt. Soc. Am. B* **2015**, *32*, 2074–2080. [[CrossRef](#)]
 23. Gric, T.; Hess, O. Surface plasmon polaritons at the interface of two nanowire metamaterials. *J. Opt.* **2017**, *19*, 085101. [[CrossRef](#)]
 24. Iorsh, I.; Orlov, A.; Belov, P.; Kivshar, Y. Interface modes in nanostructured metal-dielectric metamaterials. *Appl. Phys. Lett.* **2011**, *99*, 151914. [[CrossRef](#)]
 25. Ioannidis, T.; Gric, T.; Rafailov, E. Controlling surface plasmon polaritons propagating at the interface of low-dimensional acoustic metamaterials. *Waves Random Complex Media* **2021**, submitted.

Article 5. Ioannidis et al. (2020). Surface plasmon polariton waves propagation at the boundary of graphene based metamaterial and corrugated metal in THz range (<https://doi.org/10.1007/s11082-019-2128-x>)

Optical and Quantum Electronics (2020) 52:10
<https://doi.org/10.1007/s11082-019-2128-x>



Surface plasmon polariton waves propagation at the boundary of graphene based metamaterial and corrugated metal in THz range

Thanos Ioannidis¹ · Tatjana Gric^{1,2,3} · Edik Rafailov^{2,4}

Received: 7 October 2019 / Accepted: 26 November 2019 / Published online: 29 November 2019
 © Springer Science+Business Media, LLC, part of Springer Nature 2019

Abstract

Herein we study theoretically surface plasmon polariton (SPP) wave propagation along the nanostructured graphene-based metamaterial/corrugated metal interface. We apply the effective medium approximation formalism aiming to physically model nanostructured metamaterial. The transfer matrix approach is applied to compute the dispersion relationship for SPP waves. It has been concluded that the groove width (a) and the chemical potential (μ) parameters have a dramatical impact aiming to engineer resonance surface plasmon frequencies of the propagation modes. Moreover, one can tune the bandgap corresponding to non-propagation regime by modifying groove width parameter. The impact of the groove width (a) and the chemical potential (μ) on the propagation length was investigated. The present work may have potential applications in optical sensing in terahertz frequency range.

Keywords Graphene · Metamaterial · Surface plasmon polaritons

1 Introduction

The fundamental optical excitations that are confined to a metal/dielectric interface are the Surface Plasmon Polaritons (SPPs), as described by Ritchie (1957). SPPs can be referred to as electromagnetic excitations existing at an interface between two media, of which at least one is conducting (Raether 1988). Investigations of spoof-plasmons in a semiconductor is becoming an increasingly active area of research. As a matter of fact, the presence of surface waves was originally demonstrated either for dielectric materials placed over a metal surface or for the metallic surface with a periodic repetition of

✉ Tatjana Gric
tatjana.gric@vgtu.lt

¹ Department of Electronic Systems, Vilnius Gediminas Technical University, Vilnius, Lithuania

² Aston Institute of Photonic Technologies, Aston University, Birmingham B4 7ET, UK

³ Semiconductor Physics Institute, Center for Physical Sciences and Technology, Vilnius, Lithuania

⁴ Interdisciplinary Center of Critical Technologies in Medicine, Saratov State University, 83 Astrakhanskaya Street, Saratov, Russia 410012

obstacles or holes in the direction of propagation (Pendry et al. 2004; Garcia-Vidal et al. 2005; Jiang et al. 2009). However, these surface waves can also be excited replacing the metallic surface with the semiconductor one (Gric et al. 2015). Spoof plasmons are bound electromagnetic (EM) waves at frequencies outside the plasmonic range mimicking ("spoofing") surface plasmon polaritons (SPPs), which propagate on periodically corrugated metal surfaces (Rusina et al. 2010).

Recently, an idea of engineering surface plasmons at lower frequencies was suggested. It was concluded in Bozhevolnyi et al. (2005) that the existence of holes in the structure can lower the frequency of existing surface plasmons. Thus, by cutting holes or grooves in metal surfaces it is possible to take concepts such as highly localized waveguiding (Lamprecht et al. 2001; Maier et al. 2003) and superfocusing (Bozhevolnyi et al. 2006; Krasavin and Zheludev 2004) to lower frequencies, particularly to the THz regime (Krasavin et al. 2005), where plasmonics could enable near-field imaging and biosensing (Andrew and Barnes 2004) with unprecedented sensitivity.

In recent years, electromagnetic waves propagating at an interface between a metal and a dielectric have been of significant interest. An experimental study of propagation of a THz Zenneck surface wave on an aluminium sheet is presented in Jeon and Grischkowsky (2006). The properties of long-range SPPs are reviewed in Berini (2009). It is shown in Wang and Mittleman (2004) that a simple waveguide, namely a bare metal wire, can be used to transport terahertz pulses with virtually no dispersion, low attenuation, and with a remarkable structural simplicity.

The advent of the graphene has given rise to the unprecedented progress in actively tunable microwave, terahertz, and optical devices and structures during the last decade (Grigorenko et al. 2012; Geim and Novoselov 2007; Bonaccorso et al. 2010). Especially, we have seen significant progress in THz generation and detection over the last decade which leads to the surging demand for THz wave devices. Single-layer graphene demonstrates a dynamically changeable conductivity, permittivity, and impedance (Falkovsky 2008) while being one-atom thick and efficiently tunable by varying the chemical potential. Up to now, a single-layer uniform and patterned graphene (Yao et al. 2013; Nikitin et al. 2012; Fang et al. 2012; Hajian et al. 2016; Morozovska et al. 2017) being the simplest case for experimental studies has opened wide avenues for many applications. Though, a high degree of freedom for tunable devices is provided by double-layer graphene (Rodrigo et al. 2017) and graphene-dielectric multilayers (Grigorenko et al. 2012; Khromova et al. 2014; Crassee et al. 2011; Hajian et al. 2017; Orazbayev et al. 2016). Doing so, in contrast to noble metals, one can drastically tune graphene plasmonic resonances through electrostatic biasing. Thus, a new generation of reconfigurable plasmonic devices might be enabled. Among the new perspectives opened with graphene-dielectric multilayer structures, ENZ and near-zero-index metamaterials (Serebryannikov et al. 2018), hyperbolic metamaterials (Crassee et al. 2011; Othman et al. 2013a, b; Zhu et al. 2013; Xiang et al. 2014a, b; Iorsh et al. 2013; Xiang et al. 2014a, b), tunable beam steering (Orazbayev et al. 2016), and Tamm surface plasmons (Hajian et al. 2017) stand out. In addition, it is worthwhile noting, that surface-plasmon-polaritons (SPPs) at the interfaces of nanostructured metamaterials containing graphene (Gric 2016), tunable surface waves at the interface separating different graphene-dielectric hyperbolic metamaterials (Gric and Hess 2017a, b), and tunable perfect absorption at mid-infrared frequencies (Wu et al. 2016) are of the particular importance for the scientific community. It is worthwhile noting that dispersion of graphene-dielectric metamaterials can be engineered by changing the Fermi energy, e.g., see Refs. Othman et al. (2013a, b; Iorsh et al. 2013).

Here, we propose the nanostructured graphene-based metamaterial/corrugated metal interface. The proximity effects are already well known from the studies of other plasmonic structures (Li et al. 2010; Hajian et al. 2018). It is worthwhile noting, that new kinds of surface waves on nanostructured metamaterials, crossing the light line with a substantial portion at lower frequencies lying above the free space light line have been investigated in Trofimov and Gric (2018). The excitation of multiple surface-plasmon-polariton waves guided by the periodically corrugated interface of a homogeneous metal and a periodic multilayered isotropic dielectric material was studied theoretically in Faryad et al. (2012). The solution of the underlying canonical boundary-value problem (with a planar interface) indicates that multiple SPP waves of different polarization states, phase speeds, and attenuation rates can be guided by the periodically corrugated interface. Herein, we make a step forward by proposing an unprecedented degree of freedom while tuning the dispersion properties. We show that dispersion relation of SPPs can be adjusted by the shape of the textured grooves. Following the introduction, the remainder of this paper is structured as follows: Sect. 2 will describe the main building blocks comprising the system under consideration. In Sect. 3, the obtained results are discussed. Finally, in Sect. 4 conclusions are provided.

2 Material properties and design

The structure under consideration (Fig. 1) consists of two building blocks: grating made of Si ($\epsilon = \epsilon_g = 12.25$) and a slab of graphene-dielectric metamaterial. The function of the first building block is creation of higher-order transmission channel(s). In such a case, the coupling of the incident waves differs for the two opposite interfaces. The main its function is to attain tunability by changing the state from dielectric to ENZ, and then to plasmonic one, by engineering μ (Khromova et al. 2014).

The effective-medium approach is applied aiming to describe the optical response of such a system (Fig. 2). The former is justified if the wavelength of the radiation considered is much larger than the thickness of any layer. It is based on averaging the structure parameters. Hence, further in this paper we consider the effective homogeneous media for the semi-infinite periodic structures. The effective permittivities are as follows (Agranovich and Kravtsov 1985):

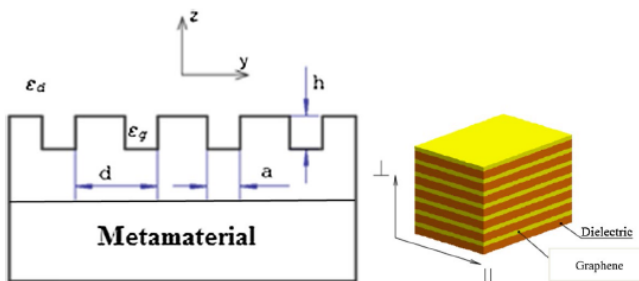


Fig. 1 Geometry of structured metamaterial surface

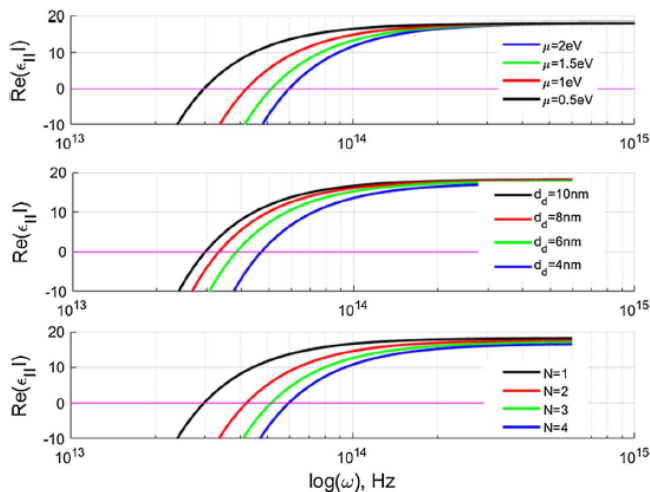


Fig. 2 The influence of **a** Fermi energy μ , **b** thickness of dielectric d_{md} , and **c** number of graphene sheets N on the real part of $\epsilon_{||}$. $N=1$, $d_{md}=10$ nm in (a), $N=1$, $\mu=0.5$ eV in (b), and $d_{md}=10$, $\mu=0.5$ eV in (c)

$$\epsilon_{||}^m = \frac{\epsilon_{mg}d_{mg} + \epsilon_{md}d_{md}}{d_{mg} + d_{md}} \quad (1)$$

$$\epsilon_{\perp}^m = \frac{\epsilon_{mg}\epsilon_{md}(d_{mg} + d_{md})}{\epsilon_{mg}d_{md} + \epsilon_{md}d_{mg}}, \quad (2)$$

where ϵ_{mg} , ϵ_{md} —are the permittivities of the graphene and dielectric layers correspondingly; d_{mg} , d_{md} —are the thicknesses of the graphene and dielectric layers correspondingly.

Matching the tangential components of the electrical and magnetic fields at the interface implies the dispersion relation for the surface modes localized at the boundary separating two anisotropic media (Iorsh et al. 2011). We assume the permittivity $\epsilon_{mg}(\omega)$ to be frequency dependent as the corresponding layer is represented by graphene.

Within the random-phase approximation and without an external magnetic field, graphene may be regarded as isotropic and the surface conductivity can be written as follows (Falkovsky 2008; Hanson 2008), $\sigma = ie^2\mu N/\pi\hbar^2(\omega + i/\tau)$, where ω , \hbar , e , μ , τ , N is the frequency, Planck constant, charge of an electron, chemical potential (Fermi energy), and phenomenological scattering rate, number of graphene layers respectively. The Fermi energy μ can be straightforwardly obtained from the carrier density n_{2D} in a graphene sheet, $\mu = \hbar v_F\sqrt{\pi n_{2D}}$, v_F is the Fermi velocity of electrons. It should be mentioned, that one can electrically control the carrier density n_{2D} by an applied gate voltage, thus leading to a voltage-controlled Fermi energy μ . Here we assumed that the electronic band structure of a graphene sheet is unaffected by the neighboring layers. Thus, the effective permittivity ϵ_{mg} of graphene can be calculated as follows (Vakil and Engheta 2011): $\epsilon_{mg} = 1 + i\sigma/\epsilon_0\omega d_{mg}$, where ϵ_0 is the permittivity in the vacuum.

One can see that $\text{Re}(\epsilon_{||})$ crosses zero at a frequency which depends on μ . For instance, this happens at 30 THz when $\mu=0.5$ eV, and at 45 THz when $\mu=1$ eV. Changing μ may drastically shift the spectral range of transition from the effectively plasmonic to the effectively dielectric state. Note that the gate positioning will be considered at the next steps. Generally, electrical gating of a multilayer graphene-dielectric metamaterial is a challenging task. One of possible gating schemes is presented in Ref. Khromova et al. (2014). In Ref. Chang et al. (2016), chemical doping has been used while preparing each graphene layer using CVD, instead of electrical gating. In Ref. Gomez-Diaz et al. (2015), the double-layer graphene has been experimentally gated, and the method was presented by the authors as the one being usable for the structures composed of a larger number of graphene monolayers. So, from a practical point of view, this approach can be utilized also in the case of graphene-dielectric metamaterial containing finite number of graphene layers.

In order to find the dielectric parameters of the effective medium describing metal grating, consider a periodic assembly of parallel plates. The effective dielectric constants of such an assembly are as follows (Born and Wolf 1999)

$$\epsilon_x = \epsilon_z = \frac{(d-a)\epsilon_{Ag} + a\epsilon_g}{d} \quad (3)$$

$$\epsilon_y = \frac{d}{(d-a)/\epsilon_{Ag} + a/\epsilon_g} \quad (4)$$

Here, ϵ_d is the permittivity of the surrounding media, ϵ_{Ag} —is the permittivity of silver.

3 Results and discussion

Herein, we present a simple example of polaritons in corrugated metal at THz frequencies. The wave vector k (Gric and Hess 2017a, b) is plotted as a function of the frequency aiming to illustrate the properties of SPPs. We deal with Ag case (Johnson and Christy 1972). It is assumed that the structure is surrounded by silicon, i.e. Si ($\epsilon = \epsilon_g = 12.25$).

Figure 3a depicts the dispersion curves of SPPs at the boundary metamaterial/structured surface with $d=10$ nm. It is of particular importance to investigate the impact of the period on the dispersion curves of SPPs. Doing so, three different groove widths a are considered. One may conclude from Fig. 3, that the asymptotic frequency, i.e. the maximum possible frequency of the propagating modes decreases with an increase in groove width. Figure 3b presents the losses of these SPPs as a function of frequency. It is worthwhile noting that the loss of SPPs is dramatically influenced by the increase in frequency. Besides that, it is of particular importance to note, that the forbidden region between the modes starts squeezing as presented in the Fig. 3a and the approach each other with the decrease of the groove width.

It is of particular interest to analyze the effect of the lattice constant (d) on the dispersion of SPPs. The dispersion curves for SPPs at the boundary metamaterial/corrugated surface with different lattice constants $d=5, 7, 10$ nm, are displayed in Fig. 4a. The groove parameter is $a=2$ nm for all cases. Figure 4b shows the losses of SPPs for three cases. It can be concluded from Fig. 4b, that a larger loss of SPPs for a given frequency takes place in case of a smaller lattice constant. One might conclude from Fig. 4b, that losses of the SPPs are drastically influenced by the lattice constant. For a given frequency, an increase of

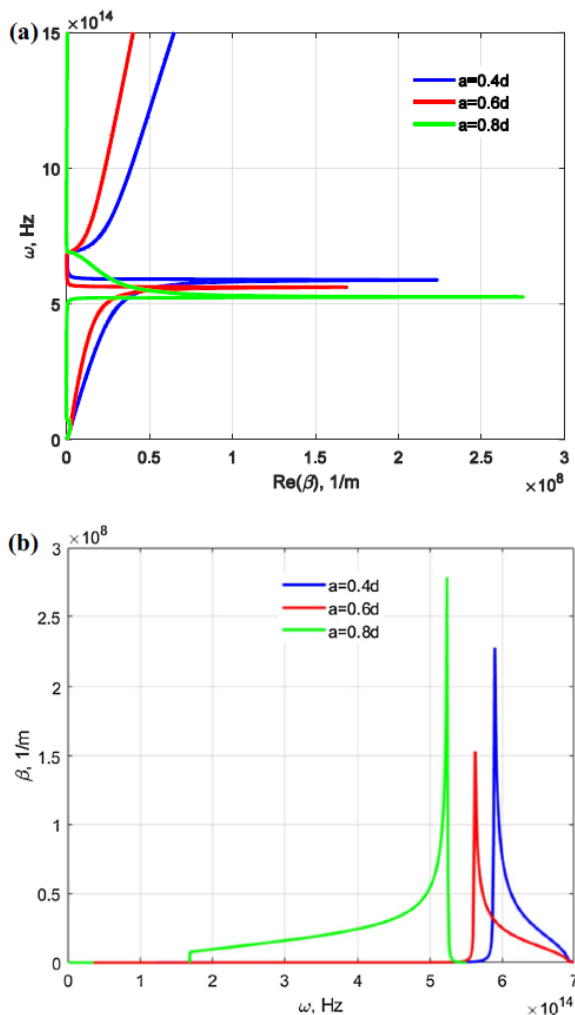


Fig. 3 **a** Dispersion curves for SPPs. **b** Attenuation coefficients of SPPs, lattice constant $d = 10$ nm

the lattice constant may cause a significant reduction of the loss of spoof SPPs. A low-loss THz waveguiding system is essential because of the need for a compact, reliable, and flexible THz system for various applications.

The impact of the chemical potential on the propagating modes along metamaterial/corrugated metal interface is depicted in Fig. 5. One may engineer the chemical potential μ of graphene by tuning the gate voltage or doping (Vakil and Engheta 2011). It is worthwhile

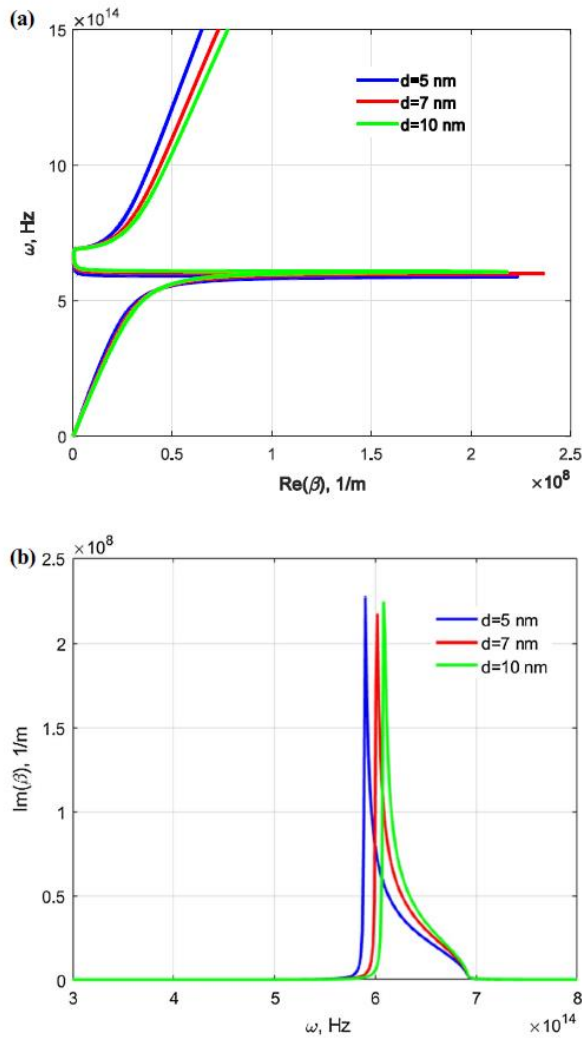


Fig. 4 Dispersion curves (a) and attenuation coefficients (b) of SPPs for different lattice constants $d = 5, 7, 10$ nm, respectively. Parameters of grooves: $a = 2$ nm

noting, that the chemical potential has different values in these dispersion curves, i.e. $\mu = 0.1$ eV, $\mu = 0.5$ eV, $\mu = 1$ eV, $\mu = 1.5$ eV. It has been confirmed that the chemical potential has a dramatic impact modulating the modes. It should be noted that the resonance frequency for the modes increases with the increase of chemical potential. In Fig. 5a, one can

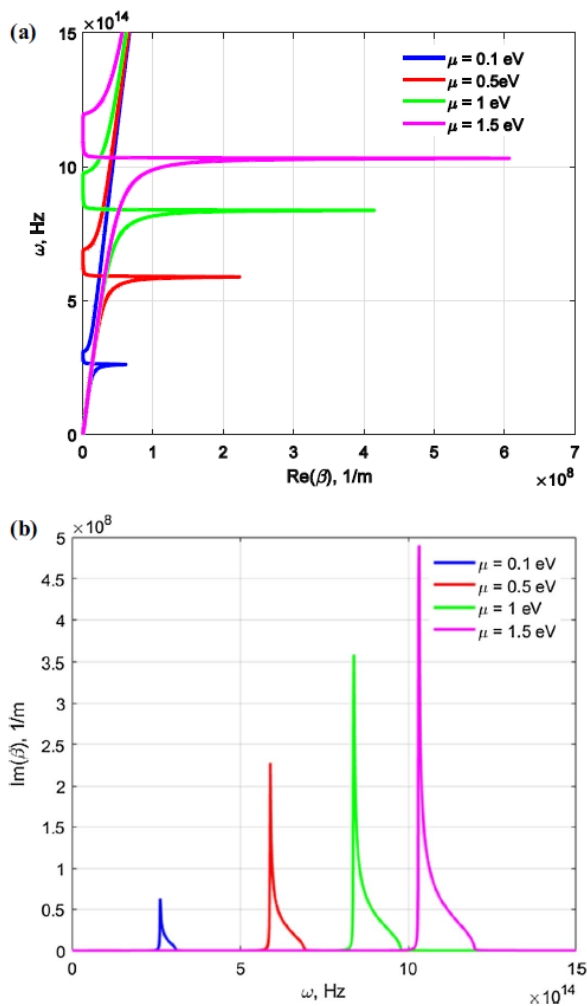


Fig. 5 Influence of chemical potential on the dispersion curves (a) and attenuation coefficients (b) of SPPs at nanostructure metamaterial interface with $d = 10$ nm, $a = 0.4d$

see that SPPs dispersion is noticeably modified as compared with the dispersion depicted in Fig. 4a. Due to the plasmon–phonon coupling, the SPPs can be supported at considerably smaller wavenumbers. It should be mentioned that decreases in the chemical potential μ will move the dispersion curves to lower frequencies; in contrast, increases in the chemical potential μ move them to higher frequencies. As seen from Fig. 5, the smallest asymptotic frequency is achieved by employing the smallest chemical potential. The former tunability

property suggests that the surface wave can be engineered by the chemical potential of the graphene sheets.

Figure 6 displays the propagation length $L_p = \frac{1}{2\text{Im}(\beta)}$ as a function of the incidence terahertz frequency ($\omega = 0.1 - 500 \text{ THz}$) for different values of groove width ($a = 0.4d$; $a = 0.6d$) and chemical potential ($\mu = 0.1 \text{ eV}$, 0.5 eV , 1 eV , 1.5 eV). It is worthwhile noting that $\mu = 0.5 \text{ eV}$ in Fig. Figure 6a and $a = 0.4d$ in Fig. 6b. It is obvious that groove width (a) and the chemical potential (μ) play a significant role in modulation of the propagation

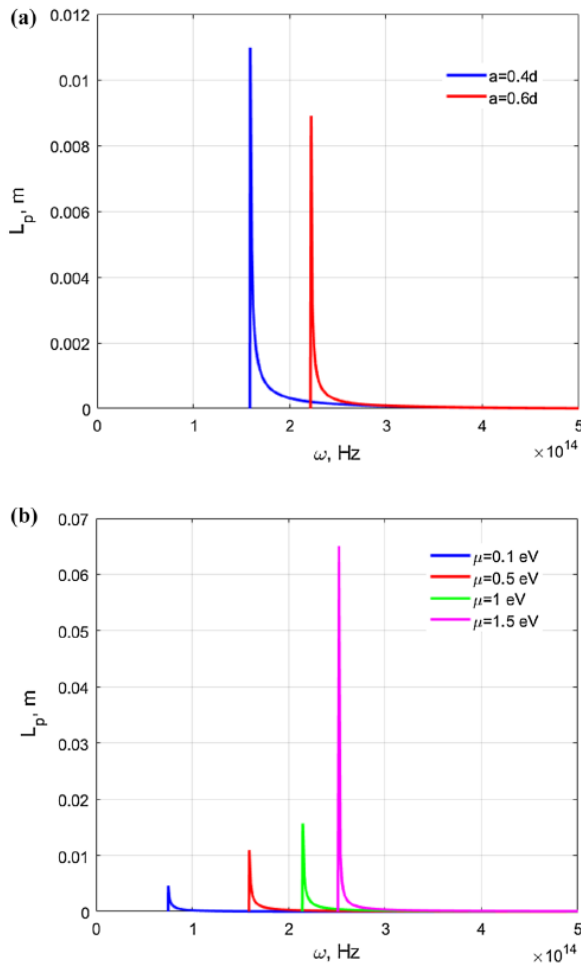


Fig. 6 Influence of groove width (a) and chemical potential (b) on the propagation length of surface wave modes as function of incidence frequency

length of the modes. The propagation length of the modes increases increasing groove width and chemical potential. It is of particular interest to mention that the propagation length profiles of the modes follow the exponential decay (Fig. 6). The usage of graphene allows for the increase the propagation length of the modes compared to ordinary interface modes.

4 Conclusion

The nanostructured metamaterial interface is used to excite the SPP waves. The dispersion relationship is computed by implementing the effective medium theory and transfer matrix approach and the following conclusions can be drawn:

- Surface wave modes propagate along the metamaterial/metal grating interface.
- One may tune the bandgap corresponding to non-propagation regime by engineering the groove width or chemical potential of graphene.
- The propagation length as a function of the terahertz frequency range is studied. It has been concluded that under appropriate parameters the propagation length can be modulated. The present method of surface wave modulation is quite simple in comparison with the corrugated structures (Anwar et al. 2017).
- One may apply the proposed geometry for optical sensing and wave propagation in the terahertz regime.

Herein, we have considered a formalism to analyze SPPs at the metamaterial/corrugated metal interface. In comparison with the previous works, our approach enables investigation the metamaterial case since it takes into account the permittivity of the metamaterial expressed by the effective medium theory. We have analyzed the properties of the dispersion and loss of SPPs at the metamaterial/corrugated metal boundary at the THz frequency range. The groove width drastically affects the asymptotic frequency of SPPs. On the other hand, the loss of SPPs is sensitive to all parameters of the surface structure. A good performance with low-loss propagation of spoof SPP can be achieved by optimizing design of the grating structure.

Acknowledgement This project has received funding from the European Union's Horizon 2020 research and innovation programme under the Marie Skłodowska Curie Grant Agreement No 713694 and from Engineering and Physical Sciences Research Council (EPSRC) (Grant No. EP/R024898/1). E.U.R. also acknowledges support and the Russian Science Foundation (Grant No. 18-15-00172).

References

- Agranovich, V.M., Kravtsov, V.E.: Notes on crystal optics of superlattices. *Solid State Commun.* **55**(1), 85–90 (1985)
- Andrew, P., Barnes, W.L.: Energy transfer across a metal film mediated by surface plasmon polaritons. *Science* **306**, 1002–1005 (2004)
- Anwar, R.S., Ning, H., Mao, L.: Recent advancements in surface plasmon polaritons-plasmonics in sub-wavelength structures at microwave and terahertz regime. *Digit. Commun. Netw.* **4**(4), 244–257 (2017)
- Berini, P.: Long-range surface plasmon polaritons. *Adv. Opt. Photon.* **1**, 484–588 (2009)
- Bonaccorso, F., Sun, Z., Hasan, T., Ferrari, A.C.: Graphene photonics and optoelectronics. *Nat. Photon.* **4**, 611–622 (2010)
- Born, M., Wolf, E.: *Principles of Optics*. Cambridge University Press, Cambridge (1999)

- Bozhevolnyi, S.I., Volkov, V.S., Devaux, E., Ebbesen, T.W.: Channel plasmon-polariton guiding by sub-wavelength metal grooves. *Phys. Rev. Lett.* **95**, 046802 (2005)
- Bozhevolnyi, S.I., Volkov, V.S., Devaux, E., Laluet, J.-Y., Ebbesen, T.W.: Channel plasmon subwavelength waveguide components including interferometers and ring resonators. *Nature* **440**, 508–511 (2006)
- Chang, Y.-C., Liu, C.-H., Liu, C.-H., Zhang, S., Marder, S.R., Narimanov, E.E., Zhong, Z., Norris, T.B.: Realization of mid-infrared graphene hyperbolic metamaterials. *Nat. Commun.* **7**, 10568 (2016)
- Crassee, I., Levallois, J., Walter, A.L., Ostler, M., Bostwick, A., Rotenberg, E., Seyller, T., van der Marel, D., Kuzmenko, A.B.: Giant Faraday rotation in single- and multilayer graphene. *Nat. Phys.* **7**, 48–51 (2011)
- Falkovsky, L.A.: Optical properties of graphene. *J. Phys. Conf. Ser.* **129**(1), 012004 (2008)
- Fang, Z., Liu, Z., Wang, Y., Ajayan, P.M., Nordlander, P., Halas, N.J.: Graphene-antenna sandwich photodetector. *Nano Lett.* **12**(7), 3808–3813 (2012)
- Faryad, M., Hall, A.S., Barber, G.D., Mallouk, T.E., Lakhtakia, A.: Excitation of multiple surface-plasmon-polariton waves guided by the periodically corrugated interface of a metal and a periodic multi-layered isotropic dielectric material. *J. Opt. Soc. Am. B* **29**(4), 704–713 (2012)
- Garcia-Vidal, F.J., Martin-Moreno, L., Pendry, J.B.: Surfaces with holes in them: new plasmonic metamaterials. *J. Opt. A-Pure Appl. Opt.* **7**, S97 (2005)
- Geim, A.K., Novoselov, K.S.: The rise of graphene. *Nat. Mater.* **6**, 183–191 (2007)
- Gomez-Diaz, J.S., Moldovan, C., Capdevila, S., Romeu, J., Bernard, L.S., Magrez, A., Ionescu, A.M., Perruisseau-Carrier, J.: Self-biased reconfigurable graphene stacks for terahertz plasmonics. *Nat. Commun.* **6**, 6334 (2015)
- Gric, T.: Surface-plasmon-polaritons at the interface of nanostructured metamaterials. *Prog. Electromagn. Res.* **46**, 165–172 (2016)
- Gric, T., Hess, O.: Tunable surface waves at the interface separating different graphene-dielectric composite hyperbolic metamaterials. *Opt. Express* **25**(10), 11466–11476 (2017a)
- Gric, T., Hess, O.: Controlling hybrid-polarization surface plasmon polaritons in dielectric-transparent conducting oxides metamaterials via their effective properties. *J. Appl. Phys.* **122**, 193105 (2017b)
- Gric, T., Wartak, M.S., Cada, M., Wood, J.J., Hess, O., Pistora, J.: Spoof plasmons in corrugated semiconductors. *J. Electromagnet. Wave* **29**, 1899–1907 (2015)
- Grigorenko, A.N., Polini, M., Novoselov, K.S.: Graphene plasmonics. *Nat. Photon.* **6**, 749–758 (2012)
- Hajian, H., Rukhlenko, I.D., Leung, P.T., Caglayan, H., Ozbay, E.: Guided plasmon modes of a graphene-coated Kerr slab. *Plasmonics* **11**(3), 735–741 (2016)
- Hajian, H., Caglayan, H., Ozbay, E.: Long-range Tamm surface plasmons supported by graphene-dielectric metamaterials. *J. Appl. Phys.* **121**(3), 033101 (2017)
- Hajian, H., Serebryannikov, A.E., Ghobadi, A., Demirag, Y., Butun, B., Vandenbosch, G.A.E., Ozbay, E.: Tailoring far-infrared surface plasmon polaritons of a single-layer graphene using plasmon-phonon hybridization in graphene-LiF heterostructures. *Sci. Rep.* **8**, 13209 (2018)
- Hanson, G.W.: Dyadic Green's functions and guided surface waves for a surface conductivity model of graphene. *J. Appl. Phys.* **103**(6), 064302 (2008)
- Iorsh, I., Orlov, A., Belov, P., Kivshar, Y.: Interface modes in nanostructured metal-dielectric metamaterials. *Appl. Phys. Lett.* **99**, 151914 (2011)
- Iorsh, I.V., Mukhin, I.S., Shadrinov, I.V., Belov, P.A., Kivshar, Y.S.: Hyperbolic metamaterials based on multilayer graphene structures. *Phys. Rev. B* **87**(7), 075416 (2013)
- Jeon, T.-I., Grischkowsky, D.: THz Zenneck surface wave (THz surface plasmon) propagation on a metal sheet. *Appl. Phys. Lett.* **88**, 061113 (2006)
- Jiang, T., Shen, L., Zhang, X., Ran, L.-X.: High-order modes of spoof surface Plasmon polaritons on periodically corrugated metal surfaces. *Prog. Electromagn. Res.* **8**, 91–102 (2009)
- Johnson, P.B., Christy, R.W.: Optical constants of the noble metals. *Phys. Rev. B* **6**, 4370 (1972)
- Khromova, I., Andryeuskii, A., Lavrinenko, A.: Ultrasensitive terahertz/infrared waveguide modulators based on multilayer graphene metamaterials. *Laser Photon. Rev.* **8**(6), 916–923 (2014)
- Krasavin, A.V., Zheludev, N.I.: Active plasmonics: controlling signals in Au/Ga waveguide using nanoscale structural transformations. *Appl. Phys. Lett.* **84**, 1416–1418 (2004)
- Krasavin, A.V., Zayats, A.V., Zheludev, N.I.: Active control of surface plasmon-polariton waves. *J. Opt. A: Pure Appl. Opt.* **7**, S85 (2005)
- Lamprecht, B., Krenn, J.R., Schider, G., Dittlbacher, H., Salerno, M., Felidj, N., Leitner, A., Aussenegg, F.R., Weeber, J.C.: Surface plasmon propagation in microscale metal stripes. *Appl. Phys. Lett.* **79**, 51 (2001)
- Li, Z., Bao, K., Fang, Y., Guan, Z., Halas, N.J., Nordlander, P., Xu, H.: Effect of a proximal substrate on plasmon propagation in silver nanowires. *Phys. Rev. B* **82**, 241402 (2010)

- Maier, S.A., Kik, P.G., Atwater, H.A., Meltzer, S., Harel, E., Koel, B.E., Requicha, A.A.G.: Local detection of electromagnetic energy transport below the diffraction limit in metal nanoparticle plasmon waveguides. *Nat. Mater.* **2**, 229–232 (2003)
- Morozovska, A.N., Kurchak, A.I., Strikha, M.V.: Graphene exfoliation at a ferroelectric domain wall induced by the piezoelectric effect: impact on the conductance of the graphene channel. *Phys. Rev. Appl.* **8**(5), 054004 (2017)
- Nikitin, A.Yu., Guinea, F., Martin-Moreno, L.: Resonant plasmonic effects in periodic graphene antidot arrays. *Appl. Phys. Lett.* **101**(15), 151119 (2012)
- Orazbayev, B., Beruete, M., Khromova, I.: Tunable beam steering enabled by graphene metamaterials. *Opt. Express* **24**(8), 8848–8861 (2016)
- Othman, M.A.K., Guclu, C., Capolino, F.: Graphene-dielectric composite metamaterials: evolution from elliptic to hyperbolic wavevector dispersion and the transverse epsilon-near-zero condition. *J. Nanophoton.* **7**(1), 073089 (2013a)
- Othman, M.A.K., Guclu, C., Capolino, F.: Graphene-based tunable hyperbolic metamaterials and enhanced near-field absorption. *Opt. Express* **21**(6), 7614–7632 (2013b)
- Pendry, J.B., Martin-Moreno, L., Garcia-Vidal, F.J.: Mimicking surface plasmons with structured surfaces. *Science* **305**, 847–848 (2004)
- Raether, H.: *Surface Plasmons on Smooth and Rough Surfaces and on Gratings*. Springer, Berlin (1988)
- Ritchie, R.H.: Plasma losses by fast electrons in thin films. *Phys. Rev.* **106**, 874 (1957)
- Rodrigo, D., Tittl, A., Limaj, O., Garcia de Abajo, F.J., Pruneri, V., Altug, H.: Double-layer graphene for enhanced tunable infrared plasmonics. *Light: Sci. Appl.* **6**, e16277 (2017)
- Rusina, A., Durach, M., Stockman, M.I.: Theory of spoof plasmons in real metals. *Appl. Phys. A* **100**(2), 375–378 (2010)
- Serebryannikov, A.E., Hajian, H., Beruete, M., Ozbay, E., Vandenbosch, G.A.E.: Tunable deflection and asymmetric transmission of THz waves using a thin slab of graphene-dielectric metamaterial, with and without ENZ components. *Opt. Mater. Express* **8**, 3887–3898 (2018)
- Trofimov, A., Gric, T.: Surface plasmon polaritons in hyperbolic nanostructured metamaterials. *J. Electromagn. Waves Appl.* **32**(14), 1857–1867 (2018)
- Vakil, A., Engheta, N.: Transformation optics using graphene. *Science* **332**(6035), 1291–1294 (2011)
- Wang, K., Mittleman, D.M.: Metal wires for terahertz wave guiding. *Nature* **432**(18), 376–379 (2004)
- Wu, J., Jiang, L., Guo, J., Dai, X., Xiang, Y., Wen, S.: Tunable perfect absorption at infrared frequencies by a graphene-hBN hyper crystal. *Opt. Express* **24**(15), 17103–17114 (2016)
- Xiang, Y., Guo, J., Dai, X., Wen, S., Tang, D.: Engineered surface Bloch waves in graphene-based hyperbolic metamaterials. *Opt. Express* **22**(3), 3054–3062 (2014a)
- Xiang, Y., Dai, X., Guo, J., Zhang, H., Wen, S., Tang, D.: Critical coupling with graphene-based hyperbolic metamaterials. *Sci. Rep.* **4**, 5483 (2014b)
- Yao, Y., Kats, M.A., Gevenet, P., Yu, N., Song, Y., Kong, J., Capasso, F.: Broad electrical tuning of graphene-loaded plasmonic antennas. *Nano Lett.* **13**(3), 1257–1264 (2013)
- Zhu, B., Ren, G., Zheng, S., Lin, Z., Jian, S.: Nanoscale dielectric-graphene-dielectric tunable infrared waveguide with ultrahigh refractive indices. *Opt. Express* **21**(14), 17089–17096 (2013)

Publisher's Note Springer Nature remains neutral with regard to jurisdictional claims in published maps and institutional affiliations.

Article 6. Ioannidis et al. (2019). Enhancing the properties of plasmonic nanowires (<https://doi.org/10.1088/2053-1591/ab0a1b>)

IOP Publishing

Mater. Res. Express 6 (2019) 065014

<https://doi.org/10.1088/2053-1591/ab0a1b>

Materials Research Express



PAPER

Enhancing the properties of plasmonic nanowires

RECEIVED
30 October 2018

REVISED
11 February 2019

ACCEPTED FOR PUBLICATION
25 February 2019

PUBLISHED
13 March 2019

Thanos Ioannidis¹, Tatjana Gric^{1,2} , Andrei Gorodetsky^{3,4} , Aleksey Trofimov¹ and Edik Rafailov⁵

¹ Department of Electronic Systems, Vilnius Gediminas Technical University, Vilnius, Lithuania

² Semiconductor Physics Institute, Center for Physical Sciences and Technology, Vilnius, Lithuania

³ ITMO University, St. Petersburg 197101, Russia

⁴ Department of Chemistry, Imperial College London, London, SW7 2AZ, United Kingdom

⁵ Aston Institute of Photonic Technologies, Aston University, Birmingham B4 7ET, United Kingdom

E-mail: tatjana.gric@vgtu.lt

Keywords: metamaterial, surface plasmons, nanowires

Abstract

In this paper, we show the approach to enhance the optical properties of the plasmonic nanowires from the perspectives of both field enhancement and tunability. Two different cases have been suggested for the consideration: the first one uses hollow-core metamaterial interface, while the other involves metallic nanowire metamaterial interface. It has been outlined, that the use of nanowire metamaterial interface allows for stretching the frequency range of surface wave existence from 500 THz (600 nm) to approximately 1000 THz (300 nm). Moreover, the nanowire metamaterial interface demonstrates better field confinement.

1. Introduction

Herein, we deal with the exceptional features of surface plasmon polaritons (SPPs) providing a fertile ground for plasmonics research. It is worthwhile noting, that the former phenomenon appears on the metal interface due to strong field localization. The strong level of interaction between light and free electrons in metals [1, 2] causes arise of quasiparticles, called SPPs. SPPs act as a surface wave propagating along the boundary between a metal and a dielectric while exponentially decaying into both the dielectric and metal. The dispersion relation of SPPs at a dielectric-metal boundary can be derived from Maxwell's equations with appropriate boundary conditions. Denoting the dielectric constant of the metal and the dielectric material as ϵ_m and ϵ_d correspondingly, the dispersion equation of SPPs is expressed as

$$\beta = \frac{\omega}{c} \sqrt{\frac{\epsilon_m \epsilon_d}{\epsilon_m + \epsilon_d}} \quad (1)$$

where ω is the angular frequency of the SPP modes, c is the speed of light, and β is the wave constant of SPPs along the propagation direction. It is worthwhile noting, that the localized SPPs are dramatically influenced by the material properties along with the size and shape of the metallic nanostructures (figure 1(a)). Doing so, it is possible to achieve an efficient coupling. It should be mentioned that the exceptional properties of SPPs, such as, subwavelength confinement and strong field enhancement give rise to a wide range of innovative applications [3–7]. Moreover, propagation of SPPs in metamaterials is a hot topic either. Coupling to the modes supported by the metamaterials has been covered in [8] opening the wide avenues for the innovative aspects. For example, owing to the excitation of SPPs, resolution of the so-called 'superlens' has reached as high as 30 nm [9]. The former opens the wide avenues for optical microscopy in terms of overcoming the diffraction limit. Alternatively, the resolution can be even higher in plasmonics-assisted spectroscopy, such as surface-enhanced Raman spectroscopy (SERS). The Raman signal can be considerably amplified by SERS approach. Doing so, the vibrational information of single molecules can be probed and recorded [10–12] by employing the strong local field enhancement of plasmonic composites and the chemical mechanism including charge transfer between the species and the metal surface. Additionally, SERS has gone beyond simply reaching single molecule spectroscopy: recently SERS was also used to determine the molecular orientation of single molecules [13]. Tip-enhanced Raman spectroscopy (TERS) may stand for the further resolution improvement. Based on the study

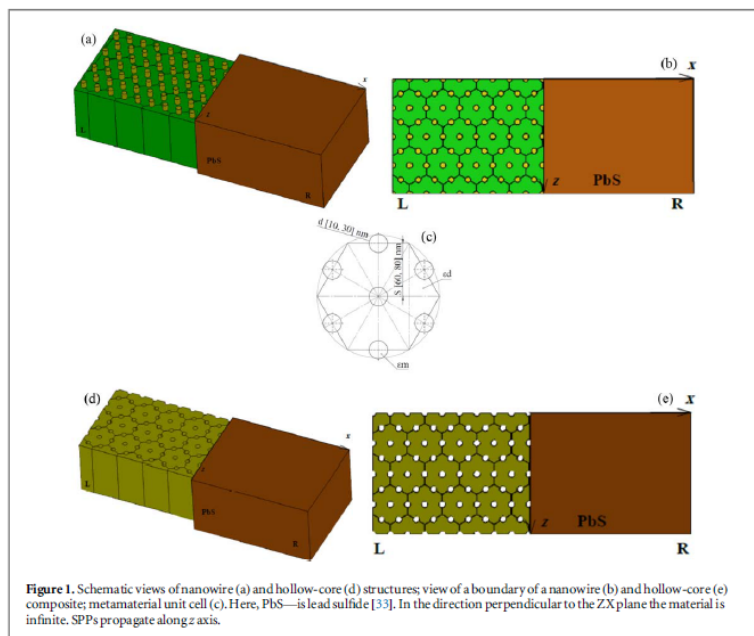


Figure 1. Schematic views of nanowire (a) and hollow-core (d) structures; view of a boundary of a nanowire (b) and hollow-core (e) composite; metamaterial unit cell (c). Here, PbS—is lead sulfide [33]. In the direction perpendicular to the ZX plane the material is infinite. SPPs propagate along z axis.

on TERS-based spectral imaging with extraordinary sub-molecular spatial resolution, one can definitely resolve the inner structure and surface configuration of a single molecule [14]. Moreover, it is worthwhile noting, that plasmonic nanoantennas give a tremendous rise to the enhancement of THz generation [15, 16].

It is worthwhile noting, that an indefinite medium with a metallic nanowire array embedded in a dielectric matrix does not rely on magnetic resonance and works over a broad range of frequency with much lower material loss [17, 18]. Such an anisotropic material has a negative electric permittivity along the nanowires and a positive permittivity perpendicular to the wires, i.e. indefinite permittivity, resulting in a hyperbolic dispersion with the ability for negative refraction of light.

Periodic metal-dielectric nanostructures open the wide avenues for applications [19–24]. In addition, a lot of investigations have been done in the field of anisotropic metamaterials, both experimentally [25] and theoretically [26–28]. Thus, a huge stream of papers is dedicated to the examination of properties of the metal-dielectric nanostructures [29–31]. However, there is still lack of studies directed towards the investigation of ways to control their properties. In this paper, we show the approach to enhance the optical properties of the plasmonic nanowires from the perspectives of both field enhancement and tunability. It should be noted, that tunability is considered as the increase of the frequency range of surface wave existence along with the ability to support tunable SPPs and up to 2-fold field enhancement. Tunability by the structure under consideration is achieved by engineering properties of SPPs. The former is possible changing the geometrical parameters of the metamaterials under study.

2. Basic model

Figure 1 displays the geometry of the nanowire structure. It is worthwhile mentioning, that in the direction perpendicular to the ZX plane the material is infinite. Metal wires with permittivity ϵ_m are implanted in a dielectric host material with permittivity $\epsilon_d = 2.4$. The mentioned materials have been chosen because of fabrication matters [32]. Doing so, we explore the optical properties of nanoscopic metallic particles prepared by electrochemically depositing metal within the pores of nanoporous alumina membranes.

The effective permittivities of the nanowire metamaterial are evaluated based on the effective medium approximation as follows [34]:

$$\varepsilon_{\perp}^L = \varepsilon_d^L \left[\frac{\varepsilon_m^L(1 + \rho^L) + \varepsilon_d^L(1 - \rho^L)}{\varepsilon_m^L(1 - \rho^L) + \varepsilon_d^L(1 + \rho^L)} \right] \quad (2)$$

$$\varepsilon_{\parallel}^L = \varepsilon_m^L \rho^L + \varepsilon_d^L(1 - \rho^L) \quad (3)$$

Here, subindices L and R refer to the left and right layer, correspondingly, and ρ is the metal filling factor which is computed as:

$$\rho = \frac{\text{nanowire area}}{\text{unit cell area}} \quad (4)$$

It should be mentioned, that $\varepsilon_{\parallel}^L$ is of the same direction as the propagating, however ε_{\perp}^L is perpendicular to it.

It is worthwhile mentioning, that metamaterial permittivity $\varepsilon_{\parallel}^L$ should be negative for SPP to exist. Aiming to investigate the features of SPPs, a Drude model is used to describe the metal. Doing so, the permittivity of silver is expressed as $\varepsilon_m(\omega) = \varepsilon_{\infty} - \frac{\omega_p^2}{\omega^2 + i\delta\omega}$. Fitting this permittivity function to a particular frequency range of bulk material [35] allows obtaining the parameters of interest. It is found [36] that a reasonable fit might be provided for silver, if the utilized values are as follows $\varepsilon_{\infty} = 5$, $\omega_p = 9.5$ eV, $\delta = 0.0987$ eV. The metal filling ratio (ρ) is calculated utilizing the parameters, such as nanowire diameter (d) and spacing (S) and dealing with a hexagonal cell, the relation [37] might be applied as follows:

$$\rho = \frac{\pi d^2}{2\sqrt{3} S^2} \quad (5)$$

Following this assumption, a dispersion equation for the SPPs concentrated at the boundary of anisotropic media might be derived. SPP mode described by the wavevector [38]

$$\beta = k \left(\frac{(\varepsilon_{\parallel}^R - \varepsilon_{\parallel}^L) \varepsilon_{\perp}^L \varepsilon_{\perp}^R}{\varepsilon_{\perp}^R \varepsilon_{\parallel}^R - \varepsilon_{\perp}^L \varepsilon_{\parallel}^L} \right)^{1/2}, \quad (6)$$

with k being the wavenumber and β is the component of the wavevector parallel to the boundary is obtained after dealing with the tangential components of the electric and magnetic fields.

It is worthwhile noting that equation (6) is valid only under the condition of surface confinement, which can be presented in the following form:

$$\begin{cases} (k^2 - \beta^2 / \varepsilon_{\parallel}^L) \varepsilon_{\perp}^L < 0 \\ (k^2 - \beta^2 / \varepsilon_{\parallel}^R) \varepsilon_{\perp}^R < 0 \end{cases} \quad (7)$$

It is worthwhile mentioning, that the proposed model was tested comparing the results obtained using equation (6) with the experimental outputs [39] for the classical case, i.e. Au/air interface. In order to apply model under consideration, we have assumed that the nanowire diameter is as follows $d \rightarrow 0$.

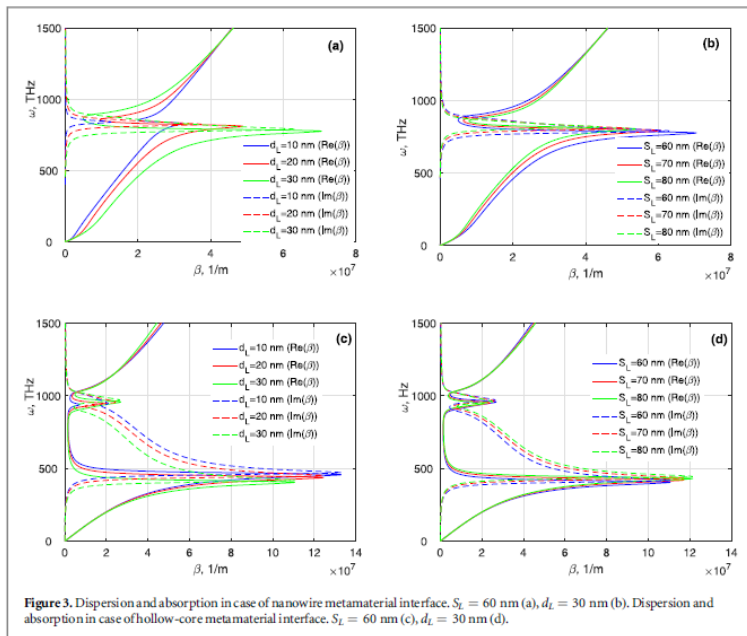
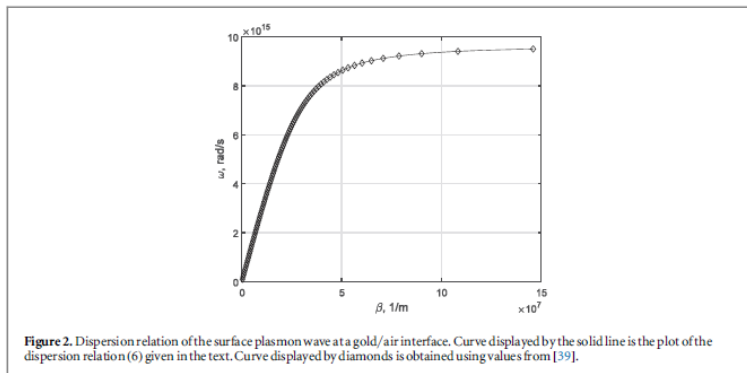
It should be noted from figure 2, that the agreement of the results is very good.

3. Simulation results and discussions

Figure 3 displays the dispersion relation (equation (6)) utilizing the complex experimental values of permittivity. Due to the metal being not treated as lossless, β is complex. Thus, a finite propagation length of surface plasmons phenomenon is caused. At this point, the divergence of the wave vector is not observed. On the contrary, it bends backwards filling the region called plasmon bandgap and connects to the Brewster mode. The range of anomalous dispersion is called quasi-bound mode [40]. One may consider how the SPP dispersion relation departs from the light line, resembling the behavior of SPPs propagating along metal at optical frequencies (see figure 3). Doing so, the TM dispersion diagram for SPP modes supported by a nanowire metamaterial are shown in figure 3. Herein, we analyze two different cases. The light line is asymptotically approached by the SPP dispersion curves at the long wavelength due to the fact that the EM is not affected by the fine periodic structure. Though, the highly localized surface bound modes are engineered along the corrugated system if the frequency increases.

3.1. Interface of the nanowire metamaterial and dielectric

First, surface modes at the boundary of the nanowire metamaterial and dielectric are studied. Figure 3 displays the dispersion diagrams of the surface modes along with the absorption graphs. In the first case (figure 3) the spacing is fixed, i.e. $S_L = 60$ nm and the pore diameter is varying, i.e. $d_L = 10$ nm, 20 nm, 30 nm. To the best of our knowledge, altering either metal or dielectric drastically affects the dispersion diagrams [41]. Herein, the impact of the spacing of the metamaterial L on the SPPs is studied. Doing so, the spacing varies from 60 to 80 nm.



The influence of the spacing parameter on the surface modes dispersion characteristics is displayed in figure 3. The increase of spacing S_L causes shift of the SPPs diagrams to the lower wavelengths. It is worthwhile noting, that it is impossible to employ the described tunability mechanisms in case of the conventional metal-dielectric interface.

3.2. Interface of the hollow-core metamaterial and dielectric

The hollow-core metamaterial is introduced by replacing the metal nanowires with the air holes. On the other hand, metal, i. e. Ag is used as the host material. The influence of the nanowire geometry on the dispersion

diagrams in case of the hollow-core metamaterial is studied in figure 3. Moreover, the influence of the distance between nanowires in the structure within different frequencies is presented in figure 3. It is worthwhile noting, that anomalous features of the dispersion diagrams can be observed near the frequency 10^{15} Hz in figure 3. The mentioned frequency is particular due to the fact that it serves as the intersection point of the effective dielectric permittivity perpendicular components obtained varying the diameter of the nanowires as well as the distance between them [34]. It is worthwhile noting, that the 'jump' point arises while $\varepsilon_{||} > 0$, $\varepsilon_{\perp} < 0$ [34] providing the possibilities to increase the frequency gap region with purely imaginary β prohibiting propagation. The mentioned property does not take place in case of the conventional metal-dielectric interface.

In figure 3 the frequency range for surface Bloch wave is narrow. Though, it is possible to extend it by dealing with the case of the nanowire metamaterial (Case A). Furthermore, the impact of the nanowire diameter on the dispersion curves (see figure 3) is discussed. It is found that both the upper and the lower limits shift to the higher frequencies as d is decreased. Though the movement of the lower limit is quicker than that of the upper one. Doing so, the broader frequency range for surface wave existence arises. This is consistent with the effect of d on the frequency range of negative $\varepsilon_{||}$. One can also broaden the frequency range of surface Bloch waves by tuning the distance S [34]. A wide spectrum of possibilities to engineer the SPP at the near-infrared frequencies is provided due to the impact of the diameter and distance on the frequency range of surface wave existence.

Figure 3 serve as a perfect evidence that at a given frequency free-space wavenumber k_0 is smaller than β , or that the wavelength λ_0 is longer than the SPP wavelength λ_{SPP} in the free space at the same frequency. Doing so, the slow wave effect is obtained. Hence, a mismatch in the phase of the free-space waves and SPPs takes place. Consequently, a coupler is needed, as in periodic leaky-wave antennas [42]. One may sometimes relate the concept of SPPs to Sommerfeld-Zenneck surface waves [43]. The former are known to occur at microwave frequencies.

It is noted that the wave vector β in the dispersion relation (figure 3) is a two-dimensional wave vector in the plane of the surface. Consequently, the constant wave vector mismatch between the light line and the SPP dispersion occurs. The described phenomenon takes place if the surface is hit by the light in an arbitrary direction. Thus, the surface plasmon polariton line will not be intersected. It means, that surface plasmons cannot be excited by light incident on an ideal surface. Nevertheless, two mechanisms, i. e. surface roughness or gratings [44], and attenuated total reflection (ATR) [45, 46] allow for the external radiation to be coupled to SPPs.

Aiming to study the possible approaches to coupling, we consider the spatial extension of the electromagnetic field associated with the SPP (see figures 4, 5). It is worthwhile noting, that only the components of \mathbf{E} in the plane of the incident wave can induce longitudinal surface charge density oscillations in the direction of propagation (z -axis) [47]. The only magnetic field component left is H_x , hence only TM-plasmon can propagate along the surface of the metamaterial. The EM field associated with TM-plasmons, also decay exponentially away from the interface into both media. Therefore, following the solution H_x can be assumed:

$$H_x = A \cdot e^{j(\omega t - \beta z)} \cdot \exp(\alpha_m x), x < 0 \quad (8)$$

$$H_x = B \cdot e^{j(\omega t - \beta z)} \cdot \exp(\alpha_d x), x > 0 \quad (9)$$

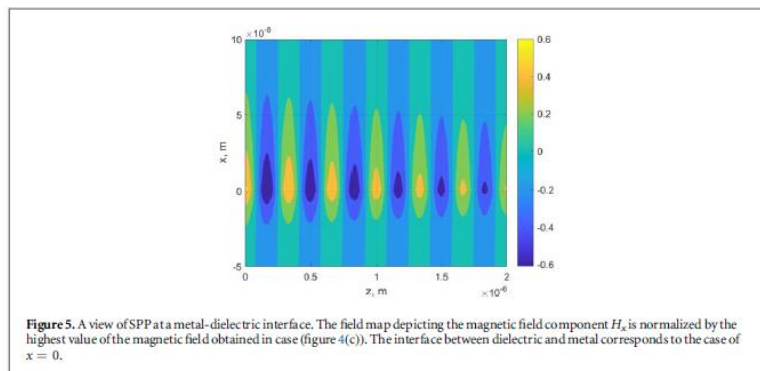
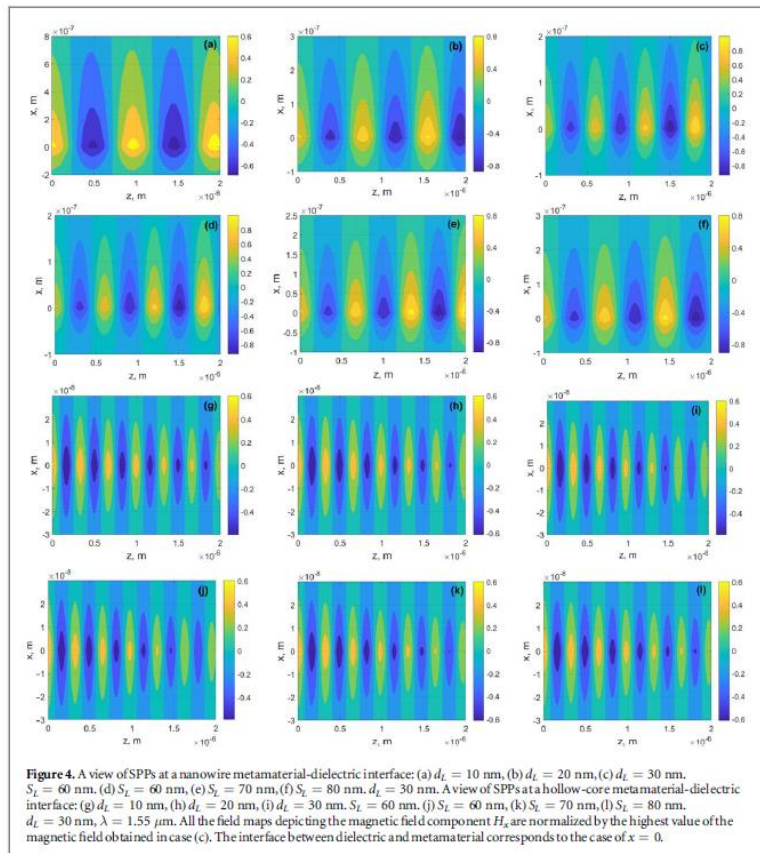
Where A and B are amplitudes to be determined by the boundary conditions, α_m and α_d are the reciprocal (positive and real) penetration depths into the metamaterial and dielectric, respectively. It is worthwhile mentioning, that the amplitude of SPPs decreases with increasing propagation distance and eventually dissipates. The penetration depth is defined as the distance from the interface at which the amplitude H_x is reduced by e^{-1} :

$$\alpha_{d/m} = \sqrt{\beta^2 - k^2 \varepsilon_{d/m}} \quad (10)$$

One may obtain the field distribution of each guide mode by the analytical approach at each eigenfrequency. Figures 4(g)–(l) show the snapshot of the fields of the modes presented in figure 3. It is worthwhile noting, that the field maps have been obtained, when $\omega = 193$ THz ($\lambda = 1.55 \mu\text{m}$). The chosen frequency corresponds to the propagation regimes for both cases under consideration (figure 3). Moreover, figures 4(g)–(l), 4 correspond to hollow-metamaterial case and metal-dielectric interface correspondingly. The former clearly demonstrates the weaker field confinement in comparison to the nanowire case.

For the sake of simplicity, the dispersion equation of SPP modes has been sketched schematically in figure 3. Herein, some properties of SPP mode on the flat metamaterial/dielectric boundary are summarized as follows.

(1) The SPP mode is an electromagnetic wave coupled with the surface electron-density oscillations. The magnetic field of the mode is perpendicular to the propagation direction (TM mode) and parallel to the metal surface. As an alternative, the electric field has both the normal (E_{\perp}) and tangent ($E_{||}$) components. On the dielectric side, $E_{\perp}/E_{||} = \sqrt{\varepsilon_{||}/\varepsilon_d}$; on the metamaterial side, $E_{\perp}/E_{||} = -\sqrt{\varepsilon_d/\varepsilon_{||}}$. Consequently, the electric field inside the metamaterial is tangent and the electrons move back and forth in the propagation direction. Then, a longitudinal electron-density wave is formed if the frequency is well below the plasma frequency. (2) The



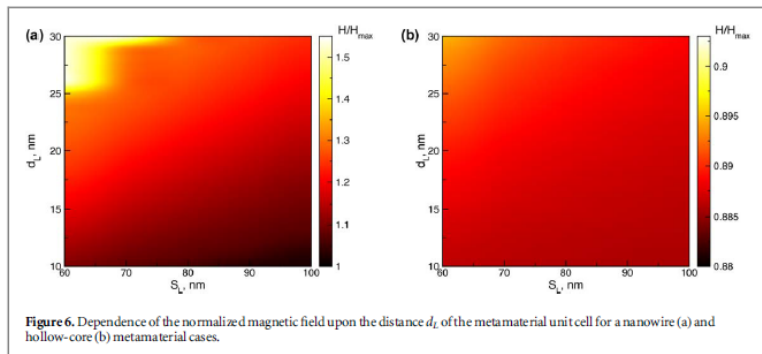


Figure 6. Dependence of the normalized magnetic field upon the distance d_c of the metamaterial unit cell for a nanowire (a) and hollow-core (b) metamaterial cases.

SPP mode can propagate along the metal surface with a larger propagation constant ($\beta > k_0 \sqrt{\epsilon_d}$). The former leads to a smaller propagation velocity of the electromagnetic wave on top of the reduced wavelength. It is worthwhile noting, that the propagation length of SPP mode is finite taking the metal absorption into account. It is shown by the detailed calculation that the energy propagation length can be expressed as $L_{app} \approx \epsilon_d^2 / k_0 \epsilon''_{||} \epsilon_d^{3/2}$, where $\epsilon'_{||}$ and $\epsilon''_{||}$ are the real and imaginary parts of permittivity of the metal, respectively. In the visible and near-infrared region, L_{app} is from several to hundreds of micrometers. (3) The SPP mode is evanescent on either side of the boundary because of the larger propagation constant. On the dielectric side, the decaying length of the field is $\delta_d \approx \sqrt{|\epsilon'_{||}| / k_0 \epsilon_d}$; on the other side, the decaying length is $\delta_m \approx 1 / k_0 \sqrt{|\epsilon'_{||}|}$. This suggests that the wave is strongly confined to the metamaterial surface, which is just desired in practice. Moreover, it is noted that a strong level of enhancement of fields near the interface can also be obtained.

To get a deeper insight into the properties of SPPs, we have sketched the dependence of the normalized magnetic field upon the distance d_c in the metamaterial unit cell (figure 6). It is worthwhile noting, that the higher field values are obtained in the case of the nanowire metamaterial.

4. Conclusion

It has been shown that usage of nanowire metamaterial interface allows the increase of the frequency range of surface wave existence from 500 THz (600 nm) to approximately 1000 THz (300 nm). Moreover, they demonstrated the ability to support tunable SPPs and up to 2-fold field enhancement. We believe that presented results provide an approach for effective realization of nanophotonic devices such as optical reflectarrays, SPP couplers, plasmonic absorbers. Plasmonic nanowires have given rise for integrated optics and nanodevices for sensing applications. Such devices could lead to efficient and delicate control on nanoscale light-matter interactions for advanced applications in photonics after further explorations on dielectric materials, structure topologies, and fabrication technologies.

ORCID iDs

Tatjana Gric <https://orcid.org/0000-0002-7850-2778>

Andrei Gorodetsky <https://orcid.org/0000-0001-5440-2185>

References

- [1] Raether H 1988 *Surface Plasmons*. (Berlin: Springer)
- [2] Maier S A 2007 *Plasmonics: Fundamentals and Applications*. (New York: Springer)
- [3] Anker J N, Paige Hall W, Lyandres O, Shah N C, Zhao J and Van Duyne R P 2008 Biosensing with plasmonic nanosensors *Nat. Mater.* **7** 442–53
- [4] Zhang X and Liu Z 2008 Superlenses to overcome the diffraction limit *Nat. Mater.* **7** 435–41
- [5] Atwater H A and Polman A 2010 Plasmonics for improved photovoltaic devices *Nat. Mater.* **9** 205–13
- [6] Srituravanich W, Fang N, Sun C, Luo Q and Zhang X 2004 Plasmonic nanolithography *Nano Lett.* **4** 1085–8
- [7] Gramotnev D K and Bozhevolnyi S I 2010 Plasmonics beyond the diffraction limit *Nat. Photon.* **4** 83–91

- [8] Dickson W, Beckett S, McClatchey C, Murphy A, O'Connor D, Wurtz G A, Pollard R and Zayats A V 2015 Hyperbolic polaritonic crystals based on nanostructured nanorod metamaterials *Adv. Mater.* **27** 5974–80
- [9] Chaturvedi P, Wu W, Logeswaran V J, Yu Z, Islam M S, Wang S Y, Stanley Williams R and Fang N X 2010 A smooth optical superlens *Appl. Phys. Lett.* **96** 043102
- [10] Nie Sand Emory S R 1997 Probing single molecules and single nanoparticles by surface-enhanced Raman scattering *Science* **275** 1102–6
- [11] Kneipp K, Wang Y, Kneipp H, Perelman L T, Itzkan I, Dasari R and Feld M S 1997 Single molecule detection using surface-enhanced Raman scattering (SERS) *Phys. Rev. Lett.* **78** 1667
- [12] Campion A and Kambhampati P 1998 Surface-enhanced Raman scattering *Chem. Soc. Rev.* **27** 241–50
- [13] Marshall A R L, Stokes J, Viscomi F N, Proctor J E, Gierschner J, Bouillard J-S G and Adawi A M 2017 Determining molecular orientation via single molecule SERS in a plasmonic nano-gap *Nanoscale* **44** 17415–21
- [14] Zhang R et al 2013 Chemical mapping of a single molecule by plasmon-enhanced Raman scattering *Nature* **498** 82–6
- [15] Lepeshov S, Gorodetsky A, Krasnok A, Rafailov E U and Belov P 2017 Enhancement of terahertz photoconductive antenna operation by optical nanoantennas *Laser & Photonics Reviews* **11** 1600199
- [16] Lepeshov S, Gorodetsky A, Krasnok A, Toropov N, Vartanyan T A, Belov P, Alù A and Rafailov E U 2018 Boosting terahertz photoconductive antenna performance with optimised plasmonic nanostructures *Sci. Rep.* **8** 6624
- [17] Yao J, Liu Z, Liu Y, Wang Y, Sun C, Bartal G, Stacy A M and Zhang X 2008 Optical negative refraction in bulk metamaterials of nanowires *Science* **321** 930
- [18] Liu Y, Bartal G and Zhang X 2008 All-angle negative refraction and imaging in a bulk medium made of metallic nanowires in the visible region *Opt. Exp.* **16** 15439–48
- [19] Ramakrishna S A and Pendry J B 2003 Optical gain removes absorption and improves resolution in a near-field lens *Phys. Rev. B* **67** 201101
- [20] Belov P A and Hao Y 2006 Subwavelength imaging at optical frequencies using a transmission device formed by a periodic layered metal-dielectric structure operating in the canalization regime *Phys. Rev. B* **73** 113110
- [21] Li X, He S and Jin Y 2007 Subwavelength focusing with a multilayered Fabry–Pérot structure at optical frequencies *Phys. Rev. B* **75** 045103
- [22] Liu Z, Lee H, Xiong Y, Sun C and Zhang X 2007 Optical hyperlens magnifying sub-diffraction limited objects *Science* **315** 1686
- [23] Xiong Y, Liu Z and Zhang X 2008 Projecting deep-subwavelength patterns from diffraction-limited masks using metal-dielectric multilayers *Appl. Phys. Lett.* **93** 111116
- [24] Engheta N 2007 Circuits with light at nanoscales: Optical nanocircuits inspired by metamaterials *Science* **317** 1698
- [25] Hoffman A J, Alekseyev L, Howard S S, Franz K J, Wasserman D, Podolskiy V A, Narimanov E E, Sivo D L and Gimach C 2007 Negative refraction in semiconductor metamaterials *Nature Mater.* **6** 946
- [26] Smith D R and Schurig D 2003 Electromagnetic wave propagation in media with indefinite permittivity and permeability tensors *Phys. Rev. Lett.* **90** 077405
- [27] Scalora M et al 2007 Negative refraction and subwavelength focusing in the visible range using transparent metallo-dielectric stacks *Opt. Express* **15** 508
- [28] Liu Y, Bartal G and Zhang X 2008 All-angle negative refraction and imaging in a bulk medium made of metallic nanowires in the visible region *Opt. Express* **16** 15439
- [29] Song Z and Jian W 2011 Splitting the surface wave in metal/dielectric nanostructures *Chinese Phys.* **20** 067901
- [30] Yeshchenko O, Bondarchuk I, Malynych S, Galabura Y, Chumanov G and Luzinov I 2015 Surface plasmon modes of sandwich-like metal-dielectric nanostructures *Plasmonics* **10** 655
- [31] Dong Z, Bosman M, Zhu D, Goh X M and Yang J K 2014 Fabrication of suspended metal-dielectric-metal plasmonic nanostructures *Nanotechnology* **25** 135303
- [32] Hornyak G L, Patrissi C J and Martin C R 1997 Fabrication, characterization, and optical properties of gold nanoparticle/porous alumina composites: the nonscattering Maxwell-Garnett limit *J. Phys. Chem. B* **101** 1548–55
- [33] Gric T and Hess O 2017 Tunable surface waves at the interface separating different graphene-dielectric composite hyperbolic metamaterials *Opt. Express* **25** 11466–76
- [34] Gric T and Hess O 2017 Surface plasmon polaritons at the interface of two nanowire metamaterials *J. Opt.* **19** 085101
- [35] Johnson P B and Christy R W 1972 Optical constants of the noble metals *Phys. Rev.* **6** 4370
- [36] Oubre C and Nordlander P 2005 Finite-difference time-domain studies of the optical properties of nanoshell dimers *J. Phys. Chem. B* **109** 10042–51
- [37] Starko-Bowes R, Atkinson J, Newman W, Hu H, Kallos T, Palikaras G, Fedosejevs R, Pramanik Sand Jacob Z 2015 Optical characterization of Epsilon near zero, epsilon near pole and hyperbolic response in nanowire metamaterials *J. Opt. Soc. Am. B* **32** 2074–80
- [38] Iorsh I, Orlov A, Belov P and Kivshar Y 2011 Interface modes in nanostructured metal-dielectric metamaterials *Appl. Phys. Lett.* **99** 151914
- [39] Pluchery O, Vayron R and Van K-M 2011 Laboratory experiments for exploring the surface plasmon resonance *Eur. J. Phys.* **32** 585–99
- [40] Dionne J A, Sweatlock L A, Atwater H A and Polman A 2005 Planar metal plasmon waveguides: frequency-dependent dispersion, propagation, localization, and loss beyond the free electron model *Phys. Rev. B* **72** 075405
- [41] Gric T 2016 Surface-Plasmon-Polaritons at the interface of nanostructured metamaterials *Pr. Elektromagn. Res. M* **46** 165–72
- [42] Jackson D R, Caloz C and Itoh T 2012 Leaky-wave antennas *Proc. IEEE* **100** 2194–206
- [43] Ishimaru A, Dexter Rockway J, Kuga Y and Lee S-W 2000 Sommerfeld and Zenneck wave propagation for a finitely conducting one-dimensional rough surface *IEEE Trans. Antennas Propag.* **48** 1475–84
- [44] Teng Y-Y and Stern E A 1967 Plasma radiation from metal grating surfaces *Phys. Rev. Lett.* **19** 511
- [45] Otto A 1968 Excitation of nonradiative surface plasma waves in silver by the method of frustrated total reflection *Z. Phys.* **216** 398
- [46] Kretschmann E and Raether H 1968 Radiative decay of non radiative surface plasmons excited by light *Z. Naturf. A* **23** 2135
- [47] Knoll W 1998 Interfaces and thin films seen by bound electromagnetic waves *Annu. Rev. Phys. Chem.* **49** 569–638

Summary in Lithuanian

Įvadas

Problemos formulavimas

Aviacijos ir antenų reikmėms tradicinių antenų medžiagų – spausdintinių plokščių, apdorotų aliuminio korpusų – dėka yra galimi išbandyti ir tikri, bet brangi antenų kūrimo būdai. Kitas didelis trūkumas yra prastos sugerties savybės, dėl kurių padidėja triukšmo lygis. Yra reikalingas naujas požiūris, kad būtų patenkinti reikalavimai naujos kartos antenoms. Tokio pobūdžio problemas galima išspręsti taikant metamedžiagas (MM). MM susideda iš nanostruktūrų, kurios vadinamos dirbtiniais atomais. Šios struktūros suteikia metamedžiagai unikalių savybių, kurių negali turėti natūralios medžiagos. Šios savybės gali būti naudojamos siekiant įveikti optines ribas, kurias sukelia keli poveikiai, pavyzdžiui, difrakcijos riba, todėl naudojant metamedžiagas gali atsirasti neįprastų įrenginių savybių. Keičiamos MM savybės buvo pasiektos taikant aktyvias medžiagas, tokias kaip vanadžio dioksidas, indžio alavo oksidas, polidimetilsiloksanas, grafenas arba skystieji kristalai. Tokiu būdu galima išspręsti valdomų charakteristikų pasiekimo problemą. Aktyvi medžiaga leidžia sukonstruoti metamedžiagą, pasižyminčią derinamumu, grįžtamumu, pakartojamumu ir greita reakcija į pokyčius. Jautrių medžiagų, tokių kaip puslaidininkiai, skystieji kristalai, fazių keitimo medžiagos arba kvantinės medžiagos (pvz.: superlaidininkai, 2D medžiagos ir kt.) naudojimas suteikia metamedžiagoms dinamines savybes, palengvindamas aktyvių ir derinamų įrenginių, turinčių patobulintą funkcionalumą arba net visiškai naujas elektromagnetines funkcijas, kūrimą.

Darbo aktualumas

Daktaro disertacijos tikslas – sukurti ir platinti naujus derinamų metamedžiagų modelius, skirtus galimam pritaikymui orlaivių pramonėje ir aukšto dažnio ruožuose. Disertacija yra daugiadalykis projektas, labai susijęs su orlaivių ir elektronikos sričių aspektais, įskaitant galimus pateiktų metodų pritaikymus antenų ir orlaivių pramonės srityse. Tyrimo rezultatai ne tik leis sukurti visiškai naujus derinamų metamedžiagų modelius, kurie gali būti pritaikyti triukšmo slopinimo funkcijoms atlikti, bet ir atvers kelią į naujas platformas, kurios galėtų pasiūlyti keletą praktinių antenų sistemų įgyvendinimo būdų.

Tyrimo objektas

Tyrimo objektas yra įvairių paviršinių plazmonų poliaritonų (SPP) sklidimo sprendimų projektavimas, remiantis nanostruktūrinių ir nanovielinių metamedžiagų modelių taikymu.

Darbo tikslas

Naujų teorinių modelių, leidžiančių ištirti paviršinių plazmonų poliaritonų (SPP), sklindančių tiriamose sandūrose, elektrodinamines savybes, sukūrimas.

Darbo uždaviniai

Darbe keliami uždaviniai:

1. Ištirti Maxwell–Garnett metodo taikymo galimybes homogenizuoti įvairių rūšių metamedžiagines struktūras, tokias kaip įprastinė nanovielinė metamedžiaga, spiralinė metamedžiaga, nanostruktūrinės metamedžiagos.
2. Ištirti paviršinių plazmonų poliaritonų (SPP), sklindančių įvairiose sandūrose, dispersines diagramas, pavyzdžiui:
 - metalinės nanovielinės ir tuščiavidurės metamedžiagos sandūra,
 - nanostruktūrinės metamedžiagos ir gofruoto metalo sandūra,
 - spiralinės vielinės metamedžiagos ir oro sandūra,
 - nanokompozito ir hiperkristalo sandūra.
3. Išanalizuoti SPP, sklindančių tiriamose sandūrose, dispersines diagramas ir nuostolių dažnines funkcijas siekiant pagerinti absorbciją, leidžiančią sukurti orlaivio dangos modelį, taip pat ir antenų sistemas, siekiant slopinti triukšmą.
4. Išanalizuoti sistemos pagrindinius konstrukcijos parametrus, tokius kaip spiralės kampas, griovelių skaičius ir kt., siekiant padaryti išvadas apie konstrukcijų savybių derinimo galimybes.

Tyrimų metodai

Darbe taikomi metodai:

1. Efektyvios terpės aproksimacijos teorija, pagrįsta Maxwell–Garnett metodu; perdavimo matricos metodas, taikomas kuriant naujus SPP sklidimo modelius, kuriais siekiama apskaičiuoti elektrodinamines charakteristikas.
2. SPP modeliavimo metodai buvo įdiegti siekiant nustatyti sklindančių modų sugerties padidėjimą, todėl galimas gautų rezultatų pritaikymas antenos konstrukcijoje.

Darbo mokslinis naujumas

1. *Matlab* programoje buvo sukurti nauji kompiuteriniai SPP sklidimo naujose metamedžiagos sandūrose modeliai, skirti tiriamose sandūrose sklindantiems SPP elektrodinaminiais parametrams apskaičiuoti.
2. Nustatyta metamedžiagų užpildymo santykio įtaka SPP perdavimo charakteristikoms, leidžiant realizuoti matmenimis valdomus SPP.
3. Sugerties stiprinimo (sklidimo konstantos menamoji dalis) kontrolė buvo ištirta modifikuojant metamedžiagos geometriją.

Darbo rezultatų praktinė reikšmė

Buvo sukurti nauji kompiuteriniai modeliai, pagrįsti naujomis metamedžiagomis, kurios gali būti naudojamos tokiuose įrenginiuose kaip antena ir triukšmą slopinančios plėvelės, o esami modeliai buvo tobulinami. Šie modeliai leidžia analizuoti SPP sklidimo savybes inovatyvios sandūrose. Jie taip pat leidžia apskaičiuoti jų parametrus ir įvertinti elektrodinamines charakteristikas. Ištirta, kaip keičiant metamedžiagos parametrus keičiasi įrenginių savybės. Buvo sukurti algoritmai ir programos, leidžiančios numatyti SPP, sklindančių naujose metamedžiagos sandūrose, elektrodinamines charakteristikas.

Ginamieji teiginiai

1. Du kartus platesnis paviršinių bangų egzistavimo dažnių diapazonas, t. y. nuo 500 THz (600 nm) iki maždaug 1000 THz (300 nm), gali būti pasiektas, jei naudojama nanovielinės metamedžiagos ($d = 10$ nm, $S = 60$ nm) sandūra vietoj tuščiaavidurės metamedžiagos sandūros ($d = 10$ nm, $S = 60$ nm).
2. Nanovielinės metamedžiagos absorbcijos padidėjimas galėtų siekti iki 10 kartų, jei nanovielinėje metamedžiagoje vietoj sidabro analogų būtų naudojami skaidrūs laidūs oksidai.
3. SPP rezonansinis dažnis gali būti padidintas nuo 250 THz iki 1000 THz padidinus cheminį potencialą nuo $\mu = 0,1$ eV iki $\mu = 1,5$ eV.
4. Suprojektuota spiralinė vielinė metamedžiaga, kurios vielos skersmuo d lygus 8 mm, leido padidinti sklidimo režimo didžiausią veikimo dažnį iki 500 THz, palyginus su mažesnio analogo leidžiamu 300 THz ($d = 4$ mm).
5. Triukšmas gali sumažėti 1,1 karto (0,83 dB), jei bus taikoma nanovielinė akustinė metamedžiaga ($d = 10$ nm, $S = 60$ nm) ir tokiu būdu pasiektas maksimalus efektyvumas, jei metamedžiagos užpildymo koeficientas bus lygus $f = 0,7$.

Darbo rezultatų apibavimas

Pagrindiniai disertacijos rezultatai paskelbti 7 mokslinėse publikacijose: 6 iš jų *Clarivate Analytics Web of Science* duomenų bazėje su citavimo indeksu ir 1 – kitose duomenų bazėse.

Tyrimo rezultatai disertacijos tema pristatyti 4-iose mokslinėse konferencijose:

- Metamaterials and Plasmonics Conference (META) 2022. Toremolinas, Ispanija.
- International Conference “Electrical, Electronic and Information Sciences“ (eStream) 2022. Vilnius, Lietuva.
- Metamaterials and Plasmonics Conference (META) 2021. Varšuva, Lenkija.
- Conference for Lithuania Junior Researchers “Science – Future of Lithuania” 2021. Vilnius, Lietuva.

Disertacijos struktūra

Disertaciją sudaro įvadas, analitinės literatūros apžvalga, tyrimo metodologijos aptarimas, apibendrinti tyrimo rezultatai ir išvados, literatūros sąrašas, autoriaus publikacijų rinkinys, santrauka lietuvių kalba. Disertaciją sudaro 138 puslapiai, 40 pateiktų lygčių, 23 paveikslai, 1 lentelė ir 69 disertacijoje cituojamos literatūros šaltiniai. Disertaciją sudaro trys pagrindiniai skyriai.

Pirmame skyriuje apžvelgiama paviršiaus plazmonų poliaritonų samprata ir jų taikymas aviacijoje. Pirmas skyrius baigiamas formuluojant pagrindinį šio tyrimo tikslą ir uždavinius.

Antrame skyriuje nagrinėjami skaitiniai metodai, taikomi metamedžiagoms tirti. Pateikiami homogenizavimo metodai, kuriais siekiama nustatyti efektyvų nagrinėjamos metamedžiagos laidumą. Apsvarstytas naujas perdavimo matricos metodas, taikomas paviršiaus plazmonų poliaritonų, sklindančių inovatyviųjų metamedžiagų sandūrose, dispersijos sąryšiui nustatyti.

Trečiame skyriuje pateikiami skaitiniai tyrimo rezultatai, analizuojant paviršinių plazmonų poliaritonų sklidimą inovatyviųjų metamedžiagų sandūrose. Šiuo atžvilgiu daktaro disertacija apima platų tyrimų spektrą, pradedant nuo įprastų nanovielinės metamedžiagos atvejų ir baigiant egzotiškais atvejais, tokiais kaip spiralinės vielinės metamedžiagos.

1. Fotoninių metamedžiagų modeliavimo metodai

Pirmame disertacijos skyriuje atlikta literatūros šaltinių disertacijos tematika apžvalga. Apžvelgti paviršiniai *plazmonų poliaritonai*, taip pat *metamedžiagos* sąvoka. Nepaisant to, kad paviršinių plazmonų poliaritonų fizikinės savybės yra ištirtos, paviršinės bangos koncepcija dar nebuvo taikyta akustikos srityje. Šis darbas parodo galimų taikymų perspektyvas aviacijoje.

Sluoksniuotų nanostruktūrinių metamedžiagų, sudarytų iš kaitaliojančių grafeno ir dielektriko sluoksnių, efektyviosios santykinės dielektrinės skvarbos gali būti apskaičiuojamos taip (Khromova et al., 2014):

$$\varepsilon_{\parallel} = \frac{\varepsilon_g d_g + \varepsilon_d d_d}{d_g + d_d}; \quad (\text{S1.1})$$

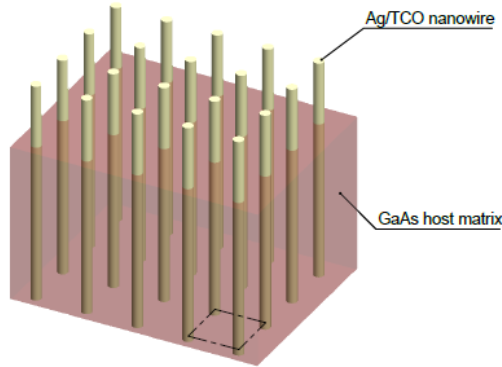
$$\varepsilon_{\perp} = \frac{\varepsilon_g \varepsilon_d (d_g + d_d)}{\varepsilon_g d_d + \varepsilon_d d_g}, \quad (\text{S1.2})$$

čia ε_g , ε_d yra grafeno ir dielektriko sluoksnių santykinės dielektrinės skvarbos; d_g , d_d yra grafeno ir dielektriko sluoksnių storiai.

2. Paviršiniai plazmoniniai polaritonai: tyrimų metodai

Antrame darbo skyriuje apžvelgti tyrimams reikalingi metodai. Parodyta, jog homogenizacijos metodas yra reikalingas nustatant anizotropinės struktūros dielektrines savybes. Siekiant gauti dispersinės lygties analitinę išraišką yra taikomas atvirkštinių matricių metodas.

Siūloma vielinės metamedžiagos geometrija parodyta S2.1 pav. Vielos, kurių santykinė dielektrinė skvarba yra ε_m^M , įterptos į pagrindinę medžiagą, kurios santykinė dielektrinė skvarba yra ε_d^M .



S2.1 pav. Vielinės metamedžiagos schematinis vaizdavimas

Remdamiesi efektyviosios terpės aproksimavimo metodu įvertiname vielinės metamedžiagos efektyviąją dielektrinę skvarbą:

$$\varepsilon_{\perp}^M = \varepsilon_d^M \left[\frac{\varepsilon_m^M (1 + \rho^M) + \varepsilon_d^M (1 - \rho^M)}{\varepsilon_m^M (1 - \rho^M) + \varepsilon_d^M (1 + \rho^M)} \right]; \quad (\text{S2.1})$$

$$\varepsilon_{\parallel}^M = \varepsilon_m^M \rho^M + \varepsilon_d^M (1 - \rho^M). \quad (\text{S2.2})$$

Čia subindeksas M žymi metamedžiaginę terpę ir ρ^M yra metalo užpildo koeficientas, apskaičiuojamas taip:

$$\rho^M = \frac{\text{nano wire area}}{\text{unit cell area}}. \quad (\text{S2.3})$$

Turint tikslą ištirti ir demonstruoti paviršinių bangų savybes taikomas *Drude* modelis (Johnson 1972) metalui (t. y. sidabru) apibūdinti, išreiškiant santykinę dielektrinę skvarbą kaip $\varepsilon_m^M(\omega) = \varepsilon_\infty - \frac{\omega_p^2}{\omega^2 + i\delta\omega}$. Parametrai gaunami pritaikant šią santykinės dielektrinės skvarbos funkciją tam tikram medžiagų dažnių diapazonui. Yra nustatyta, kad sidabro atveju vertės yra $\varepsilon_\infty = 5$, $\omega_p = 2,2971 \cdot 10^{15}$ Hz, $\delta = 2,3866 \cdot 10^{13}$ Hz. Metalo užpildo koeficientas (ρ^M) yra apskaičiuotas remiantis laidininko skersmens (d^M) ir atstumo (S^M) reikšmėmis ir darant prielaidą, kad vielos yra išsidėsčiusios pagal idealią stačiakampę struktūrą:

$$\rho^M = \frac{\pi(d^M)^2}{4(S^M)^2}. \quad (\text{S2.4})$$

Darant šią prielaidą yra įmanoma gauti dispersinę lygtį, siekiant charakterizuoti paviršinių bangų sklaidimą metamedžiagos ir PbS sandūroje. Įvertinus elektrinio ir magnetinio laukų tangentines dedamąsias sandūroje, yra gaunama sklaidimo pastoviosios išraiška:

$$\beta = k \left(\frac{(\varepsilon_{PbS} - \varepsilon_{||}^M) \varepsilon_{PbS} \varepsilon_{\perp}^M}{\varepsilon_{PbS}^2 - \varepsilon_{\perp}^M \varepsilon_{||}^M} \right)^{1/2}, \quad (\text{S2.5})$$

čia k yra bangos skaičius (bangos skaičiaus absoliučioji reikšmė vakuume) ir β yra lygiagrečioji banginio skaičiaus dedamoji.

Pagaliau spiralinės vielinės metamedžiagos efektyviųjų santykinių dielektrinių skvarbų išraiškos yra gaunamos:

$$\varepsilon_{\perp}^{SM} = -\varepsilon_d^M \frac{\varepsilon_d^M (\rho^M - 1) + \frac{ad\varepsilon_m^M \sin(2\theta)(\rho + 1)}{2}}{\varepsilon_d^M (\rho^M + 1) + \frac{ad\varepsilon_m^M \sin(2\theta)(\rho - 1)}{2}}; \quad (\text{S2.6})$$

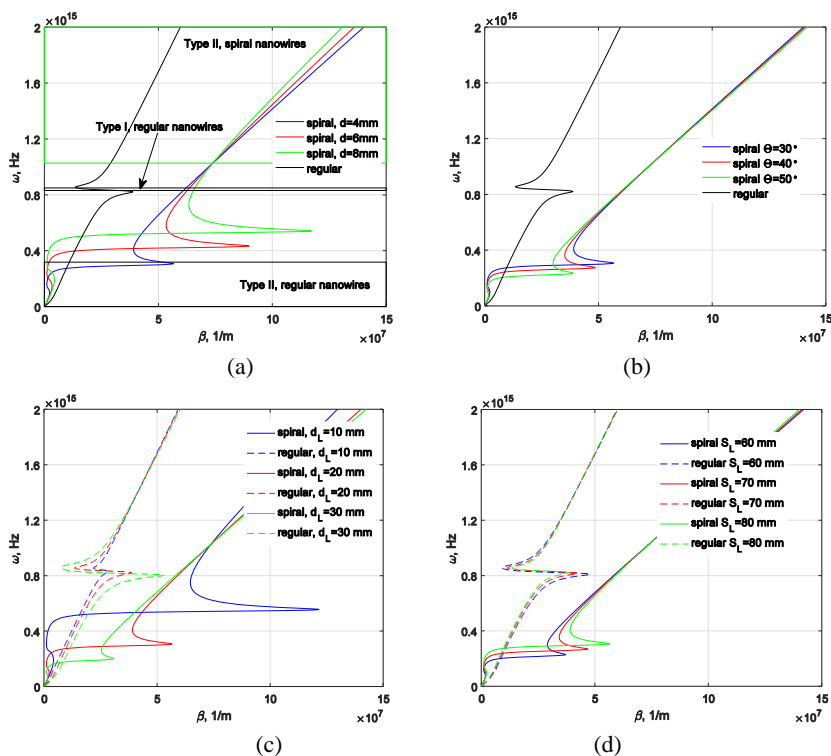
$$\varepsilon_{||}^{SM} = -\varepsilon_d^M (\rho^M - 1) - \frac{ad\varepsilon_m^M \rho^M (\cos(2\theta) + 1)}{2}. \quad (\text{S2.7})$$

Aprašytas modelis leidžia ištirti SPP, sklindančių spiralinės vielinės metamedžiagos sandūroje, savybes.

3. Paviršiniai plazmoniniai polaritonai: tyrimų rezultatai ir išvados

Trečiame skyriuje pateikti paviršinių bangų sklaidimo tyrimo rezultatai, pradedant nuo paprastų struktūrų ir baigiant novatoriškomis metamedžiagų struktūromis.

S3.1 paveiksle pavaizduotas režimo žemėlapis β - f erdvėje, iliustruojantis sritis, kuriose gali būti FB (ang. *Ferrell Berreman*) režimai. Laimei, FB režimų dažnių diapazoną galima valdyti laido periodiškumu d , spiralės kampu θ , vielų skersmeniu d^M ir atstumu tarp vielų S^M . Paviršiaus poliaritonų sklaidos santykiai kaip d funkcija parodyti S3.1 pav., a, kur $\theta = 30^\circ$, $d^M = 20$ mm, $S^M = 80$ mm. Akivaizdu, kad FB režimai egzistuoja kairėje šviesos linijos srityje. Poliaritonų dispersijos labai priklauso nuo d parametro, kaip tai aiškiai matyti S3.1 pav., a, kuriame apskaičiuojami ir nubraižomi dispersijos ryšiai pagal efektyvųjį anizotropinį laidumo tenzorį. Pažymėtina, kad FB režimų egzistavimo dažnių diapazonas didėja didėjant d , t. y. didesnis periodiškumas padidina gofruoto laido laidumą taip padidindamas efektyvų plazmoninį dažnį.



S3.1 pav. Paviršinių poliaritonų dispersijos diagramų priklausomybės nuo periodiškumo d (a), spiralės kampo θ (b), vielų skersmens d^M (c) ir atstumo tarp vielų S^M (d)

Atlikus disertacijos uždavinius, buvo gautos tokios išvados:

1. Ištyrus metalinės nanovielinės metamedžiagos ir tuščiaavidurės šerdies metamedžiagos sandūras, daromos tokios išvados:
 - Gaunamas lėtos bangos efektas. Tam tikrame dažnių diapazone ($0 < \omega < 1500$ THz) bangos skaičius k_0 vakuume yra mažesnis už β .
 - Įrodyta, kad nanovielinės metamedžiagos sandūros ($d = 10$ nm, $S = 60$ nm) naudojimas vietoj tuščiaavidurės metamedžiagos leidžia padidinti paviršinių bangų egzistavimo dažnių diapazoną nuo 500 THz (600 nm) iki maždaug 1000 THz (300 nm).
2. Ištyrus SPP sklidimą metamedžiagos ir gofruoto metalo sandūroje daromos šios išvados:
 - Griovelio plotis drastiškai veikia asimptotinį SPP dažnį atveriant plačias galimybes pasiekti aukšto derinimo režimą.
 - SPP nuostolių funkcija priklauso nuo visų paviršiaus struktūros parametrų, t. y. griovelio plotis (a) ir cheminis potencialas (μ) turi reikšmingą poveikį siekiant kontroliuoti sklindančių modų paviršinių plazmonų poliaritonų rezonansinius dažnius, suteikiant papildomą laisvės laipsnį sistemos savybių derinimui.
 - Galima kontroliuoti dažnių ruožą atitinkantį režimą, kuriam esant modos nesklinda, modifikuojant griovelio plotį, suteikiant papildomą laisvės laipsnį sistemos savybių derinimui.
 - Buvo ištirta griovelio pločio (a) ir cheminio potencialo (μ) įtaka SPP sklidimo ilgiui suteikiant papildomą laisvės laipsnį sistemos savybių derinimui.
3. Spiralinės vielinės metamedžiagos sandūros tyrimai leidžia daryti šias išvadas:
 - Sukurtas modelis leidžia kiekybiškai ištirti plazmonų poliaritonus, kuriuos galima valdyti modifikuojant spiralės kampą ir griovelį, gofruojančių idealiai laidžią vielos paviršių, skaičių suteikiant didelę sistemos savybių derinimo laisvę.
 - Buvo įrodyta, kad spiralinės vielinės supergardelės pagrindu pagamintos metamedžiagos turi unikalius mikroskopinius spinduliuojančius masinius plazmonų rezonansus, vadinamus Ferrell–Berreman modomis, kurias galima sužadinti laisvąja erdve, leidžiant išnaudoti sistemą tokiose srityse kaip jutimas, vaizdavimas ir absorbcijos spektroskopija.
4. Ištyrus SPP, sklindančias akustinės metamedžiagos riboje, gaunamos šios išvados:
 - Parodyta, kad yra dažniniai ruožai, kuriuose dinaminiai konstituciniai parametrai yra neigiami, o nagrinėjama banga tampa atgalinė (500 Hz $< f < 750$ Hz), leidžianti išnaudoti sistemą tokiems taikymams kaip priešinga jungtis, nukreipianti mikrobangų signalą į priešingus gnybtus skirtingais veikimo dažniais.
5. Ištyrus SPP, sklindančius mažų matmenų akustinių metamedžiagų sandūroje, gaunama ši išvada:
 - Gautas sugerties padidėjimas (sklidimo konstantos menamoji dalis), lygus 0,83 dB, daro didelę įtaką taikant triukšmo slopinimo metodą.

Bendrosios išvados

1. Ištyrus metalinės nanovielinės metamedžiagos ir tuščiavidurės šerdies metamedžiagos sandūras buvo gautas lėtos bangos efektas.
2. Ištyrus SPP sklidimą metamedžiagos ir gofruoto metalo sandūroje, buvo prieita išvados, kad galima kontroliuoti dažnių ruožą atitinkantį režimą, kuriam esant modos nesklinda, modifikuojant griovelio plotį, suteikiant papildomą laisvės laipsnį sistemos savybių derinimui.
3. Ištyrus spiralinės vielinės metamedžiagos sandūrą, buvo prieitą išvados, kad sukurta modelis leidžia kiekybiškai ištirti plazmonų poliaritonus, kuriuos galima valdyti modifikuojant spiralės kampą ir griovelių, gofruojančių idealiai laidžią vielos paviršių, skaičių suteikiant didelę sistemos savybių derinimo laisvę.
4. Ištyrus SPP, sklindančius mažų matmenų akustinių metamedžiagų sandūroje, buvo gautas sugerties padidėjimas (sklidimo konstantos menamoji dalis), lygus 0,83 dB, daro didelę įtaką taikant triukšmo slopinimo metodą.

Athanasios IOANNIDIS

ELECTRODYNAMICAL INVESTIGATION
OF THE PHOTONIC METAMATERIALS

Doctoral Dissertation

Technological Sciences,
Electrical and Electronic Engineering (T 001)

FOTONINIŲ METAMEDŽIAGŲ ELEKTRODINAMINIS
TYRIMAS

Daktaro disertacija

Technologijos mokslai,
elektros ir elektronikos inžinerija (T 001)

Lietuvių kalbos redaktorė Dalia Markevičiūtė
Anglų kalbos redaktorė Jūratė Griškėnaitė

2023 11 17. 11,5 sp. l. Tiražas 20 egz.
Leidinio el. versija <https://doi.org/10.20334/2023-049-M>
Vilniaus Gedimino technikos universitetas
Saulėtekio al. 11, 10223 Vilnius
Spausdino UAB „Ciklonas“,
Žirmūnų g. 68, 09124 Vilnius